THE UNIVERSITY OF
WARWICK

AUTHOR: **Shuyi Wang** DEGREE: **Ph.D.**

TITLE: **Optimization of Transmitted-Reference receivers in the Ultra-wide Bandwidth System**

DATE OF DEPOSIT: .....

I agree that this thesis shall be available in accordance with the regulations governing the University of Warwick theses.

I agree that the summary of this thesis may be submitted for publication.

I **agree** that the thesis may be photocopied (single copies for study purposes only).

Theses with no restriction on photocopying will also be made available to the British Library for microfilming. The British Library may supply copies to individuals or libraries. subject to a statement from them that the copy is supplied for non-publishing purposes. All copies supplied by the British Library will carry the following statement:

> "Attention is drawn to the fact that the copyright of this thesis rests with its author. This copy of the thesis has been supplied on the condition that anyone who consults it is understood to recognise that its copyright rests with its author and that no quotation from the thesis and no information derived from it may be published without the author's written consent."

AUTHOR'S SIGNATURE: .....

USER'S DECLARATION

1. I undertake not to quote or make use of any information from this thesis without making acknowledgement to the author.
2. I further undertake to allow no-one else to use this thesis while it is in my care.

DATE SIGNATURE ADDRESS

.....

.....

.....

.....

.....

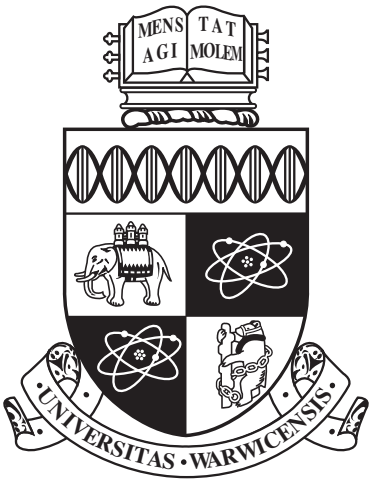

Optimization of Transmitted-Reference receivers in the Ultra-wide Bandwidth System

by

Shuyi Wang

Thesis

Submitted to the University of Warwick

for the degree of

Doctor of Philosophy

School of Engineering

November 2011

THE UNIVERSITY OF
WARWICK

Contents

List of Figures

List of Tables

Acknowledgments

I would like to acknowledge the advice and guidance of my supervisors, Dr. Yunfei Chen and Dr. Mark S. Leeson from the School of Engineering at the University of Warwick. I also thank the members of my graduate committee for their suggestions and encouragement, especially Prof. Roger J. Green.

Special thanks go to Prof. Norman C. Beaulieu from the University of Alberta Edmonton, Canada, for his knowledge and assistance in this studies.

I would like to thank my family members, especially my mother, Ms Yawei Niu, for her supporting and encouraging me to pursue this degree. Last but not least, I express my sincere appreciation to all my friends who have accompanied me during the entire period of my PhD studies.

Declarations

I herewith declare that I have produced this paper without the prohibited assistance of third parties and without making use of aids other than those specified; notions taken over directly or indirectly from other sources have been identified as such. This paper has not previously been presented in identical or similar form to any other examination board.

The thesis work was conducted from April 2008 to June 2011 under the supervision of Dr. Yunfei Chen at Warwick University.

List of Publications

Journal Papers

- **Shuyi Wang**, Yunfei Chen, Mark S. Leeson, Norman C. Beaulieu, "Channel Capacity and BER Optimization of the UWB Dual-Pulse Receiver", *Wireless Communications and Mobile Computing*, doi: 10.1002/wcm.1214, November 2011.

- **Shuyi Wang**, Yunfei Chen, M. Leeson, N.C. Beaulieu, "New receivers for generalized UWB transmitted reference systems with improved performances", *IEEE Transactions on Wireless Communications*, vol.9, no.6, pp.1837-1842, June 2010.

- Yunfei Chen, N. Beaulieu; **Shuyi Wang**, "Novel iterative receivers for TR UWB systems", *IEEE Communications Letters*, vol.13, no.4, pp.242-244, April 2009.

Conference Papers

- **Shuyi Wang**, Yunfei Chen, Mark S. Leeson, Norman C. Beaulieu, "Optimization of the Time Delay in the UWB Dual-pulse Receiver", *2011 IEEE International Conference on Ultra-Wideband*, pp. 445-449, September 2011.

Abstract

This thesis contributes the research and development of novel receiver optimization approaches conducted in ultra-wide bandwidth (UWB) systems. The ultimate goal of the improved receiver technology is to simplify the receiver structures at the cost of a tolerable performance degradation or improve the receiver performances at the cost of a tolerable complexity. Recently, UWB technology has become more and more attractive due to its increased performance. An advanced scheme that can provide a further improvement is strongly recommended and highly demanded. This research project focuses on the design of outstanding receivers suitable for the UWB system with transmitted-reference signaling. Two types of improved receivers are investigated. The first one is based on the optimization of inter-pulse time delay T_d in the traditional transmitted-reference receivers where one data pulse is transmitted T_d seconds delay after one reference pulse in a bit duration. The second one is based on the joint optimization of the number of reference symbols and the integration interval length in the generalized transmitted-reference receivers where N_d data symbols are transmitted after N_r reference symbols in a data packet. For both improved receivers, simulation and theoretical approaches are used to provide the optimization results. The numerical results show that the improved receivers by using different optimization approaches outperform the non-improved receivers significantly for most practical cases.

An up to 4.2dB performance improvement can be achieved consequently.

The principal conclusion from this thesis is that all the optimization schemes presented herein can be successfully applied to the design of receivers in the UWB transmitted-reference systems that the data decision can be obtained by thresholding the correlator output of the reference information with the data information.

Abbreviations

UWB	descriptive ultra-wide bandwidth
TR	descriptive transmitted-reference
WPAN	descriptive wireless personal area network
LLNL	descriptive Lawrence Livermore national laboratory
DoD	descriptive department of defense
FCC	descriptive Federal communications commission
Ofcom	descriptive office of communications
MIC	descriptive ministry of internal affairs and communications
EIRP	descriptive equivalent isotropically radiated power
GPS	descriptive global positioning system
LPD	descriptive low probability of detection
LPI	descriptive low probability of interception
SNR	descriptive signal-to-noise ratio
MAI	descriptive multiple access interference
NBI	descriptive narrowband interference

BER	descriptive bit error rate
S-V	descriptive Saleh-Valenzuela
LOS	descriptive line-of-sight
NLOS	descriptive non line-of-sight
PDF	descriptive probability density function
PSD	descriptive power spectral density
PPM	descriptive pulse position modulation
PAM	descriptive pulse amplitude modulation
OOK	descriptive on-off keying
BPPM	descriptive binary pulse position modulation
BPAM	descriptive binary pulse amplitude modulation
TH	descriptive time-hopping
SS	descriptive spreading spectrum
DS	descriptive direct-sequence
PN	descriptive pseudo-noise
AWGN	descriptive added white Gaussian noise
ED	descriptive energy detector

Chapter 1

Introduction

1.1 Introduction to Ultra-wide Bandwidth Systems

Over the last couple of decades, consumers' demands for wireless technologies have been dramatically increased due to the enormous convenience brought by modern technologies to the real-life world. In the near future, consumers will continuously increase their requirements for wireless connectivities to connect electronic devices, such as personal computers, portable game systems, mobile phones, photo printers and radio/video players, to each other in the home. However, today's short- or medium-range wireless communication technologies cannot meet the needs of such high compatibility which require very wide bandwidth, accommodating the needs for high capacity and data rate. For example, although the data rate can reach up to 54 Mbits per second for the IEEE 802.11 standards, the technologies have limitations in bandwidth, implementation efficiency and power consumption [1]; the bluetooth technol-

ogy (belongs to IEEE 802.15.1) trades its cost and power consumption off the data rate of up to 1 Mbit per second [2] which is not sufficient for many multiple high-bandwidth digital applications in wireless personal area networks (WPANs). A novel technology named ultra-wide bandwidth (UWB) was investigated accounting for the high-speed WPANs [3].

1.1.1 Historical development of UWB Technologies

In the long history of radio communications, the dominant electromagnetic waveform was sinusoidal. The sine-wave was so universal until the development of the sampling oscilloscope dating back to the early 1960s. The development of hardware devices attracted many institutes and companies to embark on the pulse transmitter, receiver and antenna investigations. In the 1960s, Lawrence Livermore National Laboratory (LLNL) was one of the pioneers leading the research in this area and many applications and technologies were then imported to UWB communications [4].

By the early 1970s the foundation of UWB radar systems were almost accomplished [4] and especially in 1973, Ross' US Patent [5] indicated that the comprehensive development of UWB systems had entirely started. Interested readers can refer to [4], [5] and [6] for further pioneer works for UWB all over the world. At the early stage, the UWB technologies were using base-band, carrier-less, impulse and time domain. The term 'ultra-wide bandwidth (UWB)' was first determined by the US Department of Defense (DoD) in 1989, since it occupies an extremely wide bandwidth. In the last century, UWB technologies have been diffusely used in numerous fields, such as medical applications, radar and military communications. However, there were

few applications developed for data communications like PC- or mobile-device communications [7].

In April 2002, the US Federal Communications Commission (FCC) released its report [8], first indicating that UWB technologies could be used in data communications as well. In [8], it defined UWB communication systems from many aspects, including UWB definition, bandwidth allocation and maximum transmission power. These FCC regulations have been widely accepted and applied for UWB systems, although some countries have their own variations. For example, the regulator in the UK is the Office of Communications (Ofcom) and the regulator in Japan is the Ministry of Internal Affairs and Communications (MIC), and they released their own standards for UWB communication systems in 2005 and 2004, respectively. However, the differences in UWB standards among various countries are not significant [9].

Interested readers can refer to [10], [11] and [12] for further historical reviews of UWB technologies.

1.1.2 FCC Regulations for UWB

The UWB system was defined by FCC [8] in 2002 as a transmission system with a bandwidth occupancy of more than 500 MHz or the fractional bandwidth greater than 20%, as shown in Figure 1.1, where f_L and f_H represent the lower and upper frequencies, respectively, at the -10 dB emission point. Also, $f_c = \frac{f_L+f_H}{2}$ represents the centre frequency. The fractional bandwidth is determined by $\frac{B}{f_c}$, where $B = f_H - f_L$ is the -10 dB bandwidth (10 dB below the highest emission point). According to [8], the newest UWB system either has a bandwidth no less than 500 MHz when $f_c \geq 2.5$ GHz, or has a fractional

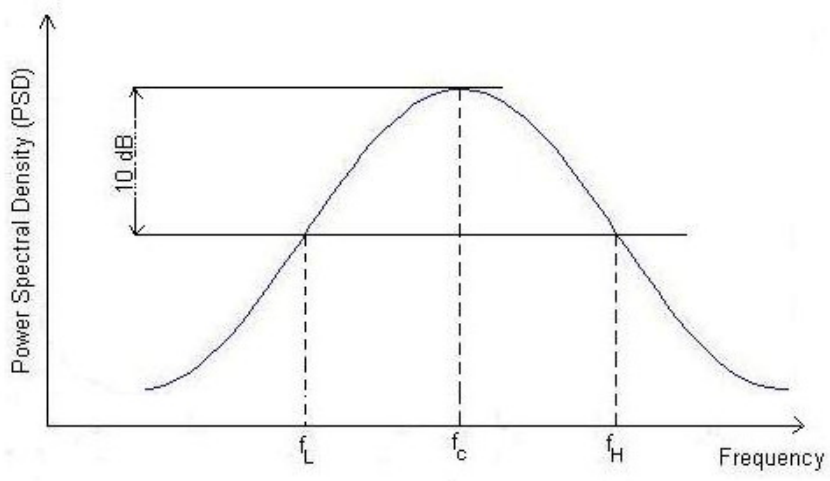

Figure 1.1: The definition of UWB systems [8].

bandwidth greater than 20% when $f_c < 2.5$ GHz.

The FCC allocated specific ranges of GHz bandwidth to UWB communication systems [8]. This extremely wide bandwidth allows UWB systems to potentially have a high data rate on the order of Gbps (Gbits per second). On the other hand, UWB has to coexist with other narrowband and wideband communication systems over the entire frequency bands. Therefore, the FCC limited the maximum transmission power such that UWB could not conflict with other existed systems.

Figure 1.2 shows the UWB spectral masks based on FCC 15.517 for indoor communications. The Equivalent Isotropically Radiated Power (EIRP) denotes the theoretical power from an isotropic antenna to produce the peak power in the direction of maximum antenna gain, taking into account the attenuations during transmission and from devices like an antenna. A conservative maximum emission power spectral density of -41.3 dBm/MHz is allowed approximately over the total 7.5 GHz bandwidth between 3.1 and 10.6 GHz, excluding the bands of 0.96-3.1 GHz where the power is restricted to as low as

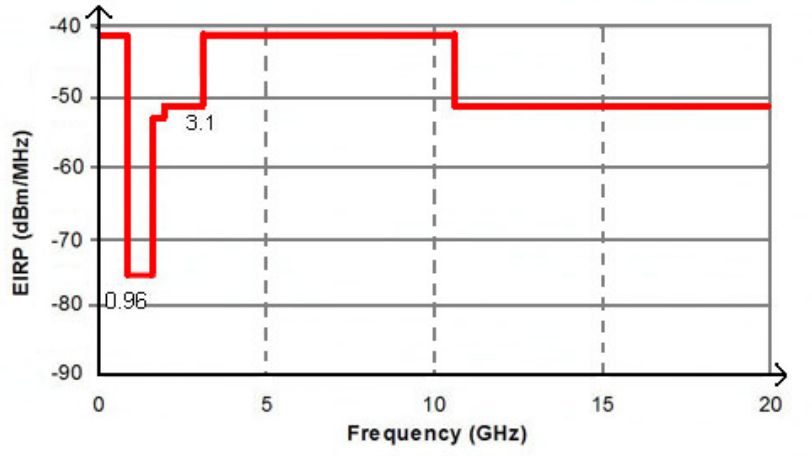

Figure 1.2: The FCC UWB spectral masks [8].

-75.3 dBm/MHz due to the existence of the global positioning systems (GPS) and some military applications.

For further detailed FCC UWB regulations, interested readers can refer to [8] or via the FCC official website '`http://www.fcc.gov/`'.

1.1.3 Characteristics of UWB

The UWB techniques have attracted great interest from both research and industry, because of some of the inherent features which make UWB optimal for low-cost, high-speed WPANs. The key benefits of UWB are listed as below:

- high data rate;
- low complexity and low cost;
- low probability of detection (LPD) and low probability of interception(LPI);
- increased capacity;
- simultaneous communications for different users.

A potential data rate in the order of Gbps can be achieved in UWB, owing to its extremely high spectral occupancy [13]. From a commercial point of view, the high data rate is the vital factor in today's manufacture for new digital applications. The UWB technologies will bring a new generation of personal wireless communications.

Unlike conventional communication systems, the UWB system generates a series of very short time-domain pulses which do not need sine-wave carriers to propagate. Consequently, the UWB system can be considered as comparably easy implementation and with low cost because no additional product is required at transmitters or receivers.

According to the UWB spectral masks shown in Figure 1.2, the UWB signal is substantially noise-like due to its low power density. This makes the signal quite difficult for unintended detection and also significantly reduces the interference between the UWB system and other existing systems. This property benefits UWB for secure and military applications [14].

Based on Shannon's theory, the channel capacity in an additive white Gaussian noise (AWGN) channel is expressed as [13]

$$C = B \log(1 + \frac{S}{N}) \tag{1.1}$$

where B is the channel bandwidth as described in section 1.1.2, and $\frac{S}{N}$ is the signal-to-noise ratio (SNR) of the channel. Clearly, the achievable channel capacity grows linearly with bandwidth but logarithmically with SNR and therefore, the bandwidth B is the dominant factor affecting the channel capacity. The UWB system thereby has a potential of relatively high channel capacity, compared with other narrowband communication systems [15].

Finally, UWB is commonly known as a low-power and short-range wireless communication system whose efficient transmission distance is normally less than 20 meters. That dramatically increases the system frequency reuse capability, as the users in different clusters can use the same frequency without interference. For example, player one (in a cluster) who is playing a wireless game (like WII) in the living room would not disturb the person (in another cluster) who is printing photos via a wireless printer in the study room, when they are using the same frequency bands.

1.1.4 UWB Applications

The UWB signal contains abundant low frequency components such that it enables the system to be capable of penetration and hence, the UWB technologies can be applied to imaging systems, such as wall radar imaging, medical imaging and surveillance systems [16].

Furthermore, owing to the fine time resolution and accurate position capabilities, UWB technologies can be applied for vehicular radar systems [17]. Consequently, they can be used to improve automotive safety and provide excellent services, such as safer airbag development and parking assistance.

For wireless communications, UWB enables a wide range of applications in WPANs. UWB wireless speaker/mouse/USB and even completely freeing cables among portable devices in the home can be realized, for example. Similarly, UWB technologies can also be applied in wireless sensor networks, due to their high power-efficiency [18].

1.1.5 Challenges for UWB

In spite of the numerous advantages of the UWB technology which make it have an optimistic future for the next generation of communications, many problems still need to be resolved for UWB to become a widely adopted technology [19].

A main problem that has always been of concern in UWB is about the cancellation of multiple access interference (MAI) and narrowband interference (NBI). Precise synchronization to the extremely short pulse, accurate channel estimation of the dense multipath coefficients, and adaptive receiver designs are also some of the key challenges that still have to be improved.

Other challenges include precise channel models in various environments, high-speed data sampling devices, appropriate multiple access and multiple access code designs, as well as compatible and universal standard/protocol solutions outside the physical layer.

1.2 Research Objective

Although UWB technology can be applied for data communications as well as radar and safety applications, this thesis focuses on investigations of UWB for data communications.

For the UWB wireless communications, receiver design is a crucial link to a successful implementation of the entire system. In an indoor environment, there exists a dense multipath propagation due to a great number of obstacles in the building. In order to take full advantage of these rich multipath components, an appropriate receiver is required to capture as much energy as possible from the multipath for reliable data detection. Consequently, an

efficient power-collection receiver with a relatively simple structure is highly desire. The current UWB receivers can be classified into two types: coherent receivers and non-coherent receivers. The transmitted-reference (TR) receiver is the most common UWB non-coherent receiver in the literature, and it can be further categorized into, for example, the traditional TR receiver or generalized TR receiver. The performances of all these receivers can be improved by either optimizing the time interval between the reference and data pulse per bit for traditional TR receivers or optimizing the number of reference symbols as well as the integration interval at the correlator for generalized TR receivers. Therefore, this thesis works on the receiver optimizations in the UWB TR system. A series of novel optimization approaches are specifically listed as below

- to determine the optimal value of the time interval T_d within pulse pairs for the traditional TR UWB receiver [52] to improve both its channel achievable capacity and BER;

- to determine the optimal value of reference symbol amount and integration interval length for the generalized TR UWB receiver [79] in order to improve its BER;

- to determine the optimal values of reference symbol amount and integration interval length for the new generalized TR UWB receivers [80] in order to improve their BERs.

1.3 Contributions to Knowledge

In the context of the objectives outlined in Section 1.2, this thesis aims to provide a significant contribution to knowledge via the demonstration of the receiver optimization investigations in UWB systems. In particular, it shows that the current UWB TR receivers [52] can be effectively optimized with respect to some inherent parameters in receiver designs; and also shows that several approaches can provide significant system improvements in terms of two criteria: maximization of channel achievable capacity and minimization of BER. The approaches proposed and investigated in this thesis will provide other researchers with a novel method for the receiver design.

1.4 Thesis outline

In *Chapter 2*, an introduction to the UWB system is presented. The main characteristic of the UWB system differing from other systems is the very dense multipath channel and thus, the properties of the UWB channel models are discussed first. Due to the extremely wide bandwidth for UWB, it makes many conventional modulation schemes unsuitable for the UWB system. Several appropriate modulation schemes for UWB are illustrated. Then, multiple-access techniques are introduced herein for real UWB communication systems. Therefore, enhanced channel capacity and reduced interference caused by multiple users can be obtained, provided that an appropriate multiple-access scheme is established. Finally, a brief description of UWB receivers is addressed.

Chapter 3 focuses on optimizations of the traditional TR receiver [52].

Both the channel achievable capacity and BER are optimized with respect to the time interval between reference and data pulses. Three approaches to the problem, being (a) simulation, (b) semi-analytical and (c) analytical, are separately discussed for the investigations. Detailed mathematical calculations are included in the chapter.

In *Chapter 4*, the generalized TR receivers [79] are optimized via simulation with respect to two parameters: the number of reference symbols in one data packet and the length of integration interval at the correlator. Then, by using the same optimization approaches as above, the new generalized TR receivers [80] are optimized similarly and the semi-analytical results for optimization are also obtained based on Gaussian approximation to the noise plus interference terms.

Chapter 5 summarizes the key results of the research presented in *Chapter 3* and *Chapter 4*. The relative merits and limitations of the approaches or methods are discussed, and suggestions for further improvement are provided as well. This chapter provides the principal conclusions and the main findings related to this work. In addition, further work is suggested.

Chapter 2

UWB systems

2.1 Introduction

In wireless communications, UWB has been considered as a very attractive technology owing to its high data rates, potential high capacity, low power consumption, low cost and low complexity for implementation [20], [21]. These benefits of the UWB system over other narrowband communication systems are all due to some inherent characteristics in UWB. The basic difference between UWB and other systems is the channel modeling where the extremely wide frequency bands of more than 500 MHz are occupied by UWB. This also results in most conventional modulation techniques being no longer applicable to UWB systems. UWB channel models are introduced and discussed in *Section 2.2*, then several modulation schemes as well as the multiple access techniques are described in *Section 2.4*. On the other hand, the UWB systems convey data information by transmitting a sequence of ultra-short pulses in the time domain. These transmission pulses are presented in *Section 2.3*. In addition, in order to take full advantage of multipath diversity in UWB channels,

the key challenge is to design an appropriate receiver with good performance and low complexity. Several commonly used UWB receivers are introduced in *Section 2.5* and conclusions are drawn in *Section 2.6*.

2.2 UWB Channel Models

In the communication system, a sequence of data information is sent from the transmitter to the receiver over a propagation environment which suffers from reflection, refraction, diffraction, polarization and scattering due to surrounding obstacles. Since a great amount of commercial UWB applications considers indoor communications, this section will focus on the indoor UWB channels only. A significant amount of research has been reported for the indoor UWB channel models in the literature, which are experiments on the signal propagating within buildings [22], [23], [24], [25]. Various measurements were evaluated for different scenarios in order to provide a precise channel model for the real system, including the delay spread, power attenuation/gain and multipath arrival time. Win, et al [24] first came up with the statistical model for UWB in the time domain using impulsive signals. After this, many accurate statistical models were proposed. In 2003, the IEEE 802.15.3a working group for wireless personal area networks released the IEEE UWB indoor channel models which are commonly used nowadays for UWB systems [26].

The proposed IEEE UWB indoor channel models [26] are based on the Saleh-Valenzuela model, as shown in [22], where multipath rays arrive in clusters and their multipath gains decay with a double-exponential function. However, the novel IEEE models differ from the Saleh-Valenzuela model [22] because the former undergoes a log-normal distribution rather than a Rayleigh

distribution for the latter one. In the following, the Saleh-Valenzuela model will be first described and the IEEE channel models will be analysed later.

2.2.1 Saleh-Valenzuela Model

One of the well-known UWB indoor channel models is the Saleh-Valenzuela (S-V) [22]. This is based on the measurements utilizing radar-like pulses with 10 ns duration and a centre frequency of 1.5 GHz. The S-V model is represented by multipath components having propagation gains of $\{a_{k,l}\}$, delays of $\{T_l, \tau_{k,l}\}$ and associated phase shifts of $\{\theta_{k,l}\}$, where l and k are the indexes of the lth cluster and the kth ray within the lth cluster, respectively. Therefore, the channel impulse response can be expressed as [22]

$$h_0(t) = \sum_{l=0}^{+\infty} \sum_{k=0}^{+\infty} a_{k,l} e^{j\theta_{k,l}} \delta(t - T_l - \tau_{k,l}) \tag{2.1}$$

where $\delta(\cdot)$ is the Dirac delta function. Referring to [22], the cluster arrival times $\{T_l\}$, i.e., the arrival times of the first ray in the clusters, are Poisson distributed random variables with rate Λ. Within each cluster, the arrival times of subsequent rays $\{\tau_{l,k}\}$ are also Poisson distributed random variables with rate λ (Normally, $\lambda >> \Lambda$ because each cluster contains numerous rays). $\{\theta_{l,k}\}$ are independent uniform random variables over the range of $[0, 2\pi)$, and $\{a_{l,k}\}$ are independent Rayleigh random variables with power $E\{a_{l,k}^2\} = \Omega_0 e^{\frac{-T_l}{\Gamma}} e^{\frac{-\tau_{l,k}}{\gamma}}$ where $\Omega_0 = E\{a_{0,0}^2\}$ is the mean energy of the first ray in the first cluster, Γ is the cluster decay rate and γ is the ray decay rate in the cluster.

From [22], the double sum term on the right side of eq.(2.1) fulfils an exponationally decaying power profile in the dense multipath environment where the number of multipath is sufficiently large.

2.2.2 IEEE Model

Instead of using a Rayleigh distribution, the channel modelling sub-committee of the IEEE 802.15.3a Task Group [26] recommends the log-normal distribution for the multipath gain, as the log-normal distribution has been verified to better fit the measured data in UWB systems. Although the IEEE 802.15.4a Task Group reports another channel model for more scenarios, this model is suitable for low data rate WPANs, especially for sensor networks [27]. In this thesis, the IEEE 802.15.3a channel model [26] is applied as a general model for the UWB system.

From [26], the UWB indoor channel models are specifically divided into four categories, according to the distance between transmitters and receivers as well as the transmission types of either line-of-sight (LOS) or non-LOS (NLOS). CM1 is based on the LOS transmission and corresponds to the very short communication range of 0 to 4 m. CM2 is defined for the same range as in CM1 but with the NLOS transmission. CM3 and CM4 are defined for the NLOS transmission. However, the communication distances are extended to 4-10 m for CM3 and over 10 m for CM4, respectively.

The IEEE UWB channel model in [26], a slightly modified version of the S-V model, has been confirmed as a precise channel modelling in reality. It identifies the number of paths, that is, it determines the number of multipath arrivals which reach within 10 dB range from the most powerful arrival. Moreover, the phase shifts $\{\theta_{l,k}\}$ are restricted to take the values of 0 or π with equal probability due to the signal inversion from reflection, and the random variables $\{X\}$ are also introduced to account for the log-normal shadowing. Consequently, the impulse response in IEEE UWB channel models is given

by [26]

$$h_0(t) = X \sum_{l=0}^{L} \sum_{k=0}^{K} a_{k,l} \delta(t - T_l - \tau_{k,l}) \tag{2.2}$$

where L represents the total number of cluster and K represents the total number of rays within each cluster. It is clear that the arrival time of the lth cluster T_l is the arrival time of the first ray in the lth cluster, for which $\tau_{0,l} = 0$. Let $\psi_l = T_l - T_{l-1}$ when $l \geq 1$ and $\psi_l = T_l$ when $l = 0$, respectively. Then the probability density function (PDF) of the cluster arrival time is given by [26] as

$$p_{\psi_l}(t) = \Lambda e^{-\Lambda t}, \quad l > 0. \tag{2.3}$$

Similarly, let $\varphi_{k,l} = \tau_{k,l} - \tau_{k-1,l}$ when $k \geq 1$ and $\varphi_{k,l} = \tau_{k,l}$ when $k = 0$, respectively. Then the PDF of the ray arrival time in the lth cluster can be written as

$$p_{\varphi_{k,l}}(t) = \lambda e^{-\lambda t}, \quad k > 0. \tag{2.4}$$

As known from *Section 2.2.1* for the S-V model, ψ_l and $\varphi_{k,l}$ are both random independent variables in the Poisson process with Λ and λ being the arrival rates for clusters and rays within their clusters, respectively. Since $T_l = \sum_{x=0}^{l} \psi_x$ and $\tau_{k,l} = \sum_{y=0}^{k} \varphi_{y,l}$, the PDFs of T_l and $\tau_{k,l}$ can be separately derived as

$$p_{T_l}(t) = \Lambda \cdot \frac{e^{-\Lambda t} \cdot (\Lambda t)^l}{l!}, \quad t > 0, l \geq 0 \tag{2.5}$$

and

$$p_{\tau_{k,l}}(t) = \lambda \cdot \frac{e^{-\lambda t} \cdot (\lambda t)^{k-1}}{(k-1)!}, \quad t > 0, k \geq 1. \tag{2.6}$$

However, for the CM1 channel model, the PDF of T_l at $l = 0$ equals zero because $T_0 = 0$ due to the LOS component. Eq.(2.5) and eq.(2.6) are both

suitable to CM2 - CM4 channel models. In addition, the selection of k excludes the value of 0 as $\tau_{0,l} = 0$.

In [26], the coefficients of multipath gain $\{a_{k,l}\}$ in (2.2) can be further represented as $a_{k,l} = p_{k,l} \cdot \chi_l \cdot \beta_{k,l}$, where $\{p_{k,l}\} = \pm 1$ with equal probabilities determining the sign of the multipath gain, χ_l represents the channel fading associated with the lth cluster and $\beta_{k,l}$ represents the channel fading associated with the kth ray in the lth cluster. The PDFs of χ_l and $\beta_{k,l}$ are separately given by [28]

$$p_{\chi_i}(z) = \frac{20}{z \ln 10 \sqrt{2\pi\sigma_1^2}} e^{-\frac{(20 \log_{10} z)^2}{2\sigma_1^2}}, \ z > 0; \tag{2.7}$$

$$p_{\beta_{k,l}}(z) = \frac{20}{z \ln 10 \sqrt{2\pi\sigma_2^2}} e^{-\frac{\left(20 \log_{10} z - \mu_{k,l}\right)^2}{2\sigma_2^2}}, \ z > 0 \tag{2.8}$$

where $\mu_{k,l} = \frac{10 \ln \Omega_0}{\ln 10} - \frac{10 T_l}{\Gamma \ln 10} - \frac{10 \tau_{k,l}}{\gamma \ln 10} - \frac{(\sigma_1^2 + \sigma_2^2) \ln 10}{20}$, Ω_0 is the average energy of the first path within the first cluster, Γ is the cluster decay rate and γ is the ray decay rate in the cluster, σ_1^2 is the variance of the log-normal fading term $20 \log_{10} \chi_l$ associated with clusters, and σ_2^2 is the variance of the term $20 \log_{10} \beta_{k,l}$ associated with rays.

Figure 2.1 shows the channel impulse response for different scenarios. All the simulation results are obtained based on 600 channel realizations. One may see that CM1 and CM2 have the similar average delay profiles. However, the strongest multipath components in CM2 are delayed by about 5 ns in comparison with those in CM1, due to the NLOS property in CM2. One can also see from CM3 and CM4 that, increasing the distance between the transmitter and the receiver results in a longer time spread, compared with CM1 and CM2.

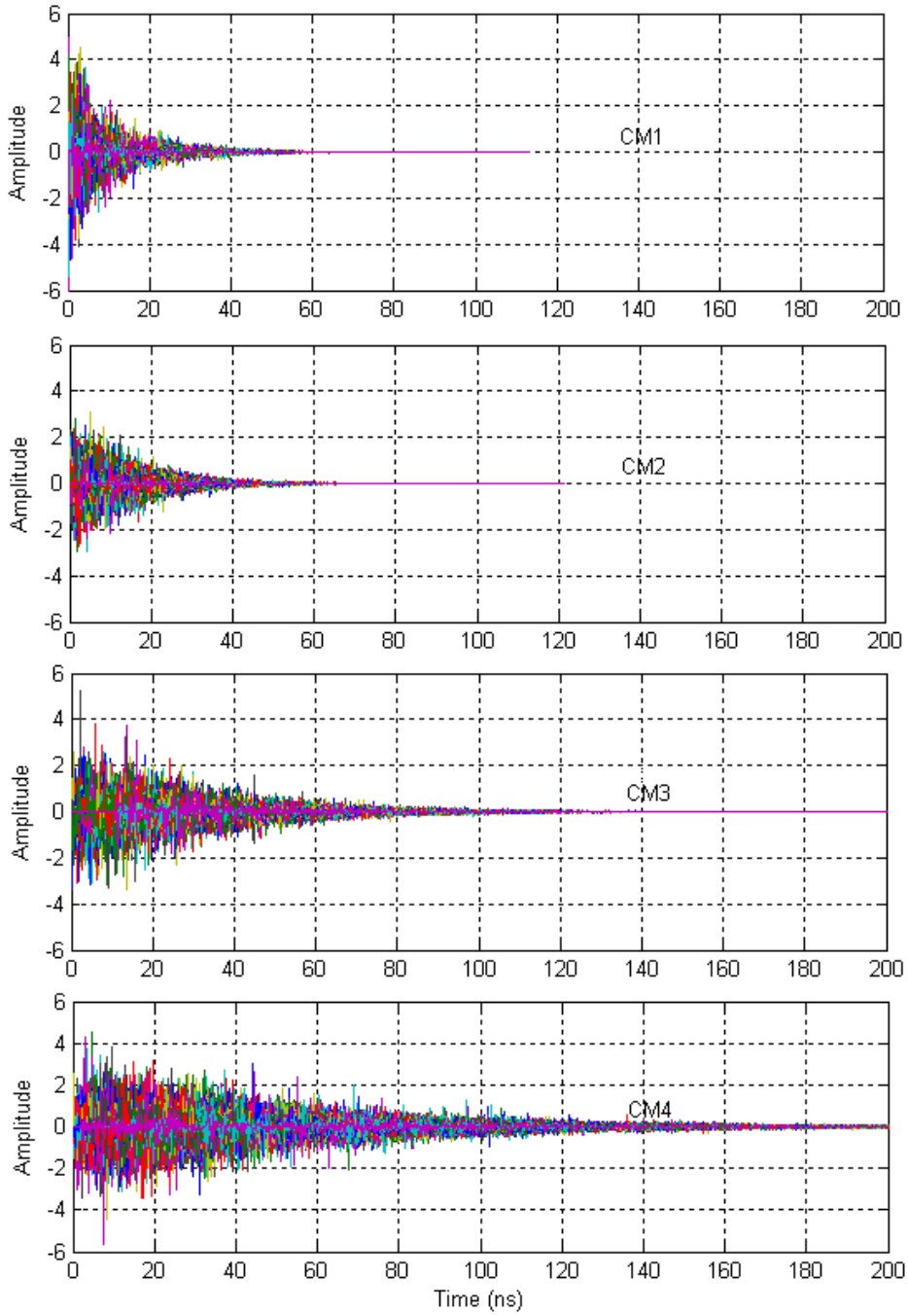

Figure 2.1: The realizations of the channel impulse response for different scenarios (CM1-CM4).

2.3 UWB Pulses

The widely used pulses $p(t)$ for UWB systems include Gaussian pulse, Gaussian monocycle (the first derivation of a Gaussian pulse) and Gaussian doublet (the second derivation of a Gaussian pulse), due to their very short pulse durations and simple functions [20], [29], [30], [31]. All these waveforms have very short duration of T_p. With T_p on the order of nanosecond, the pulse can resolve a large number of multipath components and hence, enable rich multipath diversity provided by these multipath components [21].

The mathematical definition for a typical Gaussian pulse is very similar to the Gaussian function as

$$p_0(t) = exp\left[-2\pi\left(\frac{t-\frac{t_n}{2}}{t_n}\right)^2\right] \tag{2.9}$$

where t_n is the time-scaling factor. Its nth derivation pulse has the form [32]

$$p_n(t) = \varepsilon_n \frac{d^n}{dt^n} exp\left[-2\pi\left(\frac{t-\frac{t_n}{2}}{t_n}\right)^2\right]. \tag{2.10}$$

The Gaussian doublet can be modeled by the second derivation of a Gaussian pulse as

$$p_2(t) = \left[1 - 16\pi\left(\frac{t-\frac{t_n}{2}}{t_n}\right)^2\right] \cdot exp\left(-8\pi\left[\frac{t-\frac{t_n}{2}}{t_n}\right]^2\right) \tag{2.11}$$

where the pulse is right-shifted by $\frac{t_n}{2}$ ns in the time domain in order to make the pulse starting time at the system starting point of $t = 0$ and, therefore, to make the pulse suitable for the UWB channel model which start from the "0" point. The pulse energy is $E_g = \int_{-\infty}^{\infty} p_n^2(t)dt$. On the other hand, the

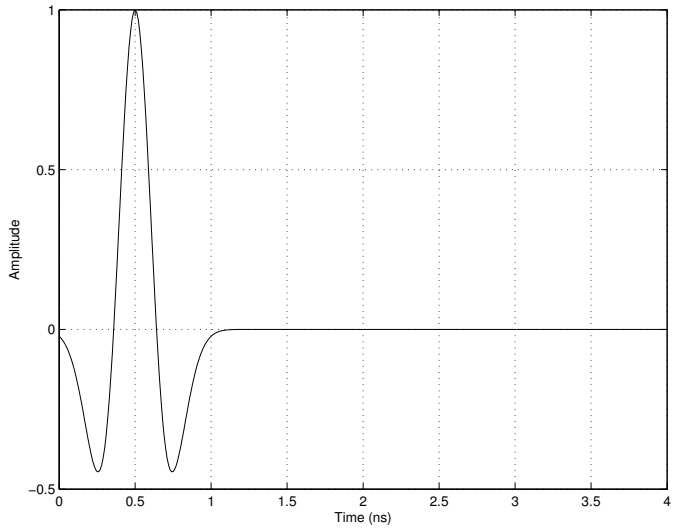

Figure 2.2: The Gaussian doublet in the time domain defined in (2.9).

representation of the Gaussian doublet $p_2(t)$ in the frequency domain can be derived by using a Fourier transform of (2.11) as

$$\begin{aligned} F_{p_2} &= \mathcal{F}\{p_2(t)\} \\ &= \int_{-\infty}^{\infty} \left[1 - 16\pi \left(\frac{t - t_n/2}{t_n}\right)^2\right] \cdot exp\left(-8\pi \left[\frac{t - t_n/2}{t_n}\right]^2\right) \cdot exp\left(-j2\pi ft\right) dt \\ &= \frac{\sqrt{\pi} t_n^3 f^2}{16} \cdot exp(j\pi t_n f - \frac{\pi t_n^2 f^2}{8}). \end{aligned} \tag{2.12}$$

The upper frequency f_H and the lower frequency f_L for the Gaussian doublet can be calculated from eq.(2.12). So that $f_H \approx 2.3$ GHz, $f_L \approx 0.99$ GHz and hence, $B = f_H - f_L \approx 1.3$ GHz and $f_c = (f_H + f_L)/2 \approx 1.7$ GHz.

Figure 2.2 and Figure 2.3 exhibit the Gaussian doublet $p(t)$ in the time domain and in the frequency domain, respectively. In the simulation, $t_n = 1\ ns$ and therefore $E_g = 0.1875$. The pulse duration $T_p = 1\ ns$ shown in Figure 2.2 also determines the bandwidth B as $B \approx \frac{1}{T_p} \approx 1$ GHz, as can be demonstrated in Figure 2.3.

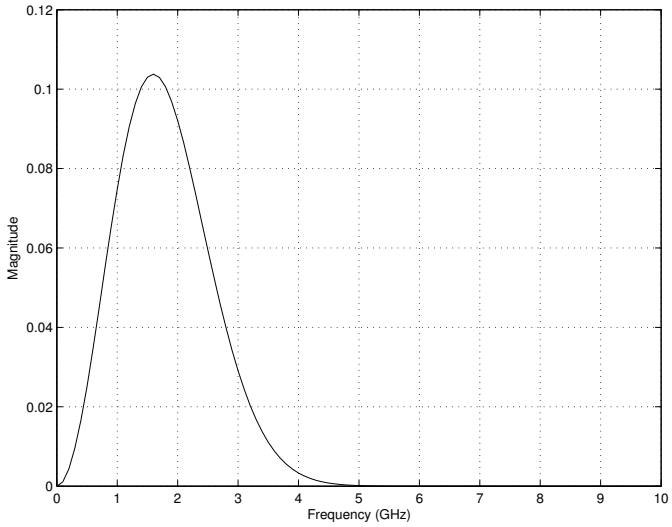

Figure 2.3: The Gaussian doublet in the frequency domain defined in (2.12).

However, the power spectral density (PSD) of the most widely used Gaussian doublet cannot meet the power spectral constraint of the FCC UWB mask unless a frequency translation is used. Only the PSD of the Gaussian pulses with an order higher than three can meet this restrictions [33]. Thus, the pulse shape design for the real UWB system needs to satisfy two conditions: i) the pulse duration T_p needs to be very short for multiple access and ii) the energy or power density needs to very low to meet the FCC frequency masks. References [34] and [35] proposed several novel methods for the UWB pulse design that meet both requirements discussed as above.

2.4 UWB Communications

As discussed previously in *Section 2.3*, a single UWB pulse does not contain any data information by itself. The digital data information need to be added to this analogue pulse, by means of modulation [13]. In spite of the benefits of UWB systems, its extremely wide frequency bands and the ultra-short trans-

mission pulse make it very difficult for the traditional modulation schemes for narrowband systems to be applied for UWB communication systems. Data rates, spectral characteristics of the transmitted signal, implementation complexity and performance are all significantly related to the employed modulation techniques. Therefore, various UWB modulations have been investigated in the literature to implement suitable modulation schemes for different scenarios [36], [37], [38], [39].

Nowadays, the most common modulation technique is pulse position modulation (PPM) where the data information is modulated by transmitting at different time instants. Specifically, the pulse is sent before or after a time scale depending on the value of the digital data. Another common technique is pulse amplitude modulation (PAM) where the data is modulated by varying the amplitude of the analogue pulse according to the data value. Other well-known modulation techniques include, for example, on-off keying (OOK) where the presence or absence of the analogue pulse determines the data information. Here, the two most commonly used modulation schemes, PPM and PAM, will be examined.

2.4.1 Binary PPM

By defining a pulse with arbitrary shape of $p(t)$, the generic transmitted signal with the binary PPM (BPPM) in a single-path and single-user environment can be written as

$$s(t) = \sum_{j=-\infty}^{\infty} p(t - jT_f - \delta d_{\lfloor j/N_f \rfloor}) \tag{2.13}$$

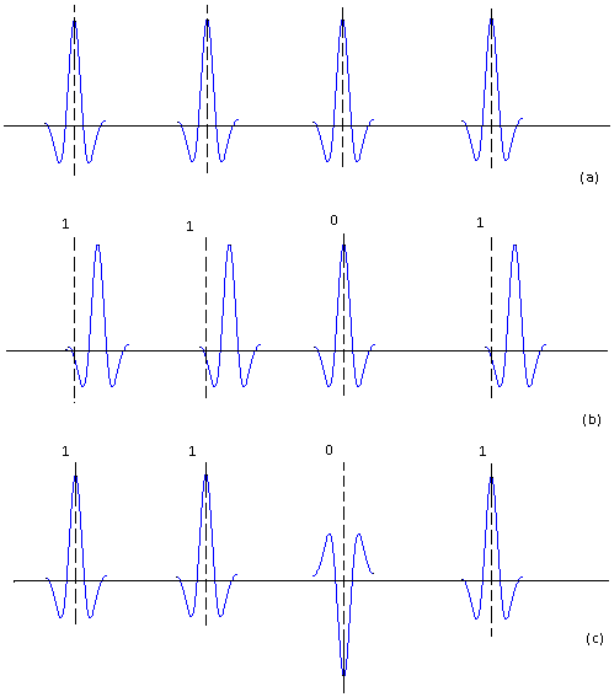

Figure 2.4: Comparison of several different modulation techniques for UWB communications: (a) unmodulated pulses, (b) BPPM and (c) PAM.

where T_f is the frame duration, j is the index of the frame number and N_f is the number of frames in one symbol. $\lfloor \cdot \rfloor$ returns the integer part of $(\cdot)$. $\delta d_{\lfloor j/N_s \rfloor}$ identifies the pulse position with $\left\{d_{\lfloor \cdot \rfloor}\right\}$ being the data information and δ being the time scale associated with BPPM. The structure diagram of BPPM is illustrated in Figure 2.4(b), while Figure 2.4(a) shows the unmodulated pulse train for comparison. One can see from Figure 2.4 (b) that the transmitted pulse containing a digital data bit of '1' is right-shifted by δ; and the transmitted pulse containing a '0' bit remains.

One can also apply this idea to a M-ary PPM system with various time shifts. That is, the time shift factor $\delta d_{\lfloor j/N_s \rfloor}$ in (2.13) is replaced by $\tau_{m,j}$ for the M-ary system, where $\tau_{m,j}$ denotes the time shift for the mth bit sequence

associated with the jth frame [40], [41]. Take a 4-ary PPM system as an example. One can make $\tau_1 = -0.75T_f$, $\tau_2 = -0.25T_f$, $\tau_3 = 0.25T_f$, and $\tau_4 = 0.75T_f$ for one frame. Thus, the four pulses corresponding to the four mapping situations can be expressed as

$$s_1(t) = \sum_{j=-\infty}^{\infty} p(t - jT_f + 0.75T_f)); \; s_2(t) = \sum_{j=-\infty}^{\infty} p(t - jT_f + 0.25T_f));$$

$$s_3(t) = \sum_{j=-\infty}^{\infty} p(t - jT_f - 0.25T_f)); \; s_4(t) = \sum_{j=-\infty}^{\infty} p(t - jT_f - 0.75T_f)).$$

In this case, each frame can be seen as divided into M individual sub-slots and each sub-slot corresponds to a bit sequence. For a single-user UWB system, the M-ary PPM modulation technique can continuously improve the system capacity with the increases of M due to the increased number of bits transmitted per symbol. However, the capacity differences among the M-ary modulation schemes with arbitrary M are reduced when the number of system users is increased. This is due to increased multi-user interference [40].

The PPM modulation scheme benefits from its structure simplicity and potential high capacity, but it requires extremely fine time control to modulate and demodulate pulses with an accuracy of a nanosecond.

2.4.2 Binary PAM

With the binary PAM (BPAM), the data is modulated by either inverting the pulse or not according to the data information. The generic transmitted signal

with BPAM in a single-path and single-user environment can be written as

$$s(t) = \sum_{j=-\infty}^{\infty} \vartheta_{\lfloor j/N_f \rfloor} p(t - jT_f) \tag{2.14}$$

where $\left\{\vartheta_{\lfloor j/N_f \rfloor}\right\}$ is the binary codes associated with the data information. $\vartheta_{\lfloor j/N_f \rfloor} = +1$ if the $\lfloor j/N_f \rfloor$th digital data '1' is transmitted and $\vartheta_{\lfloor j/N_f \rfloor} = -1$ if the $\lfloor j/N_f \rfloor$th digital data '0' is sent. An basic example of BPAM is shown in Figure 2.4(c). The inverse pulse represents the digital '0' bit, while the un-inversed pulse represents the digital '1' bit.

Compared with BPPM, the major advantage of using BPAM is due to the 3 dB gain in the power efficiency [13], [39], [40]. This is due to the fact that, BPAM can transmit twice the number of pulses and then twice the data rate over PPM because BPAM does not need to wait for the pulse transmission. Further discussions about the comparison of BPPM and BPAM can refer to [42] and [43] for interested readers.

As discussed previously, the modulation schemes can be basically divided into two categories: modelling either the pulse position or the pulse shape. These schemes all have good performances in a single-user environment, while in a multi-user system they suffer more interference from other users existing in the same system. In order to make them suitable for multiple-access communication systems, spread spectrum techniques are applied and combined with the UWB system in [29]. The most popular spreading spectrum techniques for UWB systems in the literature are: time-hopping spreading spectrum (TH-SS), and direct-sequence spreading spectrum (DS-SS).

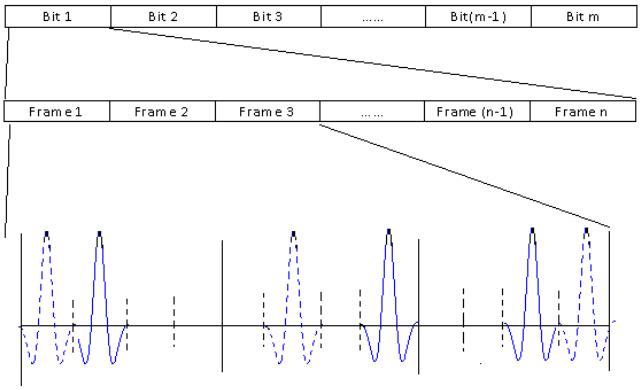

Figure 2.5: A typical structure of the UWB TH-SS system with two users.

2.4.3 TH-SS UWB systems

With TH-SS, each pulse is positioned within one frame duration T_f. Specifically, the pulse associated with one user hops in the time domain according to the pseudorandom TH sequence [29], [44]. Combining the modulation technique BPPM in eq.(2.13) with the TH-SS scheme, a typical UWB transmitted signal with TH-BPPM for the uth user is given by

$$s(u,t) = \sum_{j=-\infty}^{\infty} p(t - jT_f - T_c \cdot c_j(u) - \delta d_{\lfloor j/N_f \rfloor}) \tag{2.15}$$

where $c_j(u)$ is the TH code for the jth frame associated with the uth user, N_f is the number of frames per symbol and T_c is the chip interval. Herein, each frame is divided into $N_c = \frac{T_f}{T_c}$ individual chips and the uth user's TH code $c_j(u)$ is an arbitrary integer in the range of $[0, N_c - 1]$ within one frame. Thus, another time shift of $c_j(u) \cdot T_c$ is added to the transmitted signal, compared with that employing BPPM only as in eq.(2.13). Figure 2.5 shows a very simple example of a UWB TH-BPPM signaling structure. The solid lines

represent the desired users with a TH sequence of [2,4,3] and the dashed lines represent the interfering users with another TH sequence of [1,2,4]. One sees that, by utilizing the TH codes, increased number of users can be introduced in the system with acceptable multiple-access interference (MAI).

Similarly, TH-SS can also be combined with the BPAM scheme. In the TH-BPAM system, a typical transmitted signal for the uth user can be written as

$$s(u,t) = \sum_{j=-\infty}^{\infty} \vartheta_{\lfloor j/N_f \rfloor}(u) p(t - jT_f - T_c \cdot c_j(u)). \tag{2.16}$$

The difference between the spreading spectrum techniques applied to the UWB system and the traditional SS techniques defined in [45] is that, the signal with the former SS schemes does not occupy the entire spectrum. In the TH-SS UWB systems, each pulse is sent during an arbitrary chip interval according to the specified TH code. On the other hand, Foerster applied the DS-SS technique to UWB where one pulse containing the data information is repeatedly transmitted N_c times in one symbol duration. The DS-SS technique can reduce the impact of MAI as well [46].

2.4.4 DS-SS UWB systems

Assume that each user has a specific pseudo-noise (PN) sequence with the length of N_c and hence, the frame duration $T_f = N_c \cdot T_c$ where T_c denotes the spreading gain. A typical transmitted signal for the uth user with DS-BPAM can be expressed as

$$s(u,t) = \sum_{j=-\infty}^{\infty} \sum_{n=0}^{N_c-1} \vartheta_{\lfloor j/N_f \rfloor}(u) c_n(u) p(t - jT_f - nT_c). \tag{2.17}$$

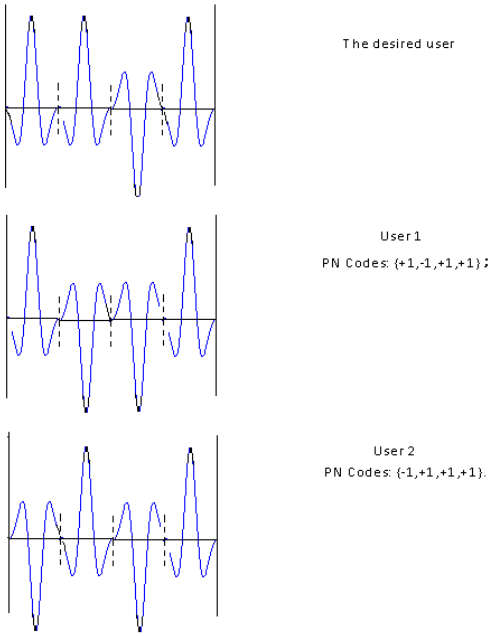

Figure 2.6: A typical structure of the UWB DS- system with three users.

where $\{c_n(u) = \pm 1\}$ are the spreading codes associated with uth user. In the DS-SS UWB systems, the frame duration T_f is decreased to a chip duration T_c and pulses are transmitted successively with a period of T_c. Figure 2.6 illustrates an example of a UWB DS-BPAM system. The PN codes $\{c_n(u)\}$ are used herein to change the polarities of the pulses to distinguished different users.

The system performance is highly related to the PN patterns. With an appropriate code design, better correlation properties can be achieved in a multi-user environment [46], [47]. The previous research have demonstrated that Gold, Kasami, Barker and PN spreading codes are all suitable for UWB DS-SS systems. Similar investigations for the TH code design in UWB TH-SS systems are presented in [48].

The comparison of the TH-SS UWB and the DS-SS UWB systems has

been discussed in [49]. The DS-SS scheme is more suitable than the TH-SS scheme in a multi-user environment, as a higher amount of collision occurs in the TH-SS scheme.

Eq.(2.15) - eq.(2.17) exhibit the transmitted signal employing various spread spectrum and modulation techniques, as TH-BPPM, TH-BPAM and DS-BPAM, respectively. These expressions can be also considered as the simplest format of the UWB transmitted signal which will pass through the multipath propagation channel to reach the receiver afterwards.

2.5 UWB Receivers

At the receiver, the distorted signal caused by interference and noise needs to be recovered for the data decision, using the TH-BPAM UWB system as an example. By substituting eq.(2.2) into eq.(2.16), the received signal for the uth user can be obtained by

$$\begin{aligned} r(u,t) &= s(u,t) * h_0(t) \\ &= \sum_{j=-\infty}^{\infty} \sum_{l=0}^{L} \sum_{k=0}^{K} \alpha_{k,l} \vartheta_{\lfloor j/N_f \rfloor}(u) p_{rx}(t - T_l - \tau_{k,l} - jT_f - T_c \cdot c_j(u)) \\ &+ n(u,t) \end{aligned} \tag{2.18}$$

where p_{rx} is the aggregate pulse taking the effects of multipath, multiple-access and spectrum spreading into account and '$*$' denotes the convolution. $n(u,t)$ represents the noise for the uth user and it is normally regarded as additive white Gaussian noise (AWGN).

The receiver design is a major challenge for a UWB system. Several receivers have been proposed for UWB in the literature, including coherent re-

ceivers such as the RAKE receiver [50] [51], and non-coherent receivers such as the transmitted-reference (TR) receiver [52] [53] [54] and the energy detection receiver [55] [56].

The Rake receiver is often applied in UWB systems to take full advantage of multipath diversity. However, it is computationally prohibitive to collect the energies of all the multipath components, as one has to employ an explicit channel estimator for each multipath component. Therefore, practical Rake receivers often adopt a limited number of 'fingers', at the cost of a degraded system performance [50], [57].

Instead of using a complicated RAKE receiver, reference [52] proposed the transmitted reference (TR) receiver, to relax the requirements on synchronization and channel estimation. The traditional TR receiver correlates the received signal corresponding to the data symbol with the template signal corresponding to the reference symbol which is transmitted before the data symbol and hence, this noisy template signal degrades the receiver performance significantly. Several template designs for reliable data detection in the UWB TR systems have been developed in [58]. Some template signals in [58] have a high time-consuming requirement due to their complex template formats. The energy detector (ED) can provide a simple receiver structure avoiding recursive algorithms, resulting in significant performance degradation. The received signal at ED is squared and then thresholded to recover the transmitted data signal. Therefore, the selection of the optimal threshold plays a very important role in the receiver performance [59], [60].

Interested readers can refer to [61] for further detailed comparison between coherent and non-coherent receivers in UWB communications. Thus, the structure of the traditional TR receiver will be described.

2.5.1 UWB TR Receivers

The attraction of the UWB TR system has been dramatically drawn from both academic and industrial environments recently. This is due to the improved system performance with an acceptable of complexity [62]. In the traditional TR system, the reference (pilot) pulse is transmitted T_d seconds before the data pulse. The part of the received signal corresponding to the reference information is used to construct the channel template, which is correlated with the part of the received signal corresponding to the data information for data detection.

Considering a multi-user UWB TH-BPM system, the transmitted signal for the ith bit (i.e., the ith symbol) in the uth user is given by

$$\begin{aligned} s(u,t) &= \sqrt{\varepsilon_i(u)} \sum_{j=0}^{N_f-1} [p(t - jT_f - T_c \cdot c_j(u)) \\ &+ \vartheta_i(u) p(t - jT_f - T_c \cdot c_j(u) - T_d(u))] \end{aligned} \tag{2.19}$$

where $\varepsilon_i(u)$ is the signal energy for the ith bit in the uth user and $T_d(u)$ is the time interval between data and reference pulses in the uth user. The expression of the received signal is similar to eq.(2.18) as

$$\begin{aligned} r(u,t) &= \sqrt{\varepsilon_i(u)} \sum_{j=0}^{N_f-1} [h(t - jT_f - T_c \cdot c_j(u)) \\ &+ \vartheta_i(u) h(t - jT_f - T_c \cdot c_j(u) - T_d(u))] + n(t) \end{aligned} \tag{2.20}$$

where $h(t) = p(t) * h_0(t)$ is the channel response to the transmitted signal. At the correlator, the reference signal is used as the channel template and thus,

the decision statistic for the ith bit in the uth user can be expressed as [63]

$$D_i(u) = \sum_{j=0}^{N_f-1} D_s(j,u) \tag{2.21}$$

where

$$D_s(j,u) = \int_{jT_f+T_c\cdot c_j(u)+T_d(u)}^{jT_f+T_c\cdot c_j(u)+T_d(u)+T_{corr}} r(u,t)r(u,t-T_d(u))dt \tag{2.22}$$

with T_{corr} being the length of integration interval and $r(u,t-T_d)$ being the channel template. Finally, the data decision is made according to

$$\hat{d}_i = \begin{cases} 0, & \text{if} \quad D_i < 0 \\ 1, & \text{if} \quad D_i \geq 0 \end{cases} \tag{2.23}$$

where $\hat{(\cdot)}$ denotes the data decision.

Unlike coherent receivers, TR receivers do not require excellent time synchronization. However, the TR receiver is very sensitive to the integration position and duration, as all the multipath components are gathered at the reception stage [64].

2.6 Conclusions

In this chapter, an overview of the basic UWB communication system was presented, starting with the multipath channel models for UWB. Nowadays, the most accurate UWB channel model, proposed by the subcommittee of the IEEE 802.15.3a group for WPANs in 2003, is a slightly different version of the S-V model. This IEEE 802.15.3a channel model was further divided into

four categories as CM1 - CM4, according to the transmission type and the communication distance. The primary parameters that significantly impact the characteristics of channels were briefly described, including the multipath fading gain and the multipath arrival times.

A commonly used second-order derivative Gaussian pulse, namely the Gaussian doublet, was discussed in both the time domain and the frequency domain. The ultra-short pulse duration in the time domain enables it to be distinguished from other unwanted multipath components due to its fine time resolution. On the other hand, this pulse in the frequency domain is spreaded over an extremely wide bandwidth so that its frequency components are low enough for the FCC regulations. Therefore, this signal can propagate very well in the UWB IEEE channels to avoid interference with other existing communication systems.

Then, two appropriate modulation schemes for the UWB systems, known as PPM and BPAM, were discussed. Multiple-access techniques for UWB were also presented. In particular, typical expressions of TH-BPPM, TH-BPAM and DS-BPAM schemes were provided. The DS-BPAM scheme benefits the TH-BPAM scheme in a multi-user environment because more collisions occurred in the TH-SS system than in the DS-SS system. Also, the TH-BPAM scheme always outperforms the TH-BPPM scheme due to the 3 dB gain in power efficiency. Moreover, a M-ary PPM technology can significantly improve the capacity with a certain number of users.

Finally, a brief description of the UWB receivers was presented. Normally, the UWB receivers in the literature can be classified as coherent and non-coherent receivers. Meanwhile, the non-coherent receivers can be further divided into several types, including the transmitted-reference receiver and the

energy detector. In a traditional TR system, the received data signal is correlated with the received reference signal for reliable data decision. A complex channel estimation process is not required for UWB TR systems. Owing to its structural simplicity and tolerable performance degradation, the TR receiver has become very attractive recently. In the next chapter onwards, the optimization for the TR receiver to improve its performance in various scenarios will be discussed.

Chapter 3

Optimization of the Traditional UWB TR Receiver

3.1 Introduction

As has been discussed previously, the UWB TR receiver was proposed to relax the requirements on synchronization and channel estimation. These properties enable the TR receiver to benefit from a simple structure and to be less computation-consuming. As a result, this also leads to simple implementations in the TR system. For the traditional TR receiver, the second pulse corresponding to the modulated signal is transmitted T_d seconds after the first pulse corresponding to the unmodulated signal [53], [62], [65]. The traditional TR receiver can be also described as an Autocorrelation Receiver (AcR) where a reference and data pair is sent per frame. The unmodulated signal containing the reference information is used as a channel template at the correlator, and the modulated signal contains the data information to detect. A significant amount of research on AcR has been conducted in UWB. In [51], Choi and

Stark presented a BER performance analysis of the AcR by using the Gaussian approximation (GA) in a single-user environment. In [53], Chao and Scholtz derived the bit error probability (BEP) of the AcR based on knowledge of the channel properties. In [66], Chao further derived the BEP of the AcR by using the orthogonal expansion concept instead of the central limit theorem in the GA for the more accurate theoretical results. In [67], Jia and Kim derived a closed-form expression for the channel-averaged signal-to-interference-plus-noise ratio (SINR) of the AcR, where multi-user interference (MAI) was considered. In [68] and [69], Witrisal and Pausini provided the statistical analysis of the correlation function considering the effect of inter-pulse interference (IPI), while [68] was based on the Volterra equivalent system model. However, none of these work has considered the best choice of T_d within the pulse pairs.

This chapter focuses on the optimization of T_d in the AcR. Since the AcR correlates the data signal with the reference signal to capture all the achievable energies from the multipath, the performance of the AcR suffers from power loss of the reference signal as well as noise in the template. Furthermore, the value of T_d determines the amount of IPI as well as the energy allocation between the reference signal and the data signal. If T_d is too large, IPI can be largely eliminated due to the sufficient interval between the reference and the data signals, but the energy allocated to the data signal could be too small, assuming fixed total signal energy, such that the useful data energy captured at the traditional TR receiver may be too small for reliable detection. This degrades the receiver performance. On the other hand, if T_d is too small, the inherent IPI could be very significant, although the energy allocated to the data signal is sufficient for reliable detection. This degrades the performance as well. Thus, there exists an optimal value of T_d that provides

the best tradeoff between interference and energy allocation. Herein, the AcR is optimized with respect to T_d for two criteria, maximization of the channel achievable capacity and minimization of the system BER. The channel capacity and BER are derived by using an accurate approximation to the SINR. Numerical results show that the optimized TR receiver can provide significant gains over the traditional TR receiver in terms of channel capacity and BER.

This chapter is organized as follows. *Section 3.2* illustrates the system model for the traditional TR receiver (AcR). The optimization with respect to T_d using the two criteria (channel capacity and BER) is addressed in *Section 3.3*. Conclusions are drawn in *Section 3.4*.

3.2 System Model for the Traditional UWB TR Receiver

A single-user UWB system is first considered. Therefore, time-hopping or direct-sequence for multiple access are not used. With BPAM applied, the ith transmitted bit can be expressed as

$$s_i(t) = \sum_{j=0}^{N_f-1} \sqrt{\varepsilon_i} \left[\sqrt{\alpha} g_{tr}(t - jT_f) + \vartheta_i \sqrt{(1-\alpha)} g_{tr}(t - jT_f - T_d) \right] \qquad (3.1)$$

where N_f is the number of frames, $j = 0, 1, \cdots, N_f - 1$ is the frame index, T_f is the frame interval, $g_{tr}(t)$ denotes the monocycle pulse with time duration T_p and energy $E_g = \int_{-\infty}^{\infty} g_{tr}^2(t)dt$, ε_i is the total energy for the ith bit, $\{\vartheta_i\} \in \{+1, -1\}$ with equal probabilities denotes the ith bit associated with the i data symbol, and T_d is the delay between the reference pulse and the data pulse, and α is the energy allocation factor. The normalized autocorrelation

function of $g_{tr}(t)$ is $R_g(\Delta) = \frac{1}{E_g}\int_{-\infty}^{\infty} g_{tr}(t)g_{tr}(t+\Delta)dt$. The energy allocation factor α is defined as

$$\alpha = \frac{\varepsilon_{ri}}{\varepsilon_i} \tag{3.2}$$

where ε_{ri} is the reference energy and T_b is the bit duration. Here, it is assumed that the energy is linearly proportional to the time interval. This assumption is based on the fact that in general energy equals the product of power and time and the observation that the average transmission power in wireless device is often fixed. Although the specific relationship between the energy and the time may be quadratic or even more complicated, the linear relationship is used as an example to give general guidance on how to choose the time delay. Using the same method presented here, one can easily replace this linear relationship with other specific relationships to find the best time delay for the specific applications. The investigations will be very similar, as the optimum time delay can be found from the optimum energy allocation factor by solving an equation using their relationships. For the reference, since the reference pulse in one frame continues until T_d seconds later when the data pulse starts, the total reference time interval can be described as $T_d \cdot N_f$ for one bit. Thus,

$$\alpha = \frac{\varepsilon_{ri}}{\varepsilon_i} = \frac{c \cdot T_d \cdot N_f}{c \cdot T_b} = \frac{T_d \cdot N_f}{T_b} \tag{3.3}$$

where the assumed linear relationship between energy ε and time interval T as $\varepsilon = c \cdot T$ is used, c is a constant. The bit energy is fixed at ε_i. Then, from eq.(3.3), the reference energy per bit is $\varepsilon_{ri} = \alpha\varepsilon_i = \frac{\varepsilon_i}{T_b} \cdot T_d \cdot N_f$. Also, from eq.(3.1), the data energy per bit is $\varepsilon_{di} = (1-\alpha)\varepsilon_i = \frac{\varepsilon_i}{T_b} \cdot (T_b - T_d \cdot N_f)$. Therefore, the reference energy ε_{ri} is different from the data energy ε_{di}. The

optimization problem can be described by using Figure 3.1. When T_d increases, from eq.(3.3), α increases. Since the reference pulse has an amplitude of $\sqrt{\alpha\varepsilon_i}$, the reference pulse amplitude increases and therefore, the reference energy increases. Also, since the data pulse has an amplitude of $\sqrt{(1-\alpha)\varepsilon_i}$, the data pulse amplitude decreases and therefore, the data energy decreases. On the other hand, when T_d increases, the time space between the reference pulse and the data pulse increases so that the inter-pulse interference is reduced. Thus, an optimal T_d exists. One notes that the choice of the time delay T_d is equivalent to the choice of α, when T_b is fixed. This selection approach can be seen as a joint study of reducing the inherent IPI and increasing the energy allocated to the data signal. In the following, the optimal α will be determined.

In order to restrict the noise, an ideal bandpass filter with one-sided bandwidth of $Bp = \frac{1}{T_p}$ (Hz) is applied at the front end of the receiver to remove excessive noise. Thus, the filtered received signal for the ith transmitted bit can be expressed as

$$r_i(t) = \sum_{j=0}^{N_s-1} \sqrt{\varepsilon_i} \left[\sqrt{\alpha} h(t - jT_f) + \vartheta_i \sqrt{(1-\alpha)} h(t - jT_f - T_d) \right] + n_i(t) \quad (3.4)$$

where $h(t) = g_{tr}(t) * h_0(t) * g_{re}(t)$ is the equivalent channel response (CR) to the transmitted waveform, $h_0(t)$ is the channel response presented in [26], $g_{re}(t)$ is the pulse shape of the bandpass filter, and $n_i(t)$ is additive white Gaussian noise (AWGN) with mean zero and variance $\delta^2 = B_p N_o$ with N_o being the one-sided noise power density. The multipath channel model used here is based on [26] and is assumed to be time-invariant over one observation interval (i.e., one data packet). Perfect synchronization is assumed. The frame

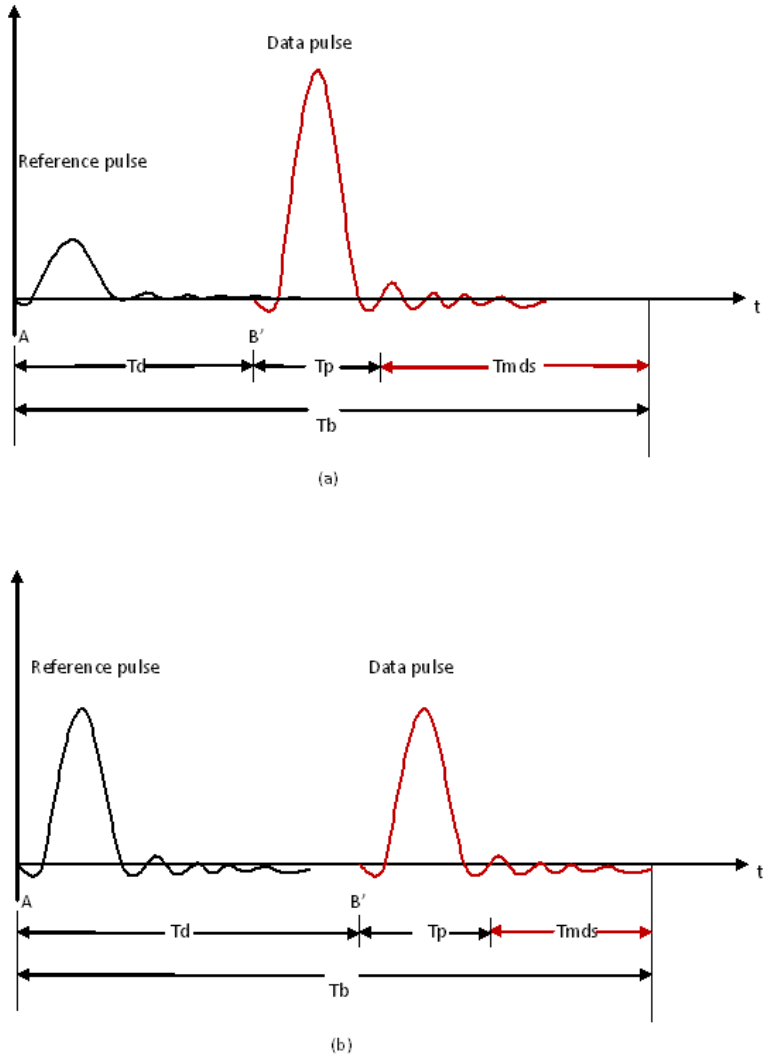

Figure 3.1: The system model of the conventional TR receiver with different values of T_d.

interval T_f is set to be $T_p + T_{dm} + T_{mds}$, where T_{mds} is the maximum channel excess delay and T_{dm} is the maximum inter-pulse delay between the reference and data pulses. Then, the bit interval T_b is $(T_p + T_{dm} + T_{mds}) \times N_f$. The optimal T_d will be chosen between T_p and T_{dm}.

By sampling the received signal in eq.(3.4) with a sample interval of T_s, one has $S = \lfloor \frac{T_f}{T_s} \rfloor$ samples in one frame duration, where $\lfloor \cdot \rfloor$ returns to the integer of $(\cdot)$. Denote $L = \lfloor \frac{T_{mds}}{T_s} \rfloor$. Then, the sampled received signal can be written as

$$\mathbf{r}_i(\alpha) = \sqrt{\varepsilon_i}(\sqrt{\alpha}\mathbf{h} + \vartheta_i\sqrt{(1-\alpha)}\mathbf{h}_d) + \mathbf{n}_i \tag{3.5}$$

where $\mathbf{h} = [h(T_1), h(T_2), \cdots, h(T_{mds}), \underbrace{0, 0, \cdots, 0}_{\lfloor \frac{T_b}{T_s} \rfloor - L}]^T$ represents the channel response to the reference signal at the sampling instants in one bit duration, $\mathbf{h}_d = [\underbrace{0, 0, \cdots, 0}_{\lfloor \frac{T_d}{T_s} \rfloor}, h(T_1 + T_d), h(T_2 + T_d), \cdots, h(T_{mds} + T_d), \underbrace{0, 0, \cdots, 0}_{\lfloor \frac{T_b - T_d}{T_s} \rfloor - L}]^T$ represents the channel response to the T_d-second-delayed data signal at the sampling instants, and $\mathbf{n}_i$ is a column vector that represents the noise corrupting the ith bit at the sampling instants. Assuming that the sampling interval T_s is small enough, the discrete sampled signal can be used to recover the continuous signal with negligible loss. For convenience, the matrix

$$\mathbf{P}_1 = \begin{bmatrix} \mathbf{0_d} & \mathbf{0_{dr}} & \mathbf{0_{r1}} \\ \mathbf{0_{dr}}^T & \mathbf{I}_{int} & \mathbf{0_{r2}} \\ \mathbf{0_{r1}}^T & \mathbf{0_{r2}}^T & \mathbf{0_{r3}} \end{bmatrix} \tag{3.6}$$

is defined, where $\mathbf{P}_1$ is a $\lfloor \frac{T_b}{T_s} \rfloor \times \lfloor \frac{T_b}{T_s} \rfloor$ matrix, $\mathbf{I}_{int}$ is a $\lfloor \frac{T_{corr}}{T_s} \rfloor \times \lfloor \frac{T_{corr}}{T_s} \rfloor$ identity matrix, T_{corr} denotes the integration interval length, $\mathbf{0_d}$ is a $\lfloor \frac{T_d}{T_s} \rfloor \times \lfloor \frac{T_d}{T_s} \rfloor$ all-zero matrix, $\mathbf{0_{dr}}$ is a $\lfloor \frac{T_d}{T_s} \rfloor \times \lfloor \frac{T_{corr}}{T_s} \rfloor$ all-zero matrix, $\mathbf{0_{r1}}$ is a $\lfloor \frac{T_d}{T_s} \rfloor \times \lfloor \frac{T_b - T_d - T_{corr}}{T_s} \rfloor$

all-zero matrix, $\mathbf{0_{r2}}$ is a $\lfloor \frac{T_{corr}}{T_s} \rfloor \times \lfloor \frac{T_b - T_d - T_{corr}}{T_s} \rfloor$ all-zero matrix, and $\mathbf{0_{r3}}$ is a $\lfloor \frac{T_b - T_d - T_{corr}}{T_s} \rfloor \times \lfloor \frac{T_b - T_d - T_{corr}}{T_s} \rfloor$ all-zero matrix. Using eq.(3.6), the received T_d-second-delayed data signal for the ith bit can be rewritten as

$$\begin{bmatrix} \mathbf{0_v} \\ \mathbf{r_{d}}_i(\alpha) \end{bmatrix} = \sqrt{\varepsilon_i}(\sqrt{\alpha}\mathbf{P}_1 \cdot \mathbf{h} + \vartheta_i \sqrt{(1-\alpha)}\mathbf{P}_1 \cdot \mathbf{h}_d) + \mathbf{P}_1 \cdot \mathbf{n}_i \tag{3.7}$$

where $\mathbf{0_v}$ denotes a $\lfloor \frac{T_d}{T_s} \rfloor \times 1$ all-zero column vector, and the received signal for the reference has been removed by $\mathbf{P}_1$. A traditional TR receiver correlates the received data signal with the received reference signal over an integration interval T_{corr}, and sums N_f correlator outputs to generate its decision statistic D as

$$D_i = \begin{bmatrix} \mathbf{r_{d}}_i(\alpha) \\ \mathbf{0_v} \end{bmatrix}^T \cdot \mathbf{P}_{int} \cdot \mathbf{r}_i(\alpha) \tag{3.8}$$

where $\begin{bmatrix} \mathbf{r_{d}}_i(\alpha) \\ \mathbf{0_v} \end{bmatrix}^T$ is the received data signal, $\mathbf{P}_{int} \cdot \mathbf{r}_i(\alpha)$ is the received reference signal, and $\mathbf{P}_{int}$ represents the correlation with $\mathbf{P}_{int} = \begin{bmatrix} \mathbf{I}_{int} & \mathbf{0_c} \\ \mathbf{0_c} & \mathbf{0_c} \end{bmatrix}$ being a $\lfloor \frac{T_b}{T_s} \rfloor \times \lfloor \frac{T_b}{T_s} \rfloor$ matrix and $\mathbf{0_c}$ is a $\lfloor \frac{T_b - T_{corr}}{T_s} \rfloor \times \left[\frac{T_b - T_{corr}}{T_s} \right]$ all-zero matrix. Finally, the data decision is made according to

$$\hat{d}_i = \begin{cases} 0, & \text{if } D_i < 0 \\ +1, & \text{if } D_i \geq 0 \end{cases} \tag{3.9}$$

where $\hat{(\cdot)}$ denotes the data decision.

3.3 The Channel Capacity Optimization

In this section, the channel achievable capacity of the traditional TR receiver is optimized with respect to α and therefore, T_d. The calculation of the signal-to-interference-pluse-noise ratio (SINR) at the correlator will be determined first. Then, by using the Shannon equation and some approximations, the capacity of the TR system with AcR signaling can be obtained accordingly. Therefore, optimizing the channel capacity is equivalent to optimizing the output SINR value. An analytical expression of SINR for the AcR has been derived in [70], however, these results were obtained in the present of multi-access interference (MAI) and did not take the optimization scheme into account.

For simplicity, it is assumed that $N_f = 1$, as the number of frames per symbol does not impact the system performance in a single-user environment. By substituting eq.(3.5) and eq.(3.7) into eq.(3.8), the decision statistic D for the ith bit can be further derived as

$$\begin{aligned} D_i &= S(\alpha) + I_1(\alpha) + I_2(\alpha) + I_3(\alpha) \\ &+ N_1(\alpha) + N_2(\alpha) + N_3(\alpha) + N_4(\alpha) + N_5 \end{aligned} \tag{3.10a}$$

where

$$
\begin{aligned}
S(\alpha) &= \vartheta_i\sqrt{\alpha(1-\alpha)}\varepsilon_i(\mathbf{h}^T\mathbf{P}_{int}\mathbf{h}) && \text{(3.10b)}\\
I_1(\alpha) &= \alpha\varepsilon_i(\mathbf{h}^T\mathbf{P}_1\mathbf{P}_{int}\mathbf{h}) && \text{(3.10c)}\\
I_2(\alpha) &= \vartheta_i\sqrt{\alpha(1-\alpha)}\varepsilon_i(\mathbf{h}^T\mathbf{P}_1\mathbf{P}_{int}\mathbf{h}_d) && \text{(3.10d)}\\
I_3(\alpha) &= (1-\alpha)\varepsilon_i(\mathbf{h}^T\mathbf{P}_{int}\mathbf{h}_d) && \text{(3.10e)}\\
N_1(\alpha) &= \sqrt{\alpha\varepsilon_i}(\mathbf{h}^T\mathbf{P}_1\mathbf{n}_i) && \text{(3.10f)}\\
N_2(\alpha) &= \vartheta_i\sqrt{(1-\alpha)\varepsilon_i}(\mathbf{h}^T\mathbf{P}_{int}\mathbf{n}_i) && \text{(3.10g)}\\
N_3(\alpha) &= \sqrt{\alpha\varepsilon_i}(\mathbf{n}_i^T\mathbf{P}_{int}\mathbf{h}) && \text{(3.10h)}\\
N_4(\alpha) &= \vartheta_i\sqrt{(1-\alpha)\varepsilon_i}(\mathbf{n}_i^T\mathbf{P}_{int}\mathbf{h}_d) && \text{(3.10i)}\\
N_5 &= (\mathbf{n}_i^T\mathbf{P}_{int}\mathbf{n}_i). && \text{(3.10j)}
\end{aligned}
$$

In (9), $S(\alpha)$ is the 'clean' signal component, $I_1(\alpha)$ is the interference caused by correlating the tail of $\mathbf{h}$ with itself, $I_2(\alpha)$ is the interference caused by correlating the tail of $\mathbf{h}$ with the T_d-second-delayed $\mathbf{h}_d$, and $I_3(\alpha)$ is the interference caused by correlating $\mathbf{h}$ with the delayed $\mathbf{h}_d$ over T_{corr}. Furthermore, the components $N_1(\alpha)$, $N_2(\alpha)$, $N_3(\alpha)$, $N_4(\alpha)$ and N_5 represent the tail of reference-times-noise part, the reference-times-noise over T_{corr} part, the noise-times-reference over T_{corr} part, the noise-times-data part, and the noise-times-noise part, respectively. Denoting $\bar{C}$ as the channel capacity, one has

$$
\bar{C}(\alpha) \approx E\{log_2(1+\rho_i)\} \approx E\left\{log_2 \left[1+\left(\frac{S(\alpha)}{I_1(\alpha)+I_2(\alpha)+I_3(\alpha)+N_1(\alpha)+N_2(\alpha)+N_3(\alpha)+N_4(\alpha)+N_5}\right)^2\right]\right\} \tag{3.11}
$$

where ρ_i is the instantaneous SINR for the ith bit and $E\{\cdot\}$ is the expectation with respect to the channel response. The approximation is due to the fact that the interference-plus-noise terms are actually not Gaussian but are assumed Gaussian to use eq.(3.11).

The optimal α that maximizes the channel achievable capacity will be found by using three different methods, including simulation, semi-analytical and analytical methods. In the examples, if not stated otherwise, the IEEE CM1 model [26] is used, and the second order derivative of a Gaussian pulse is employed with $E_g = 0.1875$ and $T_p = 1\ ns$. The maximum channel excess delay T_{mds} is restricted to 40 ns, and the frame interval T_f is set to 120 ns. The sampling interval T_s is set to $1/8\ ns$. The receiver filter is assumed to be an ideal bandpass filter with single sided bandwidth of 1 GHz.

3.3.1 Simulation Approach

In the simulation, the best value of α optimizing $\bar{C}$ can be achieved by resorting to the "brute-force" search method as

$$\alpha_{opt1} = \arg \max_{\alpha \in (0,0.5]} \left\{ \bar{C}(\alpha) \right\} \tag{3.12}$$

and, therefore, the best value of the time delay between reference and data pulses is $T_{d_{opt1}} = \alpha_{opt1} \cdot T_b$.

Figure 3.2 shows the channel achievable capacity versus T_d (i.e., α) for the improved TR receiver by using the simulation method at SNR = 0, 6, 12 and 18 dB, respectively. One sees that there indeed exists an optimal time delay between data and reference pulses. For the simulated improved TR receiver, the maximum channel achievable capacity is about 0.14

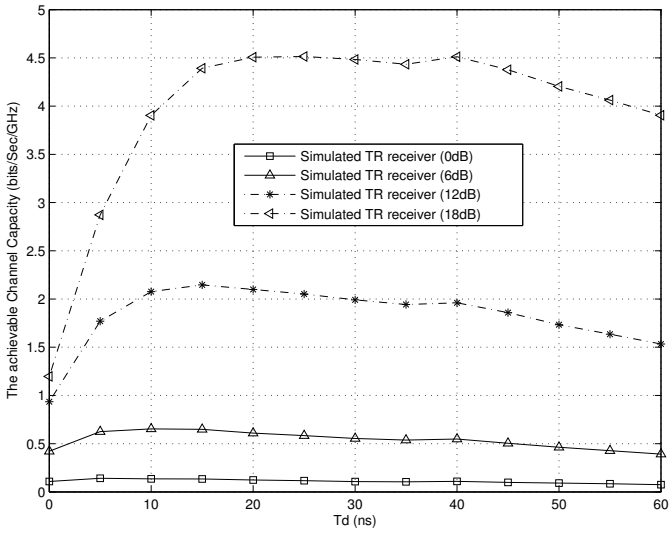

Figure 3.2: The channel achievable capacity versus T_d for the traditional TR receiver by using the simulation method.

bits/Sec/GHz at the optimum value of $T_{d_{opt1}} = 5\ ns$ at SNR = 0 dB, about 0.63 bits/Sec/GHz at the optimum value of $T_{d_{opt1}} = 10\ ns$ at SNR = 6 dB, about 2.15 bits/Sec/GHz at the optimum value of $T_{d_{opt1}} = 15\ ns$ at SNR = 12 dB, and about 4.53 bits/Sec/GHz at the optimum value of $T_{d_{opt1}} = 40\ ns$ at SNR = 18 dB. As can be seen from Figure 3.2, the optimum value of T_d approaches its maximum value of T_{mds} when SNR is increasing. This is due to the fact that, when SNR increases, the useful signal energy can be gathered in the correlator increases, and hence the optimum value of T_d has to be greater for a better data decision. In addition, the channel capacity investigated in this thesis is actually the normalized channel capacity without the consideration of channel bandwidth for convenience.

This optimum simulation method gives a highly precise result but also takes a long simulation time. In order to simplify the search for the optimal T_d, one can alternatively use the average output SINR as the performance measure.

3.3.2 Semi-analytical Approach

A semi-analytical method to maximize the averaged output SINR is developed. Similar problem has been addressed in [66], [67] and [71]. However, these works maximized the averaged SINR with respect to the integration interval length, but not the time delay T_d between the two successive pulses in a TR system. The average output SINR is defined by ξ. Since the exact value of ξ is very difficult to obtain, one can approximate it as

$$\begin{aligned}\xi(\alpha) \approx\ & E\{S^2(\alpha)\}/\left(E\{I_1^2(\alpha)\}+E\{I_2^2(\alpha)\}+E\{I_3^2(\alpha)\}+E\{N_1^2(\alpha)\}\right.\\ & \left.+E\{N_2^2(\alpha)\}+E\{N_3^2(\alpha)\}+E\{N_4^2(\alpha)\}+E\{N_5^2\}\right). \qquad (3.13a)\end{aligned}$$

From eq.(3.10b)-eq.(3.10j), the second-order moment of each component in eq.(3.13a) can be derived as

$$E\{S^2(\alpha)\} = \alpha(1-\alpha)\varepsilon_i^2 \cdot E\{||\mathbf{h}^T\mathbf{P}_{int}||^4\} \qquad (3.13b)$$

$$E\{I_1^2(\alpha)\} = \alpha^2\varepsilon_i^2 \cdot E\{||\mathbf{h}^T\mathbf{P}_{int}\mathbf{P}_1\mathbf{h}||^2\} \qquad (3.13c)$$

$$E\{I_2^2(\alpha)\} = \alpha(1-\alpha)\varepsilon_i^2 \cdot E\{||\mathbf{h}_d^T\mathbf{P}_{int}\mathbf{P}_1\mathbf{h}||^2\} \qquad (3.13d)$$

$$E\{I_3^2(\alpha)\} = (1-\alpha)^2\varepsilon_i^2 \cdot E\{||\mathbf{h}_d^T\mathbf{P}_{int}\mathbf{h}||^2\} \qquad (3.13e)$$

$$E\{N_1^2(\alpha)\} = \alpha\varepsilon_i\delta^2 \cdot E\{||\mathbf{h}^T\mathbf{P}_1\mathbf{h}||\} \qquad (3.13f)$$

$$E\{N_2^2(\alpha)\} = (1-\alpha)\varepsilon_i\delta^2 \cdot E\{||\mathbf{h}^T\mathbf{P}_{int}\mathbf{h}||\} \qquad (3.13g)$$

$$E\{N_3^2(\alpha)\} = \alpha\varepsilon_i\delta^2 \cdot E\{||\mathbf{h}_d^T\mathbf{P}_{int}\mathbf{h}_d||\} \qquad (3.13h)$$

$$E\{N_4^2(\alpha)\} = (1-\alpha)\varepsilon_i\delta^2 \cdot E\{||\mathbf{h}_d^T\mathbf{P}_{int}\mathbf{h}||\} \qquad (3.13i)$$

$$E\{N_5^2\} = E\{||\mathbf{n}_i^T\mathbf{P}_{int}\mathbf{n}_i||^2\} \qquad (3.13j)$$

where $||\mathbf{h}^T\mathbf{P}_{int}||^4 = ||\mathbf{h}^T\mathbf{P}_{int}\mathbf{h}||^2$. Note that $E\{N_5^2\}$ in eq.(3.13j) accounts for the variance of the noise-times-noise part. Using the same method as in [72], it can be calculated as

$$E\{N_5^2\} = (1-\alpha)^2\varepsilon_i^2\frac{T_{mds}}{2T_p[10^{(g/5)}]} \tag{3.13k}$$

where g is the input SNR. By substituting eq.(3.13b)-eq.(3.13i) and eq.(3.13k) into eq.(3.13a), one can obtain the average output SINR. Using $\xi(\alpha)$ in eq.(3.13a), the best value of α optimizing the channel capacity can be found as

$$\alpha_{opt2} = \arg\max_{\alpha\in(0,0.5]}\{log_2[1+\xi(\alpha)]\}\,. \tag{3.14}$$

This semi-analytical method is simpler than the simulation due to the reduced number of integrations. However, it is also less accurate than the simulation method due to the approximations used in eq.(3.13a) to achieve simplicity.

Figure 3.3 shows the channel achievable capacity versus T_d for traditional TR receivers improved by using simulation and semi-analytical methods, respectively, for different SNR scenarios. For the improved TR receiver from the semi-analytical method, it has a similar result to the improved TR receiver from the simulation method. That is, the optimum value of T_d grows with the increase of SNR. Specifically, the maximum channel achievable capacity is about 0.25 bits/Sec/GHz at the optimum value of $T_{d_{opt2}} = 10\ ns$ for the value of SNR at 6 dB, about 1.75 bits/Sec/GHz at the optimum value of $T_{d_{opt2}} = 15\ ns$ for the value of SNR at 12 dB, and about 4.4 bits/Sec/GHz at the optimum value of $T_{d_{opt2}} = 40\ ns$ for the value of SNR at 18 dB. One can see that the optimized channel achievable capacity from the semi-analytical

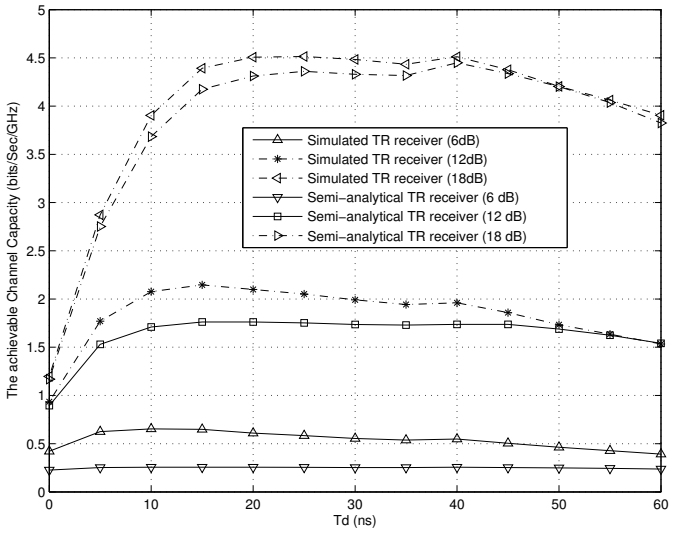

Figure 3.3: The channel achievable capacity versus T_d for the traditional TR receiver by using the simulation and semi-analytical methods.

method is smaller than that from simulation due to the applied Gaussian approximation, as expected.

The optimization results in eq.(3.12) and eq.(3.14) can be applied to any channel model. However, the semi-analytical method can be further simplified for a specific channel model and thus, the more theoretical results can be obtained relying on further calculations.

3.3.3 Analytical Approach

The UWB IEEE channel model [26] is employed such that the impulse response of the UWB fading channel is given by

$$h_0(t) = \sum_{l=0}^{L} \sum_{k=0}^{k} \alpha_{k,l} \delta(t - T_l - \tau_{k,l}) \tag{3.15}$$

where T_l is the time delay of the lth cluster, $\tau_{k,l}$ is the time delay of the kth multipath relative to the lth cluster, $\alpha_{k,l}$ is the channel gain of the kth

multipath within the lth cluster, L and K account for the total number of clusters and the total number of multipaths in each cluster, respectively. As we assume previously, the sampling rate $\frac{1}{T_s}$ is large enough such that the continuous signal can be completely replaced by its discrete form and vice versa.

By substituting eq.(3.15) into eq.(3.13b) and using a similar method to that in [28], one has

$$\begin{aligned}
& E\{S^2(\alpha)\} = \alpha(1-\alpha)\varepsilon^2 E\left\{\left|\left|\mathbf{h}^T\mathbf{P}_{int}\mathbf{h}\right|\right|^2\right\} \\
= \;& \alpha(1-\alpha)\varepsilon^2 E\left\{\left[\sum_{n_1=1}^{\bar{T}_b}\sum_{l_1=0}^{L}\sum_{k_1=0}^{K}\alpha_{k_1,l_1}\mathbf{g_{tr}}(n_1-\bar{T}_{l_1}-\bar{\tau}_{k_1,l_1})\right.\right. \\
& \left.\left.\mathbf{P}_{int}(n_1,n_1)\sum_{l_2=0}^{L}\sum_{k_2=0}^{K}\alpha_{k_2,l_2}\mathbf{g_{tr}}(n_1-\bar{T}_{l_2}-\bar{\tau}_{k_2,l_2})\right]^2\right\} \\
= \;& \alpha(1-\alpha)\varepsilon^2 E\left\{\left[\sum_{l_1=0}^{L}\sum_{k_1=0}^{K}\sum_{l_2=0}^{L}\sum_{k_2=0}^{K}\alpha_{k_1,l_1}\alpha_{k_2,l_2}\right.\right. \\
& \left.\left.\sum_{n_1=1}^{\bar{T}_b}\mathbf{g_{tr}}(n_1-\bar{T}_{l_1}-\bar{\tau}_{k_1,l_1})\mathbf{P}_{int}(n_1,n_1)\mathbf{g_{tr}}(n_1-\bar{T}_{l_2}-\bar{\tau}_{k_2,l_2})\right]^2\right\} \qquad (3.16)
\end{aligned}$$

where $\mathbf{g_{tr}}(n)$ is a $[\frac{T_b}{T_s}]\times 1$ matrix representing the discrete monocycle pulse at the sampling instants per bit with n being the column index. The notation $\bar{(\cdot)}$ indicates the discrete component after sampling. Since it is assumed that no ISI exists herein, almost the entire pulse energy is allocated within the

integration duration T_{corr}. Therefore, eq.(3.16) can be rewritten as

$$\begin{aligned} E\{S^2(\alpha)\} &\approx \alpha(1-\alpha)\varepsilon^2 E_g^2 E\left\{\left[\sum_{l_1=0}^{L}\sum_{k_1=0}^{K}\sum_{l_2=0}^{L}\sum_{k_2=0}^{K}\alpha_{k_1,l_1}\alpha_{k_2,l_2}\right]^2\right\} \\ &= \alpha(1-\alpha)\varepsilon^2 E_g^2 \sum_{l_1=0}^{L}\sum_{k_1=0}^{K}\sum_{l_2=0}^{L}\sum_{k_2=0}^{K} E\left\{\alpha_{k_1,l_1}^2\alpha_{k_2,l_2}^2\right\} \end{aligned} \tag{3.17}$$

where

$$E\{\alpha_{k_1,l_1}^2\alpha_{k_2,l_2}^2\} = \Omega_0^2 e^{\frac{(ln10)^2\sigma_1^2\sigma_2^2}{100}} E(l_1,l_2,k_1,k_2) \tag{3.18}$$

with $E(a,b,c,d) = (\frac{\Lambda\Gamma}{1+\Lambda\Gamma})^a \cdot (\frac{1+\Lambda\Gamma}{2+\Lambda\Gamma})^b \cdot (\frac{\lambda\gamma}{1+\lambda\gamma})^c \cdot (\frac{1+\lambda\gamma}{2+\lambda\gamma})^d$ are discussed in [73] corresponding to different cases.

Substituting eq.(3.15) into eq.(3.13c), one has

$$\begin{aligned} & E\{{I_1}^2(\alpha)\} = \alpha^2\varepsilon^2 E\left\{\mathbf{h}^T\mathbf{P}_{int}\mathbf{P}_1\mathbf{h}\mathbf{h}^T\mathbf{P}_1\mathbf{P}_{int}\mathbf{h}\right\} \\ = \; & \alpha^2\varepsilon^2 E\left\{\sum_{n_1=1}^{\bar{T}_b}\sum_{l_1=0}^{L}\sum_{k_1=0}^{K}\alpha_{k_1,l_1}\mathbf{g_{tr}}(n_1-\bar{T}_{l_1}-\bar{\tau}_{k_1,l_1})\mathbf{P}_{int}(n_1,n_1)\mathbf{P}_1(n_1,n_1)\right. \\ & \sum_{l_2=0}^{L}\sum_{k_2=0}^{K}\alpha_{k_2,l_2}\mathbf{g_{tr}}(n_1-\bar{T}_{l_2}-\bar{\tau}_{k_2,l_2})\sum_{n_2=1}^{\bar{T}_b}\sum_{l_3=0}^{L}\sum_{k_3=0}^{K}\alpha_{k_3,l_3}\mathbf{g_{tr}}(n_2-\bar{T}_{l_3}-\bar{\tau}_{k_3,l_3}) \\ & \left.\mathbf{P}_{int}(n_2,n_2)\mathbf{P}_1(n_2,n_2)\sum_{l_4=0}^{L}\sum_{k_4=0}^{K}\alpha_{k_4,l_4}\mathbf{g_{tr}}(n_2-\bar{T}_{l_4}-\bar{\tau}_{k_4,l_4})\mathbf{g_{tr}}(n_2-\bar{T}_{l_4}-\bar{\tau}_{k_4,l_4})\right\} \\ = \; & \alpha^2\varepsilon^2 E\left\{\left[\sum_{l_1=0}^{L}\sum_{l_2=0}^{L}\sum_{k_1=0}^{K}\sum_{k_2=0}^{K}\alpha_{k_1,l_1}\alpha_{k_2,l_2}\sum_{n_1=1}^{\bar{T}_b}\mathbf{P}_{int}(n_1,n_1)\mathbf{P}_1(n_1,n_1)\right.\right. \\ & \left.\mathbf{g_{tr}}(n_1-\bar{T}_{l_1}-\bar{\tau}_{k_1,l_1})\mathbf{g_{tr}}(n_1-\bar{T}_{l_2}-\bar{\tau}_{k_2,l_2})\right]\left[\sum_{l_3=0}^{L}\sum_{l_4=0}^{L}\sum_{k_3=0}^{K}\sum_{k_4=0}^{K}\alpha_{k_3,l_3}\alpha_{k_4,l_4}\right. \end{aligned}$$

$$\left.\left.\sum_{n_2=1}^{\bar{T}_b} \mathbf{P}_{int}(n_2,n_2)\mathbf{P}_1(n_2,n_2)\mathbf{g_{tr}}(n_2-\bar{T}_{l_3}-\bar{\tau}_{k_3,l_3})\mathbf{g_{tr}}(n_2-\bar{T}_{l_4}-\bar{\tau}_{k_4,l_4})\right]\right\} \tag{3.19}$$

where $l_1 \neq l_2$ or $k_1 \neq k_2$ and $l_3 \neq l_4$ or $k_3 \neq k_4$. Define a normalized autocorrelation function as

$$\overline{R_{g2}}(\bar{\Delta}) = \frac{1}{E_g}\sum_{n=1}^{\bar{T}_b} \mathbf{g_{tr}}(n)\mathbf{P}_{int}(n,n)\mathbf{P}_1(n,n)\mathbf{g_{tr}}(n+\bar{\Delta}). \tag{3.20}$$

Eq.(3.20) can be transformed into a continuous time form as

$$R_{g2}(\Delta) = \frac{1}{E_g}\int_{x_2}^{y_2} g_{tr}(t)g_{tr}(t+\Delta)dt \tag{3.21}$$

where x_2 and y_2 represent the lower and upper limits of integration, which can be determined by

$$\begin{cases} x_2 &= (Z_{min}-1)\times T_s \\ y_2 &= (Z_{max}-1)\times T_s \end{cases} \tag{3.22}$$

with Z_{min} and Z_{max} being the minimum and maximum row indexes of non-zero elements in $\mathbf{P}_{com}(=\mathbf{P}_{int}\mathbf{P_1})$, respectively. By using eq.(3.21) and eq.(3.22), eq.(3.19) can be rewritten as

$$\begin{aligned} & E\{{I_1}^2(\alpha)\} \\ = \;& \alpha^2\varepsilon^2{E_g}^2E\left\{\sum_{l_1=0}^{L}\sum_{l_2=0}^{L}\sum_{k_1=0}^{K}\sum_{k_2=0}^{K}\alpha_{k_1,l_1}\alpha_{k_2,l_2}R_{g2}(T_{l2}-T_{l1}+\tau_{k_2,l_2}-\tau_{k_1,l_1})\right. \\ & \left.\sum_{l_3=0}^{L}\sum_{l_4=0}^{L}\sum_{k_3=0}^{K}\sum_{k_4=0}^{K}\alpha_{k_3,l_3}\alpha_{k_4,l_4}R_{g2}(T_{l4}-T_{l3}+\tau_{k_4,l_4}-\tau_{k_3,l_3})\right\}. \end{aligned} \tag{3.23}$$

Since $E\{\alpha_{k_1,l_1}\alpha_{k_2,l_2}\} = 0$ when $l_1 \neq l_2$ or $k_1 \neq k_2$, one can further simplify eq.(3.23) under the consideration of three cases. In the first case, $l_1 = l_3$, $k_1 = k_3$ and $l_2 = l_4$, $k_2 = k_4$; in the second case, $l_1 = l_4$, $k_1 = k_4$ and $l_2 = l_3$, $k_2 = k_3$; and in the third case, $l_1 = l_2 = l_3 = l_4$ and $k_1 = k_2 = k_3 = k_4$. Then, the second-order moment of I_1 is shown as

$$\begin{aligned}
& E\left\{{I_1}^2(\alpha)\right\} \\
= \;& \alpha^2\varepsilon^2{E_g}^2E\left\{\sum_{l_1=0}^{L}\sum_{l_2=0}^{L}\sum_{k_1=0}^{K}\sum_{k_2=0}^{K}\alpha_{k_1,l_1}^2\alpha_{k_2,l_2}^2\left[R_{g2}^2(T_{l2}-T_{l1}+\tau_{k_2,l_2}-\tau_{k_1,l_1})\right.\right. \\
& \left.\left.+\; R_{g2}(T_{l2}-T_{l1}+\tau_{k_2,l_2}-\tau_{k_1,l_1})R_{g2}(T_{l1}-T_{l2}+\tau_{k_1,l_1}-\tau_{k_2,l_2})\right]\right\} \\
+ \;& \alpha^2\varepsilon^2{E_g}^2E\left\{\sum_{l_1=0}^{L}\sum_{l_2=0}^{L}\sum_{k_1=0}^{K}\sum_{k_2=0}^{K}\alpha_{k_1,l_1}^2\alpha_{k_2,l_2}^2\right\}R_{g2}^2(0) \\
+ \;& \alpha^2\varepsilon^2{E_g}^2E\left\{\sum_{l_1=0}^{L}\sum_{k_1=0}^{K}\alpha_{k_1,l_1}^4\right\}R_{g2}^2(0). \qquad (3.24)
\end{aligned}$$

Combining the last two terms on the right side of eq.(3.24) and using eq.(3.17), one has

$$E\left\{{I_1}^2(\alpha)\right\} = \alpha^2\varepsilon^2{E_g}^2\sum_{l_1=0}^{L}\sum_{l_2=0}^{L}\sum_{k_1=0}^{K}\sum_{k_2=0}^{K}(J_{11}+J_{12}) + \frac{\alpha}{1-\alpha}E\left\{S^2\right\}R_{g2}^2(0) \qquad (3.25)$$

where

$$\begin{aligned}
J_{11} &= E\left\{\alpha_{k_1,l_1}^2\alpha_{k_2,l_2}^2R_{g2}^2(T_{l_2}-T_{l_1}+\tau_{k_2,l_2}-\tau_{k_1,l_1})\right\} \\
J_{12} &= E\left\{\alpha_{k_1,l_1}^2\alpha_{k_2,l_2}^2R_{g2}(T_{l_2}-T_{l_1}+\tau_{k_2,l_2}-\tau_{k_1,l_1})R_{g2}(T_{l_1}-T_{l_2}+\tau_{k_1,l_1}-\tau_{k_2,l_2})\right\}.
\end{aligned}$$

Similarly, the second-order moments of I_2 and I_3 can be determined.

From eq.(3.13d), one has

$$
\begin{aligned}
& E\{{I_2}^2(\alpha)\} = \alpha(1-\alpha)\varepsilon^2 E\{\mathbf{h}^T\mathbf{P}_{int}\mathbf{P}_1\mathbf{h_d}\mathbf{h_d}^T\mathbf{P}_1\mathbf{P}_{int}\mathbf{h}\} \\
= \;& \alpha(1-\alpha)\varepsilon^2 E\left\{\sum_{l_1=0}^{L}\sum_{l_2=0}^{L}\sum_{k_1=0}^{K}\sum_{k_2=0}^{K}\alpha_{k_1,l_1}\alpha_{k_2,l_2}\left[\sum_{n_1=1}^{\bar{T}_b}\mathbf{P}_{int}(n_1,n_1)\mathbf{P}_1(n_1,n_1)\right.\right. \\
& \left.\mathbf{g_{tr}}(n_1-\bar{T}_{l_1}-\bar{\tau}_{k_1,l_1})\mathbf{g_{tr}}(n_1-\bar{T}_{l_2}-\bar{\tau}_{k_2,l_2}-\bar{T}_{dt})\right]\sum_{l_3=0}^{L}\sum_{l_4=0}^{L}\sum_{k_3=0}^{K}\sum_{k_4=0}^{K}\alpha_{k_3,l_3}\alpha_{k_4,l_4} \\
& \left.\left[\sum_{n_2=1}^{\bar{T}_b}\mathbf{P}_{int}(n_2,n_2)\mathbf{P}_1(n_2,n_2)\mathbf{g_{tr}}(n_2-\bar{T}_{l_3}-\bar{\tau}_{k_3,l_3})\mathbf{g_{tr}}(n_2-\bar{T}_{l_4}-\bar{\tau}_{k_4,l_4}-\bar{T}_{dt})\right]\right\}.
\end{aligned}
\tag{3.26}
$$

By employing eq.(3.21), eq.(3.26) can be rewritten as

$$
\begin{aligned}
& E\{{I_2}^2(\alpha)\} \\
= \;& \alpha(1-\alpha)\varepsilon^2 {E_g}^2 E\left\{\sum_{l_1=0}^{L}\sum_{l_2=0}^{L}\sum_{k_1=0}^{K}\sum_{k_2=0}^{K}\alpha_{k_1,l_1}^2\alpha_{k_2,l_2}^2\left[R_{g2}^2(T_{l2}-T_{l1}+\tau_{k_2,l_2}-\tau_{k_1,l_1}+T_{dt})\right.\right. \\
+ \;& \left.\left.R_{g2}(T_{l2}-T_{l1}+\tau_{k_2,l_2}-\tau_{k_1,l_1}+T_{dt})R_{g2}(T_{l1}-T_{l2}+\tau_{k_1,l_1}-\tau_{k_2,l_2}+T_{dt})\right]\right\} \\
+ \;& \alpha(1-\alpha)\varepsilon^2 {E_g}^2\cdot E\left\{\sum_{l_1=0}^{L}\sum_{l_2=0}^{L}\sum_{k_1=0}^{K}\sum_{k_2=0}^{K}\alpha_{k_1,l_1}^2\alpha_{k_2,l_2}^2\right\}R_{g2}^2(0) \\
+ \;& \alpha(1-\alpha)\varepsilon^2 {E_g}^2\cdot E\left\{\sum_{l_1=0}^{L}\sum_{k_1=0}^{K}\alpha_{k_1,l_1}^4\right\}R_{g2}^2(0).
\end{aligned}
\tag{3.27}
$$

Combining the last two terms on the right side of eq.(3.27) and using eq.(3.17), eq.(3.27) can be further simplified as

$$
E\left\{{I_2}^2(\alpha)\right\} = \alpha(1-\alpha)\varepsilon^2 {E_g}^2\sum_{l_1=0}^{L}\sum_{l_2=0}^{L}\sum_{k_1=0}^{K}\sum_{k_2=0}^{K}(J_{21}+J_{22}) + E\left\{S^2\right\}R_{g2}^2(0)
\tag{3.28}
$$

where

$$\begin{aligned} J_{21} &= E\left\{\alpha_{k_1,l_1}^2\alpha_{k_2,l_2}^2 R_{g2}^2(T_{l_2}-T_{l_1}+\tau_{k_2,l_2}-\tau_{k_1,l_1}+T_{dt})\right\} \\ J_{22} &= E\left\{\alpha_{k_1,l_1}^2\alpha_{k_2,l_2}^2 R_{g2}(T_{l_2}-T_{l_1}+\tau_{k_2,l_2}-\tau_{k_1,l_1}+T_{dt})\right. \\ &\quad \left. R_{g2}(T_{l_1}-T_{l_2}+\tau_{k_1,l_1}-\tau_{k_2,l_2}+T_{dt})\right\}. \end{aligned}$$

Meanwhile, eq.(3.13e) can be further expressed as

$$\begin{aligned} & E\{{I_3}^2(\alpha)\} = (1-\alpha)^2\varepsilon^2 E\{\mathbf{h}^T\mathbf{P}_{int}\mathbf{h_d}{\mathbf{h_d}}^T\mathbf{P}_{int}\mathbf{h}\} \\ = \; & (1-\alpha)^2\varepsilon^2 E\left\{\sum_{l_1=0}^{L}\sum_{l_2=0}^{L}\sum_{k_1=0}^{K}\sum_{k_2=0}^{K}\alpha_{k_1,l_1}\alpha_{k_2,l_2}\sum_{n_1=1}^{\bar{T}_b}\mathbf{P}_{int}(n_1,n_1)\right. \\ & \mathbf{g_{tr}}(n_1-\bar{T}_{l_1}-\bar{\tau}_{k_1,l_1})\mathbf{g_{tr}}(n_1-\bar{T}_{l_2}-\bar{\tau}_{k_2,l_2}-\bar{T}_{dt})\sum_{l_3=0}^{L}\sum_{l_4=0}^{L}\sum_{k_3=0}^{K}\sum_{k_4=0}^{K}\alpha_{k_3,l_3}\alpha_{k_4,l_4} \\ & \left.\sum_{n_2=1}^{\bar{T}_b}\mathbf{P}_{int}(n_2,n_2)\mathbf{g_{tr}}(n_2-\bar{T}_{l_3}-\bar{\tau}_{k_3,l_3})\mathbf{g_{tr}}(n_2-\bar{T}_{l_4}-\bar{\tau}_{k_4,l_4}-\bar{T}_{dt})\right\}. \end{aligned} \quad (3.29)$$

Define another normalized autocorrelation function in the continuous time domain as

$$R_{g1}(\Delta) = \frac{1}{E_g}\int_{x_1}^{y_1} g_{tr}(t)g_{tr}(t+\Delta)dt \quad (3.30)$$

where x_1 and y_1 can be determined according to eq.(3.22). In this situation, Z_{min} (Z_{max}) represents the minimum (maximum) row index of non-zero ele-

ments in $\mathbf{P}_{int}$. By substituting eq.(3.30) into eq.(3.29), one has

$$\begin{aligned}
& E\left\{{I_3}^2(\alpha)\right\} \\
= \;& (1-\alpha)^2\varepsilon^2{E_g}^2E\left\{\sum_{l_1=0}^{L}\sum_{l_2=0}^{L}\sum_{k_1=0}^{K}\sum_{k_2=0}^{K}\alpha_{k_1,l_1}^2\alpha_{k_2,l_2}^2\left[R_{g1}^2(T_{l2}-T_{l1}+\tau_{k_2,l_2}-\tau_{k_1,l_1}+T_{dt})\right.\right. \\
+ \;& \left.\left.R_{g1}(T_{l2}-T_{l1}+\tau_{k_2,l_2}-\tau_{k_1,l_1}+T_{dt})R_{g1}(T_{l1}-T_{l2}+\tau_{k_1,l_1}-\tau_{k_2,l_2}+T_{dt})\right]\right\} \\
+ \;& (1-\alpha)^2\varepsilon^2{E_g}^2E\left\{\sum_{l_1=0}^{L}\sum_{l_2=0}^{L}\sum_{k_1=0}^{K}\sum_{k_2=0}^{K}\alpha_{k_1,l_1}^2\alpha_{k_2,l_2}^2\right\}R_{g1}^2(0) \\
+ \;& (1-\alpha)^2\varepsilon^2{E_g}^2E\left\{\sum_{l_1=0}^{L}\sum_{k_1=0}^{K}\alpha_{k_1,l_1}^4\right\}R_{g1}^2(0). \qquad (3.31)
\end{aligned}$$

Then, $E\left\{{I_3}^2(\alpha)\right\}$ can be derived in a similar way as for $E\left\{{I_2}^2(\alpha)\right\}$, given by

$$E\left\{{I_3}^2(\alpha)\right\} = (1-\alpha)^2\varepsilon^2{E_g}^2\sum_{l_1=0}^{L}\sum_{l_2=0}^{L}\sum_{k_1=0}^{K}\sum_{k_2=0}^{K}(J_{31}+J_{32})+\frac{1-\alpha}{\alpha}E\left\{S^2\right\}R_{g1}^2(0) \qquad (3.32)$$

where

$$\begin{aligned}
J_{31} &= E\left\{\alpha_{k_1,l_1}^2\alpha_{k_2,l_2}^2R_{g1}^2(T_{l_2}-T_{l_1}+\tau_{k_2,l_2}-\tau_{k_1,l_1}+T_{dt})\right\} \\
J_{32} &= E\left\{\alpha_{k_1,l_1}^2\alpha_{k_2,l_2}^2R_{g1}(T_{l_2}-T_{l_1}+\tau_{k_2,l_2}-\tau_{k_1,l_1}+T_{dt})\right. \\
&\quad \left.R_{g2}(T_{l_1}-T_{l_2}+\tau_{k_1,l_1}-\tau_{k_2,l_2}+T_{dt})\right\}.
\end{aligned}$$

The second-order moments of N_1, N_2 and N_4 can be derived as follows.

From eq.(3.13f), one has

$$
\begin{aligned}
& E\left\{{N_1}^2(\alpha)\right\} \\
= \;& \alpha\varepsilon\delta_e^2 E\left\{\sum_{n_1=1}^{\bar{T}_b}\mathbf{P_1}(n_1,n_1)\right. \\
& \left.\sum_{l_1=0}^{L}\sum_{k_1=0}^{K}\alpha_{k_1,l_1}\mathbf{g_{tr}}(n_1-\bar{T}_{l_1}-\bar{\tau}_{k_1,l_1})\sum_{l_2=0}^{L}\sum_{k_2=0}^{K}\alpha_{k_2,l_2}\mathbf{g_r}(n_1-\bar{T}_{l_2}-\bar{\tau}_{k_2,l_2})\right\} \\
= \;& \alpha\varepsilon\delta_e^2 E\left\{\sum_{l_1=0}^{L}\sum_{k_1=0}^{K}\sum_{l_2=0}^{L}\sum_{k_2=0}^{K}\alpha_{k_1,l_1}\alpha_{k_2,l_2}\right. \\
& \left.\sum_{n_1=1}^{\bar{T}_b}\mathbf{g_{tr}}(n_1-\bar{T}_{l_1}-\bar{\tau}_{k_1,l_1})\mathbf{P_1}(n_1,n_1)\mathbf{g_{tr}}(n_1-\bar{T}_{l_2}-\bar{\tau}_{k_2,l_2})\right\}. \qquad (3.33)
\end{aligned}
$$

Let

$$R_{g3}(\Delta)=\frac{1}{E_g}\int_{x_3}^{y_3} g_r(t)g_{tr}(t+\Delta)dt \qquad (3.34)$$

where x_3 and y_3 can be determined using eq.(3.22) by the minimum and maximum row indexes corresponding to $\mathbf{P}_1$. The expression of eq.(3.33) can be rewritten as

$$
\begin{aligned}
E\left\{{N_1}^2(\alpha)\right\} \;=\; & \alpha\varepsilon\delta_e^2 E_g\sum_{l_1=0}^{L}\sum_{l_2=0}^{L}\sum_{k_1=0}^{K}\sum_{k_2=0}^{K} \\
& E\left\{\alpha_{k_1,l_1}\alpha_{k_2,l_2}R_{g3}(T_{l2}-T_{l1}+\tau_{k_2,l_2}-\tau_{k_1,l_1})\right\}. \qquad (3.35)
\end{aligned}
$$

Since $E\{\alpha_{k_1,l_1}\alpha_{k_2,l_2}\}=0$ when $l_1\neq l_2$ or $k_1\neq k_2$, eq.(3.35) can be simplified as

$$E\left\{{N_1}^2(\alpha)\right\}=\alpha\varepsilon\delta^2 E_g\sum_{l_1=0}^{L}\sum_{k_1=0}^{K}E\left\{\alpha_{k_1,l_1}^2\right\}R_{g3}(0) \qquad (3.36)$$

where the expectation of $\alpha_{k_1,l_1}^2=\Omega_0(\frac{\Lambda\Gamma}{1+\Lambda\Gamma})^l(\frac{\lambda\gamma}{1+\lambda\gamma})^k$ is given by [26]. Using the

same method, one has

$$E\{{N_2}^2(\alpha)\} = (1-\alpha)\varepsilon\delta^2 E_g \cdot \sum_{l_1=0}^{L}\sum_{k_1=0}^{K} E\left\{\alpha_{k_1,l_1}^2\right\} R_{g1}(0) \quad (3.37)$$

$$E\{{N_3}^2(\alpha)\} = \alpha\varepsilon\delta^2 E_g \cdot \sum_{l_1=0}^{L}\sum_{k_1=0}^{K} E\left\{\alpha_{k_1,l_1}^2\right\} R_{g1}(0) \quad (3.38)$$

$$E\{{N_4}^2(\alpha)\} = (1-\alpha)\varepsilon\delta^2 E_g \cdot \sum_{l_1=0}^{L}\sum_{k_1=0}^{K} E\left\{\alpha_{k_1,l_1}^2\right\} R_{g2}(0). \quad (3.39)$$

The expressions for $R_{g1}(\cdot)$, $R_{g2}(\cdot)$ and $R_{g3}(\cdot)$ are derived for the second-order derivative Gaussian pulse in *Section 3.3.3.1.*

Define

$$F_i(c_1,c_2,c_3,c_4,a,b,w) = \left(\frac{\Gamma\Lambda}{2+\Gamma\Lambda}\right)^{c_2}\left(\frac{\gamma\lambda}{2+\gamma\lambda}\right)^{c_4}\frac{\Lambda^{c_1-c_2}}{(c_1-c_2-1)!}\frac{\lambda^{c_3-c_4}}{(c_3-c_4-1)!} \cdot \int_0^\infty e^{-at}R_{gi}^2(t+w)t^b dt \quad (3.40)$$

and

$$G_i(c_1,c_2,c_3,c_4,a,b,w) = \left(\frac{\Gamma\Lambda}{2+\Gamma\Lambda}\right)^{c_2}\left(\frac{\gamma\lambda}{2+\gamma\lambda}\right)^{c_4}\frac{\Lambda^{c_1-c_2}}{(c_1-c_2-1)!}\frac{\lambda^{c_3-c_4}}{(c_3-c_4-1)!} \cdot \int_0^\infty e^{-at}R_{gi}(t+w)R_{gi}(t-w)t^b dt \quad (3.41)$$

where $i = 1, 2$. Λ, Γ, γ and λ represent the arrival rate of the clusters, the cluster decay rate, the arrival rate of the rays in each cluster, and the ray decay rate within one cluster, respectively [26]. The value of J_{11} can be calculated from [28] by replacing $F(\cdot)$ there with $F_2(\cdot)$ in eq.(3.40) and $T_{n,n'}$ with 0. The value of J_{12} can be obtained in the same way as J_{11} by replacing $F_2(\cdot)$ in eq.(3.40) with $G_2(\cdot)$ in eq.(3.41). The value of J_{21} can be

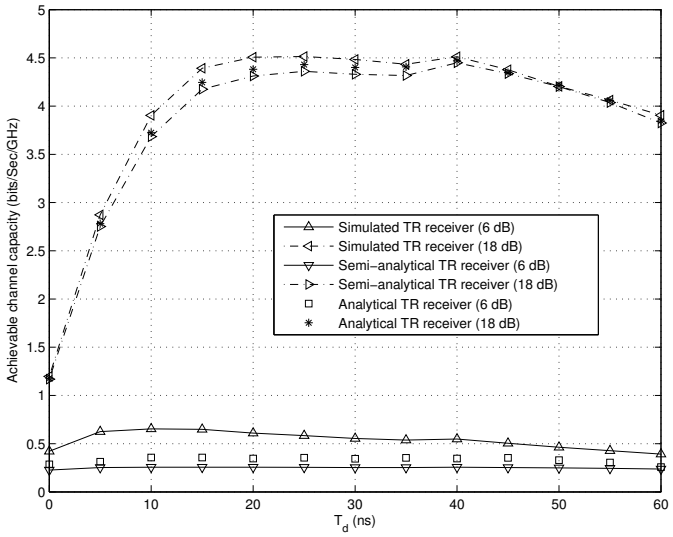

Figure 3.4: The channel achievable capacity versus T_d by using simulation, semi-analytical and analytical methods.

calculated from [28] similarly by replacing $F(\cdot)$ there with $F_2(\cdot)$ in (4.38) and $T_{n,n'}$ with T_{dt}. The value of J_{22} can be obtained in the same way as J_{21} by replacing $F_2(\cdot)$ in eq.(3.40) with $G_2(\cdot)$ in eq.(3.41). Finally, J_{31} and J_{32} can be calculated similarly by replacing $R_{g1}(\cdot)$ with $R_{g2}(\cdot)$.

By using eq.(3.17), eq.(3.25), eq.(3.28), eq.(3.32), and eq.(3.36)-eq.(3.39) in eq.(3.13a), the best value of α optimizing the channel achievable capacity is derived by setting the derivative of the channel capacity value to 0 and solving the equation

$$\alpha_{opt3} = \left\{ \frac{\partial[log_2(1+\xi(\alpha))]}{\partial(\alpha)} = 0 \right\}|_{\alpha}, \tag{3.42}$$

given an analytical method.

Figure 3.4 shows the channel achievable capacity versus T_d for the traditional TR receivers by using simulation, semi-analytical and analytical methods at SNR = 6 dB and SNR = 18 dB. One sees that similar results can be achieved as those for the simulation or the semi-analytical methods that, the

optimal T_d grows when SNR increasing. For the improved TR receiver from the analytical method, the maximum channel achievable capacity is about 0.3 bits/Sec/GHz at the optimum value of $T_{d_{opt3}} = 15\ ns$ for the value of SNR at 6 dB and about 4.45 bits/Sec/GHz at the optimum value of $T_{d_{opt3}} = 40$ ns for the value of SNR at 18 dB. Apparently, the optimum values of $T_{d_{opt}}$ from semi-analytical or analytical are not the same as those from simulation due to the approximation made in eq.(3.13a), but are very close. This demonstrates that Gaussian assumption is very accurate for the approximation of interference-pulse-noise terms. In addition, the semi-analytical or the analytical approach is very time-saving, but the simulation approach provides the most accurate result. Thus, the preferred approach can be chose for different demands: accuracy or efficiency.

Derivations of the Special Autocorrelation Functions

The special autocorrelation functions of $R_{g1}(\cdot)$, $R_{g2}(\cdot)$ and $R_{g3}(\cdot)$ are discussed in this section. The second-order derivative Gaussian pulse defined as $g_{tr}(t) = \left[1 - 16\pi\left(\frac{t-T_p/2}{T_p}\right)^2\right] \cdot e^{-8\pi\left(\frac{t-T_p/2}{T_p}\right)^2}$ is used. Then, eq.(3.21) can be further simplified as

$$\begin{aligned} R_{g2}(\Delta) &= \frac{1}{E_g}\int_{x_2}^{y_2}\left[1-16\pi\left(\frac{t-T_p/2}{T_p}\right)^2\right]e^{-8\pi\left(\frac{t-T_p/2}{T_p}\right)^2} \\ &\cdot \left[1-16\pi\left(\frac{t+\tau-T_p/2}{T_p}\right)^2\right]e^{-8\pi\left(\frac{t+\tau-T_p/2}{T_p}\right)^2}dt \end{aligned}$$

$$\begin{aligned} &= \frac{1}{E_g}\frac{8\pi^2}{{T_p}^4}e^{\left(-\frac{4\pi}{{T_p}^2}\Delta^2\right)}\int_{x_2'}^{y_2'}e^{\left(-\frac{4\pi}{{T_p}^2}x^2\right)}\cdot\left[x^4+6\left(T_p-\Delta\right)x^3\right. \\ &+ \left.6\left(T_p-\Delta\right)^2x^2+2\left(T_p-\Delta\right)^3x+\left(T_p-\Delta\right)^4\right]dx \end{aligned} \tag{3.43}$$

where $x_2' = 2x_2 + \Delta - T_p$ and $y_2' = 2y_2 + \Delta - T_p$. According to [74], one has

$$\begin{aligned} R_{g2}(\Delta) &= -\frac{1}{E_g} e^{(-\frac{4\pi}{T_p^2}\Delta^2)} \cdot \Big\{ f_0 (y_2')^3 U_1 - f_0 (x_2')^3 U_0 + f_1 (y_2')^2 U_1 \\ &- f_1 (x_2')^2 U_0 + f_2 (y_2') U_1 - f_2 (x_2') U_0 + f_3 U_1 - f_3 U_0 \\ &+ f_4 \left[\Phi\left(\frac{2\sqrt{(2\pi)}}{T_p} \right) x_2' - \Phi\left(\frac{2\sqrt{(2\pi)}}{T_p} \right) y_2' \right] \Big\} \end{aligned} \tag{3.44}$$

where

$$\begin{aligned} f_0 &= \frac{\pi}{T_p^2} \\ f_1 &= \frac{6\pi(T_p - \Delta) + 4\pi}{T_p^2} \\ f_2 &= \frac{12\pi {T_p}^2 + 10\pi\Delta^2 - 24\pi T_p \Delta + 12\pi T_p - 12\pi\Delta}{T_p^2} - \frac{1}{8} \\ f_3 &= \frac{\pi}{2{T_p}^2}(44{T_p}^3 - 60{T_p}^2\Delta + 57T_p\Delta^2 - 48T_p\Delta + 24\Delta^2 - 17\Delta^3) + \frac{3(T_p - \Delta)}{2} + 1 \\ f_4 &= \frac{40{\pi^2}^3}{T_p}\Delta^4 + \frac{16{\pi^2}^2}{T_p}(2 + \frac{1}{T_p})\Delta^3 + 3\pi(16\pi + \frac{40\pi}{T_p} + \frac{9}{T_p} + \frac{16\pi^2}{T_p})\Delta^2 + \\ &\quad \pi(48\pi T_p - 64\pi + \frac{752\pi}{T_p} - \frac{6}{T_p} - 10)\Delta + (\frac{3}{16}T_p + 5\pi T_p - 12\pi^2)T_p + 6\pi \\ U_0 &= e^{(-\frac{4\pi}{T_p^2}{x_2'}^2)} \\ U_1 &= e^{(-\frac{4\pi}{T_p^2}{y_2'}^2)}, \end{aligned}$$

and $\Phi(x) = \frac{1}{\sqrt{2\pi}} \int_{-\infty}^{x} e^{-\frac{1}{2}t^2} dt$ is the normal cumulative distribution function.

Similarly, $R_{g1}(\Delta)$ ($R_{g3}(\Delta)$) can be obtained from eq.(3.44) by switching x_2' with x_1' (x_3'), y_2' with y_1' (y_3') where

$$\begin{cases} x_1' = 2x_1 + \Delta - T_p, & y_1' = 2y_1 + \Delta - T_p; \\ x_3' = 2x_3 + \Delta - T_p, & y_3' = 2y_3 + \Delta - T_p. \end{cases} \tag{3.45}$$

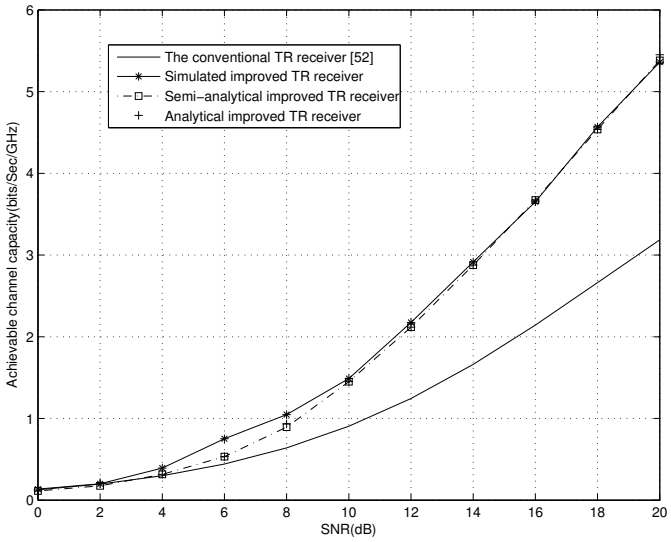

Figure 3.5: The channel achievable capacity versus SNR for the traditional and improved TR receivers for CM1.

3.3.4 Numerical Results and Discussion

Figure 3.5 shows the channel achievable capacity using the optimized T_d for different SNRs in the CM1 channel model. As can be seen from Figure 3.5 that, the improved TR receivers can provide significant performance gains over the traditional TR receiver. The improved TR receiver from the simulation method has a predicted improvement of up to 2.2 bits/Sec/GHz, the improved TR receiver from the semi-analytical method has a predicted improvement of up to 2.1 bits/Sec/GHz, and the improved TR receiver from the analytical method has a predicted improvement of up to 2.3 bits/Sec/GHz. One can also see that, for medium values of SNR between 4 dB and 10 dB, the channel achievable capacity at optimized T_d from simulation is greater than that from the semi-analytical or analytical approaches. This is because that the optimized T_d from theoretical methods is less accurate than that from the simulation method due to the Gaussian overestimation of noise.

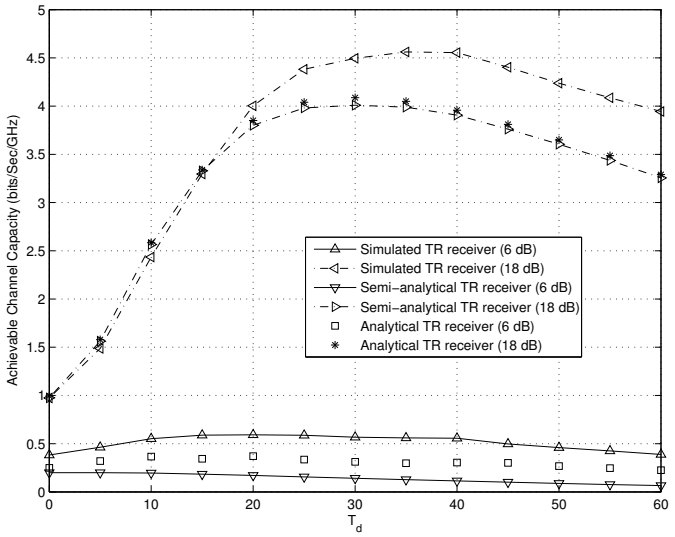

Figure 3.6: The channel achievable capacity versus T_d by using simulation, semi-analytical and analytical methods for CM2.

Figure 3.6 shows the channel achievable capacity versus T_d for the IEEE CM2 channel model in [26]. In this case, one can obtain the similar optimization results as those in Figure 3.4 for the CM1 channel model. However, the curves in Figure 3.6 are not as flat as those in Figure 3.4, as the channel model CM2 incurs more IPI and the value of T_d has more significant effect on the channel achievable capacity. For the simulated improved TR receiver, the maximum channel achievable capacity is about 0.6 bits/Sec/GHz at the optimum value of $T_{d_{opt}} = 20\ ns$ for the value of SNR at 6 dB and about 4.5 bits/Sec/GHz at the optimum value of $T_{d_{opt}} = 35\ ns$ for the value of SNR at 18 dB. For the semi-analytical improved TR receiver, the maximum channel achievable capacity is about 0.2 bits/Sec/GHz at the optimum value of $T_{d_{opt}} = 5\ ns$ for the value of SNR at 6 dB and about 4 bits/Sec/GHz at the optimum value of $T_{d_{opt}} = 30\ ns$ for the value of SNR at 18 dB. Also, for the analytical optimized TR receiver, the maximum achievable channel capacity is about 0.4 bits/Sec/GHz at the optimum value of $T_{d_{opt}} = 10\ ns$ for the value of

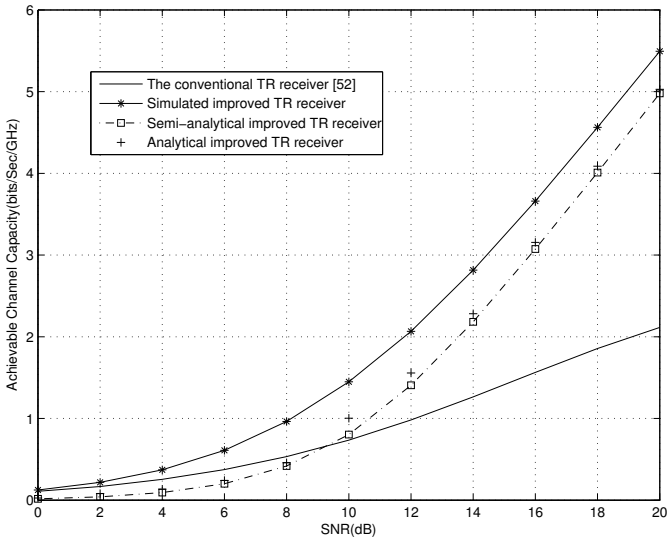

Figure 3.7: The channel achievable capacity versus SNR for the traditional and improved TR receivers for CM2.

SNR at 6 dB and about 4.5 bits/Sec/GHz at the optimum value of $T_{d_{opt}} = 40$ ns for the value of SNR at 18 dB.

Figure 3.7 shows the channel achievable capacity using the optimized T_d for the CM2 channel model. In this case, the improved TR receiver can provide a performance improvement of up to 3.4 bits/Sec/GHz, greater than that for the CM1 channel model. This is due to the fact that, the CM2 channel is more sensitive to the interference caused by the time delay T_d than the CM1 channel. The optimized channel achievable capacities for the CM1 and CM2 channel models are approximately the same. On the other hand, both semi-analytical and analytical methods give less accurate predictions, because the Gaussian approximation is less accurate due to the increased IPI, compared with the CM1 channel model. Also, in low SNR regions from 0 to 10 dB, the theoretical improved TR receivers unperform the non-improved TR receiver. This is because that Gaussian approximation for the interference-pulse-noise

terms in CM2 is not as accurate as in CM1, due to the increased IPI in CM2 as well.

Table 3.1 lists the optimum values of T_d calculated from the simulation, semi-analytical and analytical methods for different scenarios and used in the receivers improved in Figure 3.5 and Figure 3.7, respectively. T_{dopt1} denotes the time delay T_d optimizing the channel achievable capacity obtained from the simulation method, T_{dopt2} denotes the time delay T_d optimizing the channel achievable capacity estimated by using the semi-analytical method, and T_{dopt3} denotes the time delay T_d optimizing the channel achievable capacity estimated by using the analytical method. All these optimum values of T_d could be used as a guideline for practical receiver designs in different SNR environments. One sees that the optimal values from the semi-analytical and analytical methods are very close to each other for most values of SNR, while the optimum values from the simulation method are close to those from semi-analytical and analytical methods for large values of SNR. This is because the approximation used in eq.(3.13a) is more accurate when SNR is large. Although the approximation error in eq.(3.13a) is large for small values of SNR, it can be shown that the optimized channel achievable capacity is almost independent of the methods used, as seen from Figure 3.5 and Figure 3.7.

Table 3.1: **The Best Values of T_d (ns) for Different SNRs.**

SNR	CM1			CM2		
(dB)	T_{dopt1}	T_{dopt2}	T_{dopt3}	T_{dopt1}	T_{dopt2}	T_{dopt3}
0	5.000	10.00	10.00	11.24	0.000	1.278
1	5.000	10.00	10.00	17.48	0.000	1.278
2	5.000	10.00	11.24	23.72	0.000	1.278
3	8.716	11.24	11.24	23.72	0.000	1.278
4	12.56	12.56	12.56	23.72	0.000	1.278
5	13.76	13.76	12.56	23.72	2.476	2.476
6	13.76	13.76	13.76	23.72	6.211	6.211
7	13.76	13.76	26.24	23.72	8.721	8.721
8	13.76	13.76	40.00	23.72	9.921	9.921
9	13.76	26.24	40.00	23.72	13.76	13.76
10	13.76	40.00	40.00	23.72	16.28	16.28
11	16.28	40.00	40.00	23.72	16.28	16.28
12	17.48	40.00	40.00	23.72	17.48	18.78
13	17.48	40.00	40.00	26.24	18.78	18.78
14	17.48	40.00	40.00	27.56	20.00	20.00
15	17.48	40.00	40.00	30.00	23.72	25.00
16	17.48	40.00	40.00	33.76	26.24	26.24
17	27.56	40.00	40.00	33.76	27.56	30.00
18	40.00	40.00	40.00	33.76	30.00	30.00
19	40.00	40.00	40.00	40.00	35.00	35.00
20	40.00	40.00	40.00	40.00	35.00	35.00

3.4 BER Optimization

In this section, the BER performance of the traditional TR receiver is optimized with respect to the time delay T_d between reference and data pulses.

$$BER = \frac{P_{b\_e}}{P_b} \tag{3.46}$$

where P_{b_e} is the average number of bits in error out of P_b total transmitted bits, and the value of α optimizing the BER performance is found from

$$\alpha_{opt4} = \arg \min_{\alpha \in (0,0.5]} \{BER(\alpha)\}. \tag{3.47}$$

In practice, the value of α_{opt4} does not equal the value of α_{opt1} in eq.(3.12). This is due to the fact that the value of α_{opt1} maximizing the averaged channel capacity does not necessarily minimize the system BER, and the value of α_{opt4} minimizing the system BER does not necessarily maximize the averaged channel capacity.

Figure 3.8 shows the BER performance versus T_d for the traditional TR receiver by using the simulation method at SNR = 0 dB, 6 dB, 12 dB and 18 dB, respectively. One sees that the curves for small values of SNR are too flat to have an optimization, because in this case, the impact of the noise is greater that the impact of the interference such that the effect of IPI can be neglected. While the optimizations do exist for large values of SNR, as the effect of IPI becomes significant due to the increased signal energy. Specifically, the optimum value of $T_{d_{opt4}}$ is about 5 ns at SNR = 12 dB and about 10 ns at SNR = 18 dB. One can also see that the optimum values of $T_{d_{opt4}}$ increase when SNR is growing, as the noise is further compressed such that IPI will greatly

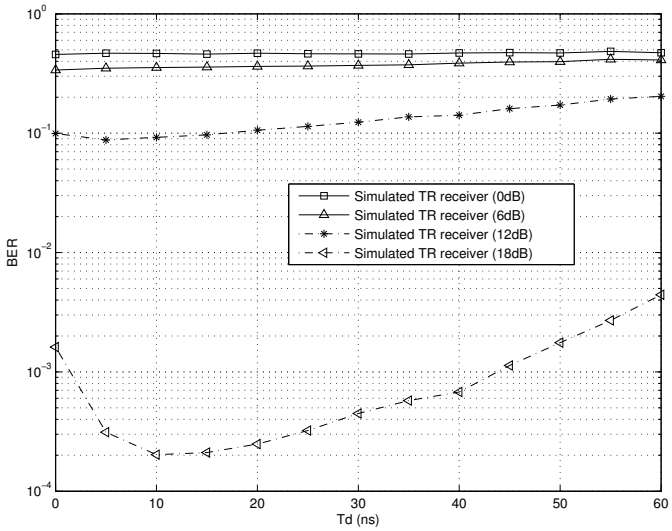

Figure 3.8: The BER versus T_d for the traditional TR receiver at different SNRs for CM1.

impact the receiver performance. To reduce this interference, the optimum value of $T_{d_{opt}}$ has to be increased for reliable detection.

Using a Gaussian approximation to the interference-plus-noise terms, the approximate BER can be obtained as $BER_{semi_analy} = Q(\sqrt{\xi(\alpha)})$ where $\xi(\alpha)$ is derived by *Section 3.3*. First, by using the average SINR from the semi-analytical approach in *Section 3.3.2*, the best value of α optimizing the approximate BER can be found as

$$\alpha_{opt5} = \arg \min_{\alpha \in (0,0.5]} \left\{ Q(\sqrt{\xi(\alpha)}) \right\}. \tag{3.48}$$

Similarly, by using the average SINR from the analytical approach in *Section 3.3.3*, the best value of α can be obtained by solving the derivation function of the approximate BER as

$$\alpha_{opt6} = \left\{ \frac{\partial [Q(\sqrt{\xi(\alpha)})]}{\partial(\alpha)} = 0 \right\} |_{\alpha}. \tag{3.49}$$

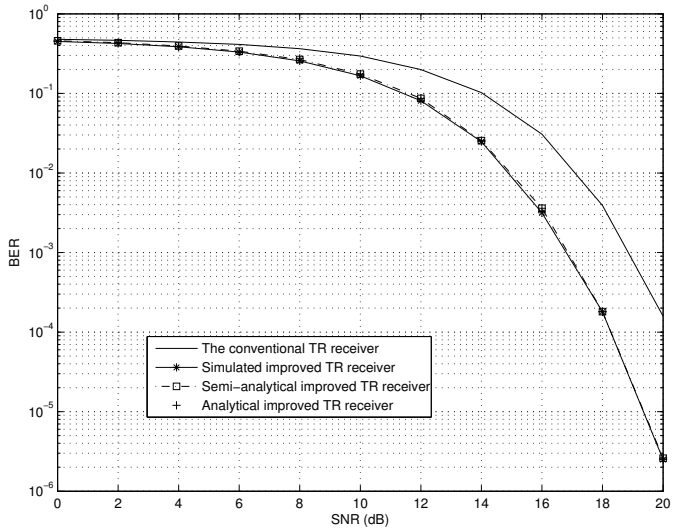

Figure 3.9: The BER versus SNR for the traditional and improved TR receivers for CM1.

Since $log_2(x)$ monotonically increases when x increases, while $Q(x)$ monotonically decreases when x increases, the value of α_{opt5} equals the value of α_{opt2} in eq.(3.14) and the value of α_{opt6} equals the value of α_{opt3} in eq.(3.42).

Figure 3.9 shows the BER performance versus SNR for the traditional TR receiver and the optimized TR receivers for the CM1 channel model. One sees that the improved receivers outperform the traditional TR receiver in all the cases considered. The performance improvements achieved by optimizing T_d are significant. For example, at BER = 10^{-1}, the improved TR receiver by using simulation can provide a performance gain of up to 2.4 dB, the improved TR receiver from the semi-analytical approach can provide a performance gain of up to 2.1 dB and the improved TR receiver from the analytical approach can provide a performance gain of up to 2.2 dB, over the traditional TR receiver. There is little performance difference between the methods applied and hence, the Gaussian approximation used for the theoretical methods is suitable for T_d optimization in the traditional TR system.

3.5 Conclusions

In this chapter, the issue of finding optimum values of the time delay T_d between the reference and the data pulses for the traditional TR receiver has been investigated. This problem was transformed into the problem of finding the optimum values of the energy allocation factor α. The numerical results have demonstrated that there exists an optimal value of time delay between reference and data pulses that maximizes the channel capacity or minimizes the BER with significant improvements.

Simulation, semi-analytical and analytical methods have been investigated to calculate the optimum values of $T_{d_{opt}}$ for the CM1 and CM2 channel models. For both criteria (channel capacity and BER), the simulation method provides the most accurate optimization result, while semi-analytical and analytical methods provide the comparatively inferior results. However, the former one consumes more time and resource than the latter ones. All the improved TR receivers at the optimized T_d can offer significant performance gains over the traditional TR receiver. Since the optimization results from theoretical methods by using Gaussian approximation are very close the those from the simulation method, all the optimal T_d values from each method will be used to guide UWB receiver designs. One can also use the similar optimization method as in this chapter for other receiver designs.

Chapter 4

Optimization of Generalized UWB TR Receivers

Due to the transceiver properties of the TR system, it is very suitable for low-data-rate applications such as sensor networks and body area networks, where power consumption is more important than data rate [75], [76]. In the previous chapter, the optimization of the traditional TR receiver has been investigated. There, a reference and data pulse pair are transmitted in one frame and then the received data signal is correlated with the reference signal in the same pair for detection. The two pulses within a pair are separated with a time delay T_d at the transmitter. However, a template based on one reference is not reliable, and hence generalized TR receivers are proposed [77] for easy implementation and also they can provide better performance [58] compared with AcR. Thus, this chapter will concentrate on the optimization of generalized TR receivers in UWB systems.

4.1 Introduction

Unlike a traditional TR system, a generalized TR system transmits N_r reference symbols and N_d data symbols per data packet, where N_r and N_d are arbitrary integers. For the conventional generalized TR receiver, all the N_r previous reference symbols per data packet are used to construct the channel template which is later correlated with the received data signal for detection. Specifically, the template signal is the average value of the N_r previous reference symbols [78]. As a result, the generalized TR receiver enables an increase in the bandwidth efficiency and an improvement in the bit error rate (BER) performance significantly [54], [79].

One of the widely used generalized TR receivers is the training-based (TB) receiver, which constructs the channel template using the received signals of the reference symbols only. This is also known as the conventional generalized TR receiver. Compared to this simple receiver, the maximum-likelihood (ML) and the generalized likelihood ratio test (GLRT)-based receivers proposed in [79] can provide significant performance improvements in terms of the template signals constructed by the reference and the received data symbols. However, their structures are complicated, as they require calculation of many extra parameters as well as matrix inversion. Thus, new ML and GLRT receivers are proposed in [80] to simplify the receiver structures from avoiding iteration algorithms with acceptable performance degradations. For convenience, the recursive ML and recursive GLRT receivers are denoted as the ML-I and GLRT-I receivers, and the non-recursive ML and non-recursive GLRT receivers are denoted as the ML-II and GLRT-II receivers. In [81], three better TR receivers with simpler structures are derived. These receivers make

use of the part of the received signal corresponding to the reference symbols, the part of the received signal corresponding to the data symbols, as well as the past data decisions. They provide considerable performance gains over the receivers in both [79] and [80]. However, none of them is optimized for the best BER performance.

Assuming perfect synchronization of the receiver, the performances of the TR receivers are very sensitive to the energy allocation between the reference symbols and the data symbols [77]. An optimal allocation between the reference energy and the data energy exists when the total energy is fixed. Furthermore, the length of the correlation integration interval is another important parameter that affects the receiver performance significantly [79], [82], [83]. In [77], Yang and Giannakis improved the TB-based receiver with respect to the energy allocation between reference and data symbols in one data packet by increasing the average channel capacity. In [79], Franz and Mitra improved the ML- and GLRT-based receivers with respect to the energy allocation and the correlation integration interval length by increasing the effective signal-to-noise ratio (SNR). In this chapter, the receivers proposed in [79], [84], [80] are improved with respect to the length of the integration interval and the energy allocation of reference and data symbols by reducing the BER. Both the best number of reference symbols and the best length of the integration interval are derived for different scenarios.

This chapter is organized as follows. The system model for the generalized TR receivers is provided in *Section 4.2*. In *Section 4.3*, the optimization with respect to the energy allocation and the length of integration interval for each receiver is investigated by simulation. Similarly, the optimization for the receivers in [79], [84], [80] by using the simulation and theoretical methods is

specifically discussed in *Section 4.4*. Finally, the concluding remarks are given in *Section 4.5*.

4.2 System Model

Consider a TH UWB system with the BPM scheme. The received signal for the TR system can be expressed as [80]

$$r(t) = \sum_{i} \sqrt{\varepsilon_i}\vartheta_i \sum_{j=0}^{N_f-1} h(t - iN_fT_f - jT_f - c_jT_c) + n(t) \tag{4.1}$$

where ε_i represents the energy of the ith symbol/bit, N_f is the number of frames per symbol, T_f is the frame duration, $c_j \in [0, N_h]$ is the time hopping code for the jth frame, N_h is the maximum value of c_j, T_c is the chip duration, $h(t)$ is the channel response (CR) to the transmitted waveform, and $n(t)$ is additive white Gaussian noise with mean zero and variance δ^2. The multipath channel used herein is based on the IEEE UWB CM1-CM4 channel models [26]. It is assumed to be time-invariant in one data packet.

Assuming that N_r reference symbols are transmitted followed by N_d data symbols in one data packet and hence, a total of $M = N_r + N_d$ symbols are sent per data packet. The energy of the reference signal per frame is $\varepsilon_{ri} = \frac{\varepsilon_r}{N_rN_f}$ for $i = 0, 1, \cdots, N_r - 1$ and the energy of the data signal per frame is $\varepsilon_{di} = \frac{\varepsilon_d}{N_dN_f}$ for $i = N_r, N_r + 1, \cdots, M - 1$, where ε_r and ε_d are the total energies of the reference symbols and the data symbols in one data packet, respectively. $\varepsilon = \varepsilon_r + \varepsilon_d$ denotes the total signal energy per packet. Assume that the frame energy of the reference signal equals the frame energy of the data signal (i.e., $\varepsilon_{ri} = \varepsilon_{di}$) and define $\alpha = \frac{\varepsilon_r}{\varepsilon_r+\varepsilon_d}$ as the energy allocation factor

such that

$$\alpha = \frac{N_r}{N_r + N_d} = \frac{N_r}{M}, \tag{4.2}$$

so that the total reference energy per data packet is $\varepsilon_r = \alpha\varepsilon$ and the total data energy per packet is $\varepsilon_d = (1-\alpha)\varepsilon$. Therefore, the choice of α is equivalent to the choice of the number of reference symbols N_r when the number of data symbols N_d is fixed. If α is too small, the energy allocated to the reference symbols per packet is too small and hence, the receiver will suffer from an inaccurate channel template. In this case, the receiver performance will be degraded. On the other hand, if α is too large, the energy allocated to the reference symbols per packet is too large and hence the data symbols will be more vulnerable to noise. The receiver performance will be degraded again. The value of α will be selected later in this chapter.

It may also be assumed that the receiver is perfectly synchronized. Let $T_f \geq T_{mds} + T_c N_h$, where T_{mds} is the channel maximum excess delay. Thus, there is no inter-frame interference (IFI) or intersymbol interference (ISI). The presented results are only applicable to UWB systems with large values of T_f where IFI and ISI can be ignored. They may not be applicable to small values of T_f with possibly considerable IFI and ISI. The received signal in eq.(4.1) is sampled at a sampling interval of T_s, resulting in $MS = \lfloor \frac{T_f}{T_s} \rfloor$ samples per frame in total. Among them, only $L = \lfloor \frac{T_{mds}}{T_s} \rfloor$ $(L \leq MS)$ samples contain useful data energy. By averaging the sampled received signal over frames within one data symbol, one has

$$\mathbf{r}_i(\alpha) = \sqrt{\varepsilon_i(\alpha)} d_i \mathbf{h} + \mathbf{n}_i \tag{4.3}$$

where $\mathbf{h} = [h_{T_1}, h_{T_2}, \cdots, h_{T_{mds}}]^T$ is a $L \times 1$ column vector that represents the CR at different sampling instants, $\varepsilon_i(\alpha)$ is the ith symbol energy function of α due to the energy allocation, and $\mathbf{n}_i = [n_{T_1}, n_{T_2}, \cdots, n_{T_{mds}}]^T$ is a $L \times 1$ column vector that represents the noise samples in the ith received symbol with variance $\delta_e^2 = \delta^2/N_f$.

After correlating the received signals with the channel template and thresholding the result, the data decision before demodulation is given by

$$\hat{\vartheta}_i(\alpha, T_N) = sgn\left\{\mathbf{r}_i^T(\alpha)\mathbf{P}_{T_N}\hat{\mathbf{h}}_i(\alpha)\right\} \tag{4.4}$$

where $\mathbf{r}_i(\alpha)$ and $\hat{\mathbf{h}}_i(\alpha, T_N)$ are the received signal and the channel template for the ith symbol, respectively, $i = N_r, N_r + 1, \cdots, M-1$, $\mathbf{P}_{T_N} = \begin{bmatrix} \mathbf{I}_{T_N} & \mathbf{0} \\ \mathbf{0} & \mathbf{0} \end{bmatrix}$ is a $L \times L$ matrix, $\mathbf{I}_{T_N}$ is the $\lfloor \frac{T_N}{T_s} \rfloor \times \lfloor \frac{T_N}{T_s} \rfloor$ identity matrix with T_N representing the length of the integration interval, and $sgn(\cdot)$ is the *signum* function with $sgn(x) = 1$ if $x > 0$ and $sgn(x) = -1$ if $x \leq 0$. The final data decision can be obtained after demodulation that the digital data is '1' if $\hat{\vartheta}_i = +1$ and the digital data is '0' if $\hat{\vartheta}_i = -1$. Assuming perfect synchronization of the receiver (i.e.,$\tau_0 = 0$), the performances of generalized TR receivers are very sensitive to the length of integration interval T_N [64] [71]. If T_N is too small, only a small amount of useful signal energy will be captured and the receiver performance will be degraded. If N is too large, an excessive amount of noise can be introduced, as the signal often decays with time. In this case, the receiver performance will be degraded again. There must exist an optimal length of integration interval, where the integration in the correlator contains enough signal energy but no excessive noise. The choice of T_N will be also

discussed later in this chapter.

4.3 Optimization for the Generalized TR Receivers by Simulation

In the following, the BER performances of the generalized TB, ML and GLRT receivers [79] are improved with respect to the energy allocation factor of α and the integration interval length of T_N. This may be done by conducting a joint optimization of α and T_N; on the other hand, it may also be done by conducting two separate optimizations of α and T_N. The joint optimization requires a time-consuming two-dimensional search. In order to save simulation time, two separate optimizations of α and T_N are performed in this chapter. This gives suboptimal results that are not necessarily the same as the overall optimal results achieved by a joint optimization, and the receivers may be described as improved but not fully optimized in this sense. The two separate optimizations can be done by optimizing α with an initial value of T_N then optimizing T_N at the optimized α, or by optimizing T_N with an initial value of α then optimizing α at the optimized T_N. It will be shown via simulation results later that there is little performance difference between these two schemes. Hence, in this chapter, the improvement will be done in the following two steps. In the first, the value of α is optimized with an initial integration interval length of $T_N = T_{ds}$. In the second, the length of T_N is optimized at the optimized value of α obtained in the first step.

In the examination, the second order derivative of a Gaussian pulse is used, which is normalized to unit energy with duration 1 ns. The frame

interval T_f is set to 110 ns. Also, $N_f = 1$, $T_c = 2$ ns, and $N_h = 24$. The number of data symbols N_d is fixed to 20 while the number of the reference symbols N_r varies. The IEEE CM1 model [26] is used. The maximum excess delay T_{mds} is restricted to 50 ns. The sampling interval T_s is set to 1/8 ns. In this case, there are $L = 400$ samples within one frame that contain useful energy. These parameters are chosen to be the same as those in [81] to facilitate the comparison. If not stated otherwise, the "brute-force" method is applied for simulation throughout the whole chapter.

4.3.1 The generalized TB, ML-I and GLRT-I receivers

From [79], the channel template for the TB receiver is constructed by using the received signal corresponding to the reference symbols only, which is give by

$$\hat{\mathbf{h}}_{i,TB}(\alpha) = \sqrt{\frac{N_f}{\alpha\varepsilon N_r}} \sum_{m=0}^{N_r-1} \vartheta_m \mathbf{r}_m \quad (i = N_r, N_r+1, \cdots, N_s-1). \tag{4.5}$$

For the ML-I and the GLRT-I receivers in [79], both of their channel templates are constructed by combining the received signal with a weighted factor and the reference signal, as well as the nonlinearly *tanh* function with respect to the past-decision-data as

$$\begin{aligned} \hat{\mathbf{h}}_{i,ML-I} &= \frac{1}{\varepsilon}\Bigg(\sqrt{\frac{\alpha\varepsilon N_f}{N_r}} \sum_{m=0}^{N_r-1} \vartheta_m \mathbf{r}_m \\ &+ \sqrt{\frac{(1-\alpha)\varepsilon N_f}{N_d}} \sum_{n=N_r}^{N_s-1} tanh\left(\frac{\sqrt{\varepsilon_n}}{\delta_e^2} \mathbf{r}_n^T \hat{\mathbf{h}}_{i,ML-I}\right)\mathbf{r}_n\Bigg) \end{aligned} \tag{4.6}$$

and

$$\hat{\mathbf{h}}_{i,GLRT-I} = \frac{1}{\varepsilon - \frac{(1-\alpha)\varepsilon}{N_d}} \left(\sqrt{\frac{\alpha\varepsilon N_f}{N_r}} \sum_{m=0}^{N_r-1} \vartheta_m \mathbf{r}_m + \sqrt{\frac{(1-\alpha)\varepsilon N_f}{N_d}} \sum_{n=N_r, n\neq i}^{N_s-1} tanh\left(\frac{\sqrt{\varepsilon_n}}{{\delta_e}^2} \mathbf{r}_n^T \hat{\mathbf{h}}_{i,GLRT-I} \right) \mathbf{r}_n \right). \quad (4.7)$$

The Best Value of the Energy Allocation Factor

In this section, the simulation is performed with respect to the energy allocation factor α first, without taking the effect of the integration interval length T_N into account. In this situation, T_N is fixed to T_{ds} and the best value of α can be found by searching over the possible values of α that may minimize BER as

$$\alpha_{opt1} = \arg \min_{\alpha \in (0,1)} \{BER(\alpha, T_{ds})\}. \quad (4.8)$$

Figure 4.1 shows the BER performances versus α for the TB receiver, at the SNR values of 0 dB, 6 dB and 12 dB, respectively, and $T_N = T_{mds}$. As can be seen from Figure 4.1 that, the effect of α for a small value of SNR at 0 dB is hardly to be recognized, due to the very huge amount of noise component compared to the useful signal component. The optimal α is about 0.5 for a value of SNR at 6 dB, and the optimal α is about 0.35 for a value of SNR at 12 dB. One sees that, the effect of α becomes more distinct with the increase of SNR, as the useful signal is strongly dominated by the noise and hence, the BER performance is very sensitive to α which affects the quality of the received signal significantly. One can also see that, the optimum value of α_{opt} at SNR = 12 dB is smaller than the optimum value of α_{opt} at SNR = 6 dB. This is due to the fact that, with SNR increasing, the signal energy

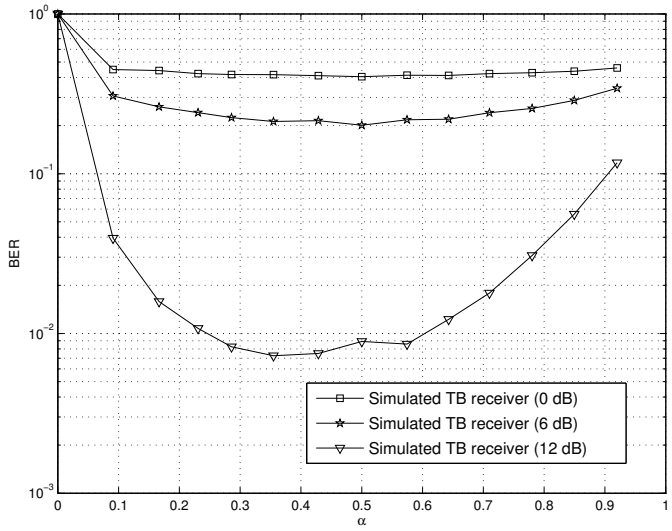

Figure 4.1: The BER versus α for the generalized TB receiver at $T_N = T_{ds}$ for different SNR scenarios.

for reference symbols per packet is enhanced. However, the energy allocated to data symbols per packet is accordingly reduced when the total energy per packet is fixed. This will result in a performance degradation. Therefore, the number of reference symbols per packet (i.e., α) has to be decreased to provide a sufficient useful signal component for the data decision.

Figure 4.2 exhibits the effect of α for the generalized ML-I receivers with one, four and nine iteration numbers, respectively. At SNR = 6 dB, the optimal values of α for the ML-I receivers with one, four and nine iterations are all about 0.43; at SNR = 12 dB, the optimal values of α for the ML-I receiver with one, four and nine iterations are all about 0.28. It is clear that the optimal values of α for the ML-I receivers are not related to the receiver recursive number. One has the same results for the ML-I receivers in Figure 4.2 as those for the TB receiver in Figure 4.1 that, the optimum values of α for the large SNR of 12 dB are less than those for the small SNR of 6 dB due to the increased energy of reference symbols. The BER performance versus α

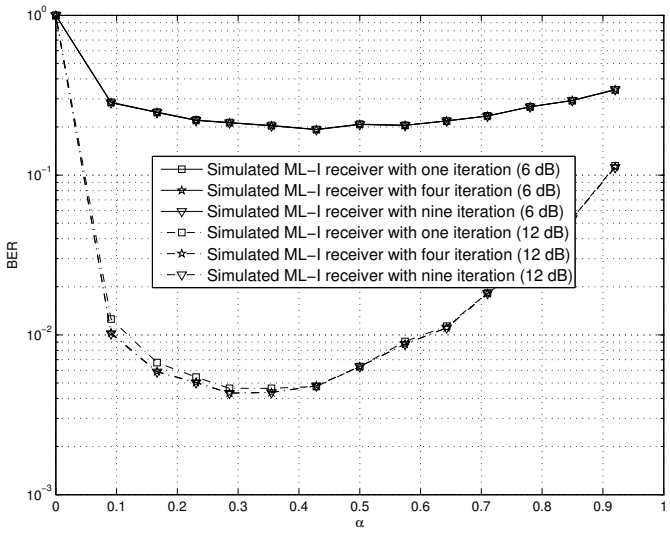

Figure 4.2: The BER versus α for the generalized ML-I receivers at $T_N = T_{ds}$ for different SNR scenarios.

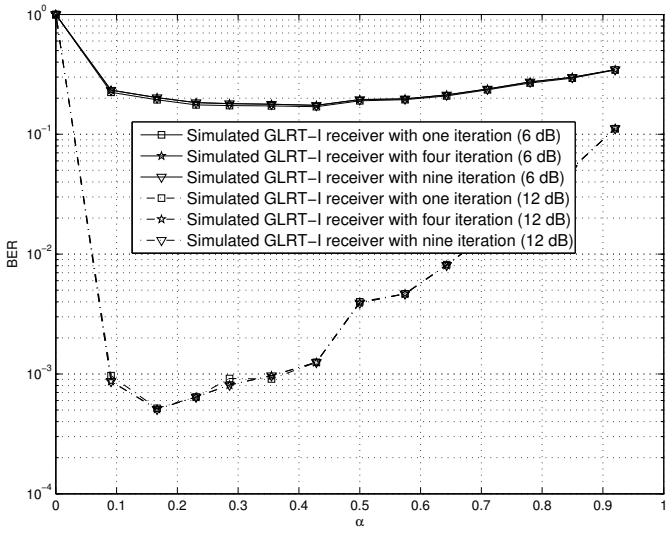

Figure 4.3: The BER versus α for the generalized GLRT-I receivers at $T_N = T_{ds}$ for different SNR scenarios.

for the GLRT-I receivers are depicted in Figure 4.3. In this case, the optimum values of α are about 0.43 at SNR = 6 dB and about 0.17 at SNR = 12 dB, which depend a little on the recursive number.

Figure 4.4 shows the optimized BER performances versus SNR at α_{opt} achieved as above for the generalized TB and ML-I receivers. At BER = 10^{-1}, the simulated improved TB receiver can provide about 3.3 dB performance advantage over the non-improved TB receiver. For the simulated improved ML-I receivers, the receivers with one, four and nine iterations can separately provide about 2.1 dB, 1.8 dB and 1.8 dB performance advantage over the non-improved ML-I ones with one, four and nine iterations, at BER = 10^{-1}. Meanwhile, Figure 4.5 shows the optimized BER performance versus SNR at the optimized α for the generalized GLRT-I receivers. At BER = 10^{-1}, the GLRT-I receivers can all provide about 1.2 dB performance advantage over the non-improved ones. As can be seen from Figure 4.4 and Figure 4.5 that, all the improved generalized TR receivers can offer significant performance gains over the non-improved ones.

The Best Value of the Integration Interval Length

In this section, the best choice of the integration interval length T_N at the optimized α achieved in the previous section is discussed. In this case, the number of $\alpha_{opt}M$ reference symbols in one observation is applied for the channel templates and the optimal length of integration interval T_N can be found as

$$T_{N_{opt1},\alpha_{opt1}} = \arg \min_{T_N \in [0,T_{ds}]} P_r \left\{ z_i(\alpha_{opt}, T_N) < 0 \right\} \tag{4.9}$$

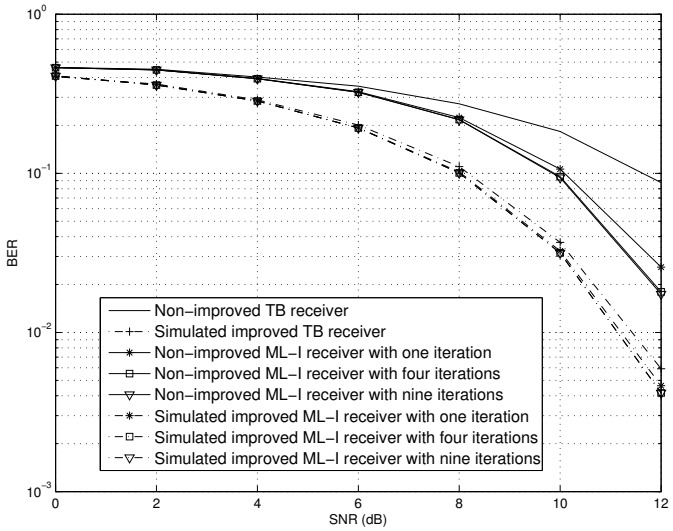

Figure 4.4: The BER versus SNR at the optimal α for the generalized TB and ML-I receivers.

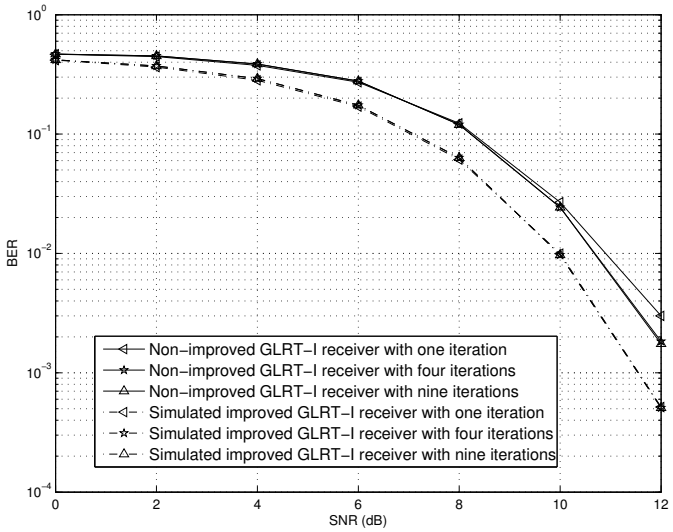

Figure 4.5: The BER versus SNR at the optimal α for the generalized GLRT-I receivers.

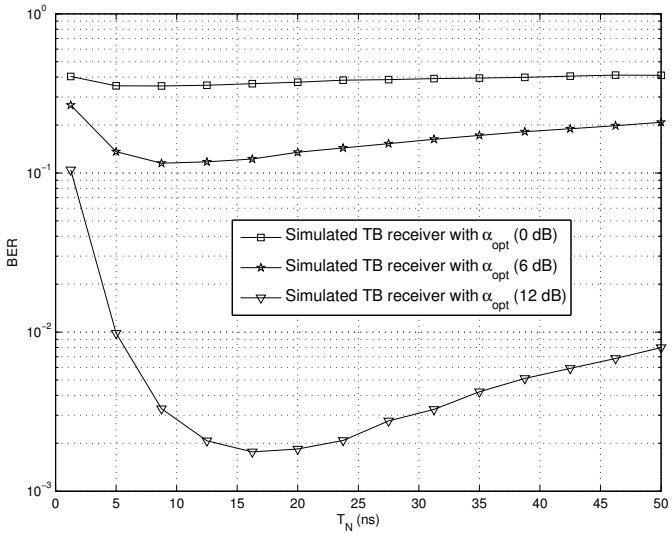

Figure 4.6: The BER versus T_N at the optimum values of α for the generalized TB receiver.

assuming that $d_i = 1$ is sent, where α_{opt} is the best value of the energy allocation factor derived in (4.8) and $z_i(\alpha_{opt}, T_N) = \mathbf{r}_i^T(\alpha)\mathbf{P}_{T_N}\hat{\mathbf{h}}_i(\alpha)$ is the decision variable.

Figure 4.6, Figure 4.7 and Figure 4.8 illustrate the optimum values of T_N at α_{opt} for the generalized TB, ML-I and GLRT-I receivers, respectively. For the improved TB receiver as in Figure 4.6, the optimal T_N for the value of SNR at 0 dB is about 5 ns, the optimal T_N for the value of SNR at 6 dB is about 8.75 ns, and the optimal T_N for the value of SNR at 12 dB is about 11.25 ns. For the improved ML-I and GLRT-I receivers, the optimal T_N relys little on the receiver recursive numbers, as can be seen from Figure 4.6 and Figure 4.7. The optimum values of $T_{N\,opt}, \alpha_{opt}$ for the ML-I receivers are all about 8.75 ns at SNR = 6 dB and all about 11.25 ns at SNR = 12 dB. Meanwhile, the optimum values of $T_{N\,opt}, \alpha_{opt}$ for the GLRT-I receivers are all about 12.5 ns at SNR = 6 dB and all about 20 ns at SNR = 12 dB. It is clear that the optimum values of $T_{N\,opt}, \alpha_{opt}$ grow with the increase of SNR,

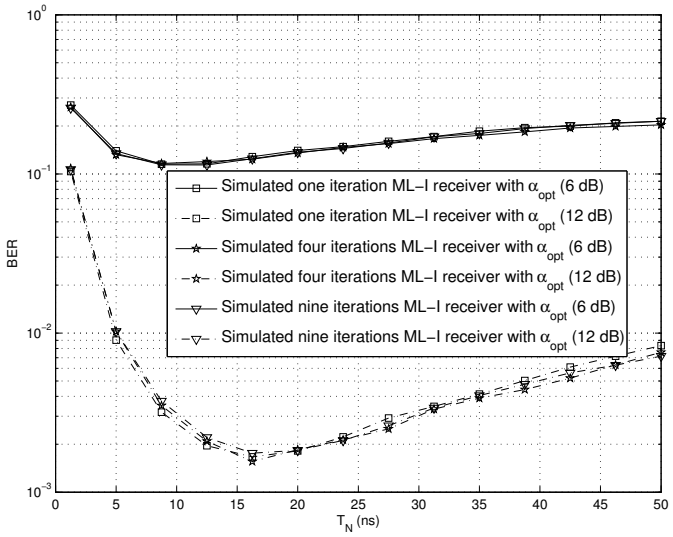

Figure 4.7: The BER versus T_N at the optimum values of α for the generalized ML-I receivers.

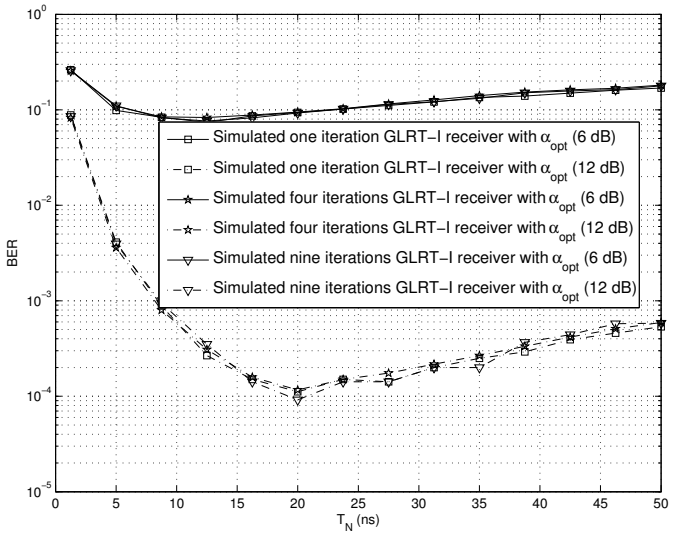

Figure 4.8: The BER versus T_N at the optimum values of α for the generalized GLRT-I receivers.

as the useful signal energy is becoming enhanced and the data is increasingly dominated by the noise. Thus, the more useful signal energy will be gathered at the correlator for the better data decision. If SNR is continuously increased, the optimal value T_N may approach its maximum value of T_{mds}.

Figure 4.9 shows the overall improved BER performance versus SNR for the generalized TB and ML-I receivers. In this case, both the optimum value of α_{opt} obtained from Figure 4.6 and the optimum value of $T_{N\,opt}, \alpha_{opt}$ obtained from Figure 4.7 are applied for the system optimization. At SNR $= 10^{-1}$, the simulated improved TB receiver can provide 4.6 dB performance improvement over the non-improved TB receiver. For the simulated improved ML-I receivers, the receivers with one, four and nine iterations can separately provide 3.8 dB, 3.5 dB and 3.5 dB performance improvements over the non-improved ones, at BER $= 10^{-1}$. One can see that the receivers with both α and T_N optimized can provide further performance improvements over the receivers with only α optimized. Specifically, a performance improvement of up to 1.3 dB can be achieved for the TB receiver, a performance improvement of up to 1.0 dB can be achieved for the ML-I receivers, and a performance improvement of up to 1.7 dB can be achieved for the GLRT-I receivers.

In addition, the overall improved BER performance versus SNR for the GLRT-I receivers is depicted in Figure 4.10. The GLRT-I receivers with one, four and nine iterations can separately provide 2.9 dB, 2.8 dB and 2.9 dB performance improvements over the non-improved ones, at BER $= 10^{-1}$. Similarly, the further improvement of up to 1.7 dB can be achieved for the GLRT-I receivers with both α and T_N optimized, compared to the ones with only α optimized.

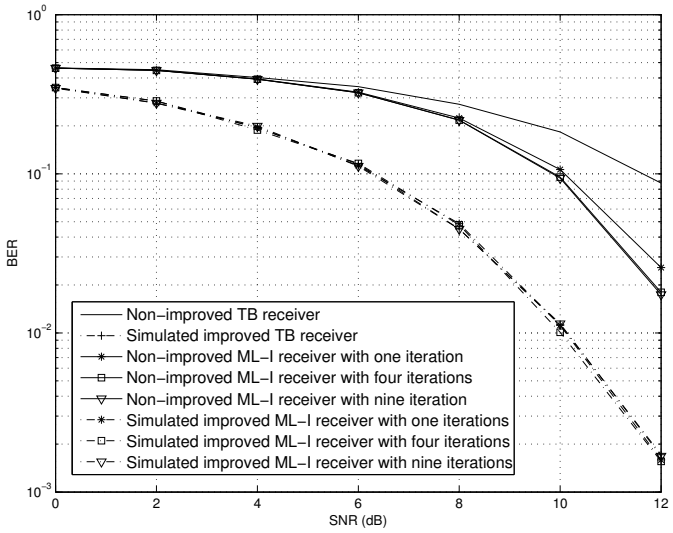

Figure 4.9: The BER versus SNR at $T_{N\,opt}, \alpha_{opt}$ and α_{opt} for the generalized TB and ML-I receivers.

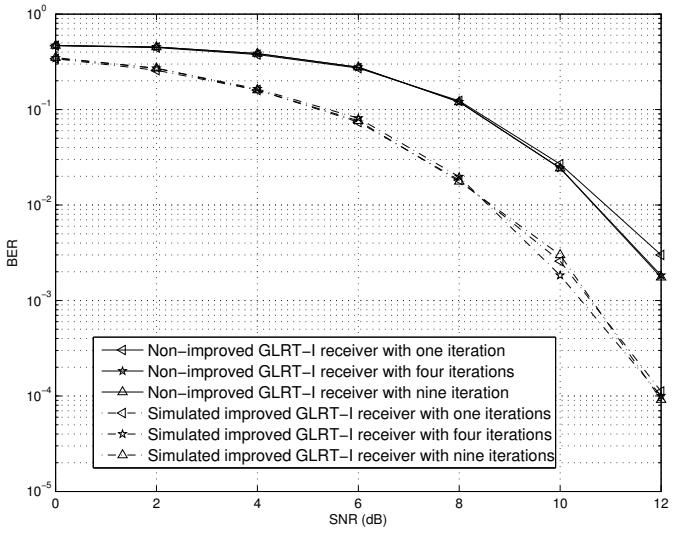

Figure 4.10: The BER versus SNR at both α and T_N optimized for the generalized GLRT-I receivers.

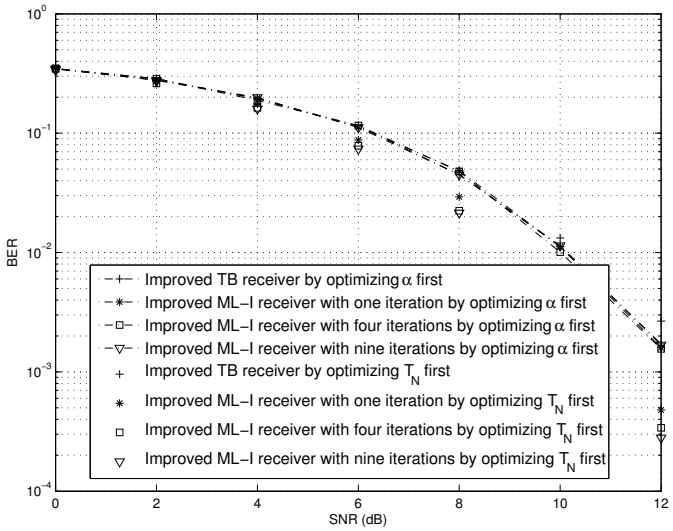

Figure 4.11: Comparison of the improved TB and ML-I receivers that optimize α first and the improved TB and ML-I receivers that optimize T_N first.

Investigations on the Optimization Order

There is no rule addressing that the energy allocation factor α has to be optimized first. Therefore, another approach for the generalized TR receivers optimization is to optimize T_N first with an initial value of α, then optimized α at $T_{N\,opt}$ obtained previously.

Figure 4.11 and Figure 4.12 compare the simulated improved TR receivers that optimize α first with those that optimize T_N first. One can see that, the performance difference for the TB receivers is less than 0.5 dB, the performance difference for the Ml-I receivers is less than 1.0 dB, and the performance difference for the GLRT-I receivers is less than 0.3 dB in all the scenarios considered. Thus, one may conduct two separate one-dimensional optimizations by either optimizing α first or optimizing T_N first, without much difference. This implies that the result from two separate one-dimensional optimizations depends little on the initial condition.

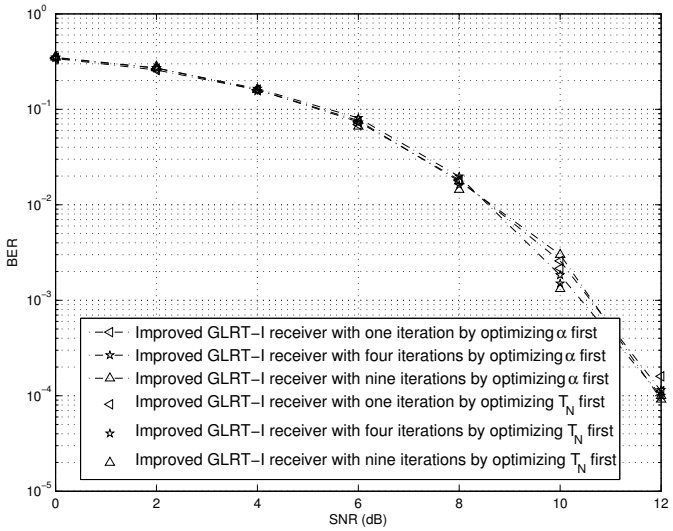

Figure 4.12: Comparison of the improved GLRT-I receivers that optimize α first and the improved GLRT-I receivers that optimize T_N first.

4.3.2 The ML-II and GLRT-II receivers

To avoid solving the formulas of $\hat{\mathbf{h}}_{i,ML-I}$ and $\hat{\mathbf{h}}_{i,GLRT-I}$ in eq.(4.6) and eq.(4.7) iteratively, the approximate ML and the approximate GLRT receivers are proposed accordingly by employing the closed-form assumption in [80]. In this chapter, they are denoted as the ML-II and the GLRT-II receivers of which the template signals are separately shown as

$$\hat{\mathbf{h}}_{i,ML-II}(\alpha) \approx \left[\mathbf{I}_L - \frac{(1-\alpha)}{N_d}\sum_{n=N_r}^{N_s-1}\frac{1-|G_i|}{\delta_e^2}\mathbf{r}_n\mathbf{r}_n^T\right]^{-1}\frac{\mathbf{c}_0}{\varepsilon} \tag{4.10}$$

and

$$\hat{\mathbf{h}}_{i,GLRT-II}(\alpha) \approx \left[\mathbf{I}_L - \frac{(1-\alpha)}{N_d-1+\alpha}\sum_{n=N_r,n\neq i}^{N_s-1}\frac{1-|G_i|}{\delta_e^2}\mathbf{r}_n\mathbf{r}_n^T\right]^{-1}\frac{\mathbf{c}_1}{\varepsilon-\frac{\varepsilon_d}{N_d}} \tag{4.11}$$

where $\mathbf{I}_L$ is a $L\times L$ identity matrix and $(\cdot)^{-1}$ denotes the inverse matrix. The coefficients of c_0, c_1 and G_i are all determined in [80].

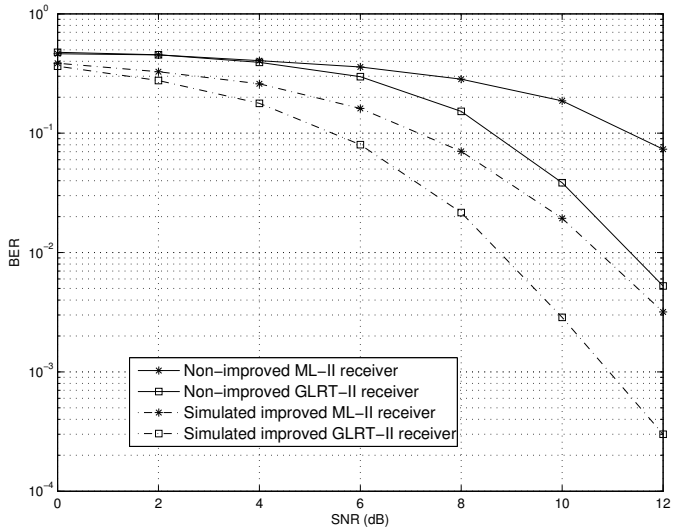

Figure 4.13: The BER versus SNR at $T_{N\,opt}, \alpha_{opt}$ and α_{opt} for the generalized ML-II and GLRT-II receivers.

By using the similar methods as in the previous section, the optimization with respect to α and/or T_N for the generalized ML-II and GLRT-II receivers are investigated as follows. In this case, the process starts with optimizing α at $T_N = T_{ds}$ by making use of eq.(4.8), then optimizing T_N at the α_{opt} by using eq.(4.9).

Figure 4.13 shows the overall BER performace versus SNR by using both the optimized α and the optimized T_N for the non-recursive receivers. At BER $= 10^{-1}$, the simulated improved ML-II receiver can provide about 4.2 dB performance gain over the non-improved ML-II receiver, and the simulated improved GLRT-II receiver can provide about 3.1 dB performance gain over the non-improved GLRT-II receiver. One can see that significant performance improvements can be achieved from the joint optimization with respect to α and T_N, for the non-recursive ML and GLRT receivers. Figure 4.14 compare the simulated improved ML-II and GLRT-II receivers that optimize α first with those that optimize T_N first. One sees that the performance difference is

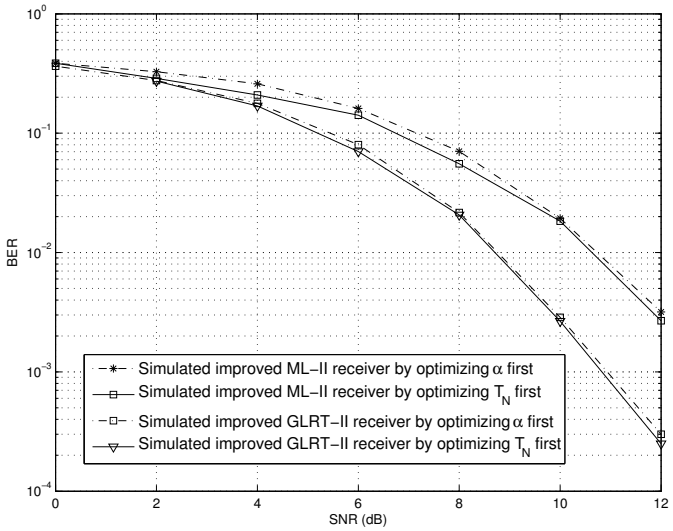

Figure 4.14: Comparison of the improved ML-II and GLRT-II receivers that optimize α first and those that optimize T_N first.

very negligible in all cases considered, as expected.

4.4 The RD, RI and RDI receivers

Three new improved generalized TR receivers with simple structures were proposed in [81], and the channel templates for them are given by

$$\hat{\mathbf{h}}_{i,RD}(\alpha) = a_1\sqrt{\frac{N_f}{\alpha\varepsilon N_r}}\sum_{m=0}^{N_r-1} d_m\mathbf{r}_m(\alpha) + b_1\sqrt{\frac{N_f}{(1-\alpha)\varepsilon N_d}}\sum_{k=N_r}^{i-1}\hat{d}_k\mathbf{r}_k(\alpha) \quad (4.12)$$

$$\begin{aligned}\hat{\mathbf{h}}_{i,RI}(\alpha) &= a_2\sqrt{\frac{N_f}{\alpha\varepsilon N_r}}\sum_{m=0}^{N_r-1} d_m\mathbf{r}_m(\alpha) + b_2\sqrt{\frac{N_f}{(1-\alpha)\varepsilon N_d}} \\ &\quad \sum_{k=N_r,k\neq i}^{N_s-1} tanh\left(\sqrt{\frac{(1-\alpha)\varepsilon}{N_d N_f {\delta_e}^4}}\mathbf{r}_k^T(\alpha)\mathbf{P}_{T_N}\hat{\mathbf{h}}_{TB}(\alpha)\right)\mathbf{r}_k(\alpha) \quad (4.13)\end{aligned}$$

$$\begin{aligned}\hat{\mathbf{h}}_{i,RDI}(\alpha) &= a_3\left(a_1\sqrt{\frac{N_f}{\alpha\varepsilon N_r}}\sum_{m=0}^{N_r-1} d_m\mathbf{r}_m(\alpha) + b_1\sqrt{\frac{N_f}{(1-\alpha)\varepsilon N_d}}\sum_{k=N_r}^{i-1}\hat{d}_k\mathbf{r}_k(\alpha)\right) \\ &+ b_3\sqrt{\frac{N_f}{(1-\alpha)\varepsilon N_d}}\sum_{l=i+1}^{N_s-1} tanh\left(\sqrt{\frac{(1-\alpha)\varepsilon}{N_d N_f {\delta_e}^4}}\mathbf{r}_l^T(\alpha)\mathbf{P}_{T_N}\hat{\mathbf{h}}_{TB}(\alpha)\right)\mathbf{r}_l(\alpha) \quad (4.14)\end{aligned}$$

respectively, where the coefficients of a_1, a_2, a_3, b_1, b_2 and b_3 are all derived in [81], and $\hat{\mathbf{h}}_{TB}(\alpha)$ is the channel template for the TB-based receiver given by eq.(4.5). The receiver using eq.(4.12) is defined as the reference-decision (RD) receiver, the receiver using eq.(4.13) as the reference-information (RI) receiver, and the receiver using eq.(4.14) as the reference-decision-information (RDI) receiver.

In the next section, the BERs of the RD, RI and RDI receivers are improved with respect to α and T_N. An analytical method for the improvement is difficult, if not impossible. To the best of the author's knowledge, there is no exact closed-form expression for the BER of the TR receiver in the literature. This is mainly caused by the multipath fading channel in $\mathbf{r}_i(\alpha)$,

the complicated structure of $\hat{\mathbf{h}}_i(\alpha)$ in the correlator, and the cross terms in the decision variable. In order to overcome this difficulty, one may resort to a semi-analytical method, similar to that in [79], by approximating the cross terms as Gaussian to obtain the effective SNR and therefore, the approximate BER. However, the values of α and T_N optimize the effective SNR or the approximate BER do not necessarily optimize the real BER.

4.4.1 BER Improvements

In this section, both semi-analytical and simulation methods are investigated. It will be shown that values of α and T_N optimizing the effective SNR or the approximate BER in the semi-analytical method are different from values of α and T_N optimizing the real BER in the simulation.

In the semi-analytical method, the decision variable for the ith symbol/bit is derived as

$$z_i(\alpha, T_N) = \mathbf{r}_i^T(\alpha)\mathbf{P}_{T_N}\hat{\mathbf{h}}_i(\alpha, T_N). \tag{4.15}$$

For the RD receiver, by substituting eq.(4.3) and eq.(4.12) into eq.(4.15), one has $z_{i,RD}(\alpha, T_N) = d_i S_{RD}(\alpha, T_N) + N_{RD}(\alpha, T_N)$ with

$$\begin{aligned} S_{RD}(\alpha, T_N) &= a_1\sqrt{\frac{\varepsilon_i(\alpha)N_f}{\alpha\varepsilon N_r}}\left(\sum_{m=0}^{N_r-1}\sqrt{\varepsilon_m(\alpha)}\right)\mathbf{h}_{RD}{}^T\mathbf{P}_{T_N}\mathbf{h}_{RD} \\ &+ b_1\sqrt{\frac{\varepsilon_i(\alpha)N_f}{(1-\alpha)\varepsilon N_d}}\left(\sum_{k=N_r}^{i-1}\hat{d}_k d_k\sqrt{\varepsilon_k(\alpha)}\right)\mathbf{h}_{RD}{}^T\mathbf{P}_{T_N}\mathbf{h}_{RD} \end{aligned} \tag{4.16}$$

and

$$
\begin{aligned}
N_{RD}(\alpha, T_N) &= d_i a_1 \sqrt{\frac{\varepsilon_i(\alpha) N_f}{\alpha \varepsilon N_r}} \mathbf{h}_{RD}^T \mathbf{P}_{T_N} \left(\sum_{m=0}^{N_r-1} d_m \mathbf{n}_m \right) \\
&+ d_i b_1 \sqrt{\frac{\varepsilon_i(\alpha) N_f}{(1-\alpha)\varepsilon N_d}} \mathbf{h}_{RD}^T \mathbf{P}_{T_N} \left(\sum_{k=N_r}^{i-1} \hat{d}_k \mathbf{n}_k \right) \\
&+ a_1 \sqrt{\frac{N_f}{\alpha \varepsilon N_r}} \left[\sum_{m=0}^{N_r-1} \sqrt{\varepsilon_m(\alpha)} \right] \mathbf{n}_i^T \mathbf{P}_{T_N} \mathbf{h}_{RD} \\
&+ b_1 \sqrt{\frac{N_f}{(1-\alpha)\varepsilon N_d}} \left[\sum_{k=N_r}^{i-1} \hat{d}_k d_k \sqrt{\varepsilon_k(\alpha)} \right] \mathbf{n}_i^T \mathbf{P}_{T_N} \mathbf{h}_{RD} \\
&+ a_1 \sqrt{\frac{N_f}{\alpha \varepsilon N_r}} \mathbf{n}_i^T \mathbf{P}_{T_N} \left(\sum_{m=0}^{N_r-1} d_m \mathbf{n}_m \right) \\
&+ b_1 \sqrt{\frac{N_f}{(1-\alpha)\varepsilon N_d}} \mathbf{n}_i^T \mathbf{P}_{T_N} \left(\sum_{k=N_r}^{i-1} \hat{d}_k \mathbf{n}_k \right). \qquad (4.17)
\end{aligned}
$$

The effective SNR can be derived from eq.(4.16) and eq.(4.17) as

$$
\begin{aligned}
\rho_{RD}(\alpha, T_N) &= \frac{S_{RD}^2(\alpha, T_N)}{N_{RD}^2(\alpha, T_N)} \\
&= \frac{\left(a_1^2 + \frac{b_1^2 c_2^2}{N_d^2} \right) N_f^2 \varepsilon_i(\alpha) \|\mathbf{h}_{RD}(T_N)\|^4}{\left[\left(\frac{1-\alpha+\alpha N_d}{\alpha N_d} \right) a_1^2 + \left(\frac{i-N_r+{c_2}^2}{N_d^2} \right) b_1^2 \right] {\delta_e}^2 \|\mathbf{h}_{RD}(T_N)\|^2 + \left[\frac{a_1^2}{\alpha} + \frac{b_1^2 (i-N_r)}{(1-\alpha)N_d} \right] \frac{T_N + T_s}{\varepsilon N_f^2 T_s} {\delta_e}^4} \qquad (4.18)
\end{aligned}
$$

where $c_2 = \sum_{k=N_r}^{i-1} \hat{d}_k d_k$ and $\|\mathbf{h}(T_N)\|^4 = \left\| \mathbf{h}^T \mathbf{P}_{T_N} \mathbf{h} \right\|^2$.

For the RI receiver, by substituting eq.(4.3) and eq.(4.13) into eq.(4.15),

one has $z_{i,RI}(\alpha, T_N) = d_i S_{RI}(\alpha, T_N) + N_{RI}(\alpha, T_N)$ with

$$\begin{aligned} S_{RI}(\alpha, T_N) &= a_2 \sqrt{\frac{\varepsilon_i(\alpha) N_f}{\alpha \varepsilon N_r}} \left(\sum_{m=0}^{N_r-1} \sqrt{\varepsilon_m(\alpha)} \right) \mathbf{h}_{RI}{}^T \mathbf{P}_{T_N} \mathbf{h}_{RI} \\ &+ b_2 \frac{N_f}{N_d^2} \sqrt{\varepsilon_i(\alpha)} \left[\sum_{k=N_r, k\neq i}^{M-1} d_k \cdot tanh(z) \right] \mathbf{h}_{RI}{}^T \mathbf{P}_{T_N} \mathbf{h}_{RI} \end{aligned} \quad (4.19)$$

and

$$\begin{aligned} N_{RI}(\alpha, T_N) &= d_i a_2 \sqrt{\frac{\varepsilon_i(\alpha) N_f}{\alpha \varepsilon N_r}} \mathbf{h}_{RI}^T \mathbf{P}_{T_N} \left(\sum_{m=0}^{N_r-1} d_m \mathbf{n}_m \right) \\ &+ d_i b_2 \frac{N_f}{N_d^2} \mathbf{h}_{RI}^T \mathbf{P}_{T_N} \left[\sum_{k=N_r, k\neq i}^{M-1} \mathbf{n}_k \cdot tanh(z) \right] \\ &+ a_2 \sqrt{\frac{N_f}{\alpha \varepsilon N_r}} \left[\sum_{m=0}^{N_r-1} \sqrt{\varepsilon_m(\alpha)} \right] \mathbf{n}_i^T \mathbf{P}_{T_N} \mathbf{h}_{RI} \\ &+ b_2 \frac{N_f}{N_d^2} \left[\sum_{k=N_r, k\neq i}^{M-1} d_k \cdot tanh(z) \right] \mathbf{n}_i^T \mathbf{P}_{T_N} \mathbf{h}_{RI} \\ &+ a_2 \sqrt{\frac{N_f}{\alpha \varepsilon N_r}} \mathbf{n}_i^T \mathbf{P}_{T_N} \left(\sum_{m=0}^{N_r-1} d_m \mathbf{n}_m \right) \\ &+ b_2 \frac{N_f}{N_d^2} \frac{1}{\sqrt{\varepsilon_i(\alpha)}} \mathbf{n}_k^T \mathbf{P}_{T_N} \left[\sum_{k=N_r, k\neq i}^{M-1} \mathbf{n}_k \cdot tanh(z) \right] \end{aligned} \quad (4.20)$$

where

$$\begin{aligned} tanh(z) &= tanh \left\{ \sqrt{\frac{1}{N_r^2 \delta_e^4}} \left[d_k \varepsilon_k(\alpha) N_r \mathbf{h}_{RI}^T \mathbf{P}_{T_N} \mathbf{h}_{RI} \right. \right. \\ &+ d_k \sqrt{\varepsilon_k(\alpha)} \mathbf{h}_{RI}^T \mathbf{P}_{T_N} \left(\sum_{m=0}^{N_r-1} d_m \mathbf{n}_m \right) \\ &+ N_r \sqrt{\varepsilon_k(\alpha)} \mathbf{n}_k^T \mathbf{P}_{T_N} \mathbf{h}_{RI} \\ &+ \left. \left. \mathbf{n}_k^T \mathbf{P}_{T_N} \left(\sum_{m=0}^{N_r-1} d_m \mathbf{n}_m \right) \right] \right\} \end{aligned} \quad (4.21)$$

is a tangent function. Using similar methods, the effective SNRs for the RI receiver can be derived as

$$\begin{aligned}\rho_{RI}(\alpha, T_N) &= \frac{S_{RI}^2(\alpha, T_N)}{N_{RI}^2(\alpha, T_N)} \\ &= \frac{\left(a_2^2 + \frac{b_2^2 d_1^2 N_f}{N_d^4}\right) N_f \varepsilon_i(\alpha) \|\mathbf{h}_{RI}(T_N)\|^4}{\left[\left(\frac{1-\alpha+\alpha N_d}{\alpha N_d N_f}\right) a_2^2 + \left(\frac{d_2+d_1^2}{N_d^4}\right) b_2^2\right] {\delta_e}^2 \|\mathbf{h}_{RI}(T_N)\|^2 + \left[\frac{a_2^2}{\alpha N_f} + \frac{b_2^2 d_2}{(1-\alpha) N_d^3}\right] \frac{T_N + T_s}{\varepsilon N_f^2 T_s} {\delta_e}^4}\end{aligned} \tag{4.22}$$

where $d_1 = \sum_{k=N_r, \neq i}^{N_s-1} a_k x$, $d_2 = \sum_{k=N_r, \neq i}^{N_s-1} x^2$, and $x = tanh\left(\sqrt{\frac{(1-\alpha)\varepsilon}{N_d N_f {\delta_e}^4}} \mathbf{r}_k^T(\alpha) \mathbf{P}_{T_N} \hat{\mathbf{h}}_{TB}(\alpha)\right)$.

For the RDI receiver, by substituting eq.(4.3) and eq.(4.14) into eq.(4.15), one has $z_{i,RDI}(\alpha, T_N) = d_i S_{RDI}(\alpha, T_N) + N_{RDI}(\alpha, T_N)$ with

$$\begin{aligned} S_{RDI}(\alpha, T_N) &= a_3 a_1 \sqrt{\frac{\varepsilon_i(\alpha) N_f}{\alpha \varepsilon N_r}} \left(\sum_{m=0}^{N_r-1} \sqrt{\varepsilon_m(\alpha)}\right) \mathbf{h}_{RDI}^T \mathbf{P}_{T_N} \mathbf{h}_{RDI} \\ &+ a_3 b_1 \sqrt{\frac{\varepsilon_i(\alpha) N_f}{(1-\alpha) \varepsilon N_d}} \left(\sum_{k=N_r}^{i-1} \hat{d}_k d_k \sqrt{\varepsilon_k(\alpha)}\right) \mathbf{h}_{RDI}^T \mathbf{P}_{T_N} \mathbf{h}_{RDI} \\ &+ b_3 \frac{N_f}{N_d^2} \sqrt{\varepsilon_i(\alpha)} \left[\sum_{k=N_r, k\neq i}^{M-1} d_k \cdot tanh(z)\right] \mathbf{h}_{RDI}^T \mathbf{P}_{T_N} \mathbf{h}_{RDI} \end{aligned} \tag{4.23}$$

and

$$\begin{aligned} N_{RDI}(\alpha, T_N) &= d_i a_3 a_1 \sqrt{\frac{\varepsilon_i(\alpha) N_f}{\alpha \varepsilon N_r}} \mathbf{h}_{RDI}^T \mathbf{P}_{T_N} \left(\sum_{m=0}^{N_r-1} d_m \mathbf{n}_m\right) \\ &+ d_i a_3 b_1 \sqrt{\frac{\varepsilon_i(\alpha) N_f}{(1-\alpha) \varepsilon N_d}} \mathbf{h}_{RDI}^T \mathbf{P}_{T_N} \left(\sum_{k=N_r}^{i-1} \hat{d}_k \mathbf{n}_k\right) \\ &+ a_3 a_1 \sqrt{\frac{N_f}{\alpha \varepsilon N_r}} \left[\sum_{m=0}^{N_r-1} \sqrt{\varepsilon_m(\alpha)}\right] \mathbf{n}_i^T \mathbf{P}_{T_N} \mathbf{h}_{RDI} \\ &+ a_3 b_1 \sqrt{\frac{N_f}{(1-\alpha) \varepsilon N_d}} \left[\sum_{k=N_r}^{i-1} \hat{d}_k d_k \sqrt{\varepsilon_k(\alpha)}\right] \mathbf{n}_i^T \mathbf{P}_{T_N} \mathbf{h}_{RDI} \end{aligned}$$

$$
\begin{aligned}
&+ \quad a_3 a_1 \sqrt{\frac{N_f}{\alpha \varepsilon N_r}} \mathbf{n}_i^T \mathbf{P}_{T_N} \left(\sum_{m=0}^{N_r-1} d_m \mathbf{n}_m \right) \\
&+ \quad a_3 b_1 \sqrt{\frac{N_f}{(1-\alpha)\varepsilon N_d}} \mathbf{n}_i^T \mathbf{P}_{T_N} \left(\sum_{k=N_r}^{i-1} \hat{d}_k \mathbf{n}_k \right) \\
&+ \quad d_i b_3 \frac{N_f}{N_d^2} \mathbf{h}_{RDI}^T \mathbf{P}_{T_N} \left[\sum_{k=N_r, k\neq i}^{M-1} \mathbf{n}_k \cdot tanh(z) \right] \\
&+ \quad b_3 \frac{N_f}{N_d^2} \left[\sum_{k=N_r, k\neq i}^{M-1} d_k \cdot tanh(z) \right] \mathbf{n}_i^T \mathbf{P}_{T_N} \mathbf{h}_{RDI} \\
&+ \quad b_3 \frac{N_f}{N_d^2} \frac{1}{\sqrt{\varepsilon_i(\alpha)}} \mathbf{n}_k^T \mathbf{P}_{T_N} \left[\sum_{k=N_r, k\neq i}^{M-1} \mathbf{n}_k \cdot tanh(z) \right]. \qquad (4.24)
\end{aligned}
$$

Therefore, the effective SNRs for the RDI receiver can be similarly derived as

$$
\begin{aligned}
\rho_{RDI}(\alpha, T_N) &= \frac{S_{RDI}^2(\alpha, T_N)}{N_{RDI}^2(\alpha, T_N)} \\
&= \frac{\left(a_1^2 a_3^2 + \frac{a_3^2 b_1^2 c_2}{N_d^2} + \frac{d_1^2 b_3^2 N_f}{N_d^4} \right) {N_f}^2 \varepsilon_i(\alpha) \|\mathbf{h}_{RDI}(T_N)\|^4}{\left[\left(\frac{1-\alpha+\alpha N_d}{\alpha N_d} \right) a_1^2 a_3^2 + \left(\frac{i-N_r+c^2}{N_d^2} \right) b_1^2 a_3^2 + \frac{(d_2+{d_1}^2) {b_3}^2 N_f}{N_d^4} \right] {\delta_e}^2 \|\mathbf{h}_{RDI}(T_N)\|^2 + Y \frac{T_N+T_s}{\varepsilon N_f^2 T_s} {\delta_e}^4} \qquad (4.25)
\end{aligned}
$$

where $Y = \frac{a_1^2 a_3^2}{\alpha} + \frac{(i-N_r) a_3^2 {b_1}^2}{(1-\alpha) N_d} + \frac{d_2 b_3^2 N_f}{(1-\alpha) N_d^3}$.

Then, using the Gaussian approximation, the approximate BER can be written as $BER_{semi-analy} = Q\left(\sqrt{\rho_x(\alpha, T_N)} \right)$, for $x \in \{RD, RI, RDI\}$. Thus, the best value of α optimizing $BER_{semi-analy}$ can be found as

$$
\alpha_{opt2} = \arg \min_{\alpha \in (0,1)} Q\left(\sqrt{\rho_x(\alpha, T_N)} \right), \qquad (4.26)
$$

where the length of the integration interval is fixed at $T_N = T_{mds}$, and the best

value of the integration interval length can be found as

$$T_{N_{opt2},\alpha_{opt2}} = \arg \min_{T_N \in (0,T_{ds}]} Q\left(\sqrt{\rho_x(\alpha_{opt2}, T_N)}\right) \tag{4.27}$$

where α_{opt2} is the best value of the energy allocation factor derived in eq.(4.26). One sees that the values of α and T_N minimizing $BER_{semi-analy}$ are actually the same as those maximizing the effective SNR $\rho_x(\alpha, T_N)$, similar to [79].

In the simulation, the best value of α and the best length of the integration interval for the RD, RI and RDI receivers can be similarly found from eq.(4.8) and eq.(4.9), by using the "brute-force" method. The novelty of this work lies in the fact that it uses the semi-analytical method to minimize the approximate BER or to maximize the effective SNR as well as the simulation method to minimize the real BER for the receivers in [81], with respect to the energy allocation and the correlator integration interval length. Reference [79] used a semi-analytical method to minimize the approximate BER or to maximize the effective SNR for the receivers in [79]. This does not present a direct improvement of the real BER performance.

4.4.2 Numerical Results and Discussion

In this section, the performances of the improved receivers are examined. One may use the same method to examine systems with other parameters.

Figure 4.15 shows the BER versus α for the SNR value of 10 dB and $T_N = T_{mds}$. Several observations can be made. First, the BERs of all the improved receivers first decrease then increase when α increases. The performance difference for different values of α is significant. For example, for the simulated improved RDI receiver, the BER at $\alpha = 0.167$ is almost ten times

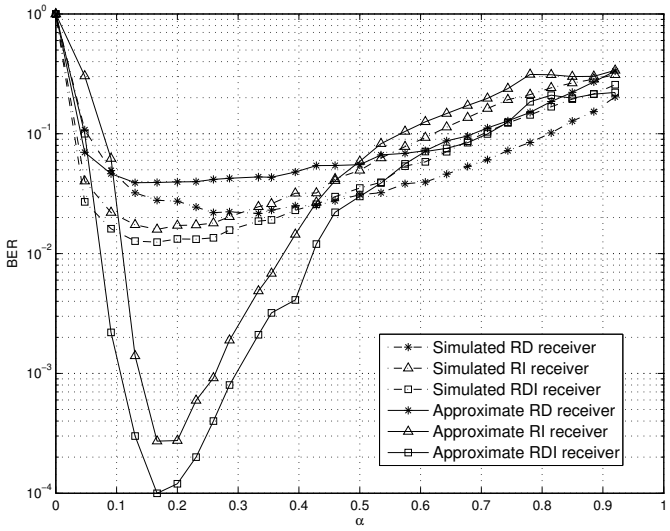

Figure 4.15: The BER versus α at SNR = 10 dB and $T_N = T_{mds}$.

smaller than that at $\alpha = 0.85$. The effect of α on the performances of the approximate improved RI and RDI receivers using the Gaussian approximation is larger than that on the performances of the simulated improved RI and RDI receivers, due to the over-estimation of the Gaussian approximation. Second, the best value of α is about $\alpha = 0.33$ for the simulated improved RD receiver and about $\alpha = 0.167$ for the simulated improved RI and RDI receivers, as the RD receiver only uses $(i-1)$ previous data decisions in the channel template and therefore, it requires more reference energy to achieve a channel template with sufficient accuracy. Third, the simulated improved receivers do not have exactly the same best values of α as the approximate improved receivers, as expected, as the best values of α minimize the real BER for the simulated improved receivers, while they maximize the effective SNR for the approximate improved receivers. It should be noted that α gives the ratio of the number of reference symbols to the total number of symbols in one data packet. Additional simulations not described in detail here for brevity show that the best

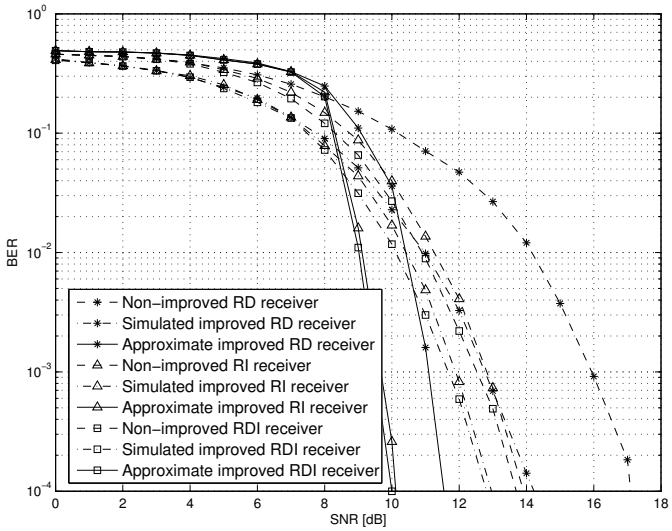

Figure 4.16: The BER versus SNR for non-improved receivers and improved receivers using α_{opt}.

value of α is not related to the bin size in the channel model.

Figure 4.16 shows the BER versus SNR for optimized α and non-optimized α at $T_N = T_{mds}$. When the SNR is smaller than 8dB, the approximate improved receivers underperform the simulated improved receivers, as the approximate improved receivers cannot find the real best α in this case due to the under-estimation of the Gaussian approximation for the interference-plus-noise terms. When the SNR is larger than 8dB, the approximate improved receivers outperform the simulated improved receivers, due to the over-estimation of the Gaussian approximation. One also sees that all the simulated improved receivers outperform the non-improved receivers. For example, at BER = 10^{-3}, the simulated improved RD receiver has a performance gain of about 3.1 dB over the non-improved RD receiver, the simulated improved RI receiver has a performance gain of about 1.1 dB over the non-improved RI receiver, and the simulated improved RDI receiver has a performance gain of about 0.9 dB over the non-improved RDI receiver. The performance gains are

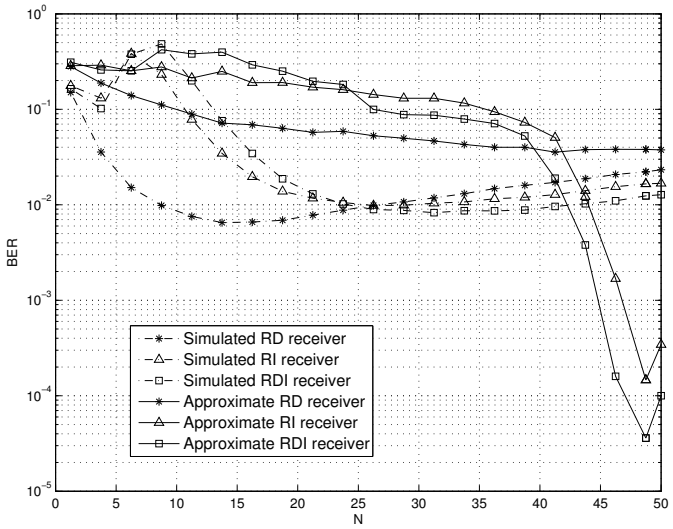

Figure 4.17: The BER versus T_N using α_{opt} at SNR = 10 dB.

significant. Furthermore, the performance gain of the simulated improved RD receiver is the largest, while the performance gain of the simulated improved RDI receiver is the smallest. This suggests that the RD receiver benefits the most from optimization of α. This might be caused by the fact that the channel template for the RD receiver does not use the received signal corresponding to the data symbols, while the channel templates for both the RI and RDI receivers do use the received signal corresponding to the data symbols. Therefore, the RD receiver suffers more from non-optimized α. Also, comparing the RDI receiver with the RD receiver and the RI receiver, one sees that the simulated improved RDI receiver performs best when the SNR is larger than 7 dB. The performance gain increases as the SNR increases. However, it is not as large as that among the non-improved receivers, as the improved receivers are closer to the performance limits and thus, they have less room for improvement from each other.

Figure 4.17 shows the BER versus T_N for the SNR value of 10 dB using

α_{opt}. The BER changes significantly when T_N increases. The best value of T_N is about $15ns$ for the simulated improved RD receiver, about $25ns$ for the simulated improved RI receiver, and about $31.25ns$ for the simulated improved RDI receiver. Thus, the RD receiver has the smallest optimum integration interval length, while the RDI receiver has the largest optimum integration interval length. As a result, the simulated improved RD receiver requires the least amount of memory as well as computation to achieve improved performance. Notice that the BER curves for the simulated improved RI and RDI receivers are not smooth when T_N is small, as their channel templates use the received data symbols (the last term in eq.(4.13) or eq.(4.14)). This term contains a *tanh* function. When the value of T_N is small such that the input of *tanh* is small, the *tanh* function in the last term of eq.(4.13) or eq.(4.14) is large due to the large slope of the *tanh* function. In this case, a noise term to a power of larger than two occurs in the decision variable, in addition to the squared noise. This causes the fluctuation. When the value of T_N is large such that the input of *tanh* is large, the *tanh* function will be hard-limited. In this case, the squared noise term becomes dominant. As a result, the curves for the RI and RDI receivers become as smooth as the RD receivers. Thus, the fluctuation at small T_N is inherent in the RI and RDI receivers, and it cannot be removed by averaging many channel realizations. One sees that the simulated improved RD receiver does not have the *tanh* function in its template and thus, it does not have this behavior. For the approximate improved receivers, the best T_N for the RD receiver is $T_N = 41.25ns$, while the best T_N for the RI and RDI receivers is $T_N = 48.75ns$.

Figure 4.18 shows the BER versus SNR when neither α or T_N is optimized and when both α and T_N are optimized. Again, all the improved re-

ceivers outperform the non-improved receivers in all the cases considered. The performance gains using α_{opt} and $T_{N\,opt,\alpha_{opt}}$ are much larger than those using α_{opt} only in Figure 4.16. For example, at BER = 10^{-3}, the performance gain of the improved RD receiver over the non-improved RD receiver is about 4.2 dB, the performance gain of the improved RI receiver over the non-improved RI receiver is about 1.4 dB, and the performance gain of the improved RDI receiver over the non-improved RDI receiver is about 1.2 dB. The performance gains increase as the SNR increases. Again, the RD receiver has the largest performance gain, while the RDI receiver has the smallest performance gain. Thus, the RD receiver benefits the most from optimization of α and T_N. In fact, the improved RD receiver performs the best when the SNR is larger than 0 dB and smaller than 11 dB. This is explained as follows. The channel templates for the RI and RDI receivers use the received signal corresponding to the data symbols. Thus, they suffer more from the noise when the SNR is small. The BERs of the RI and RDI receivers decay quickly when the SNR is large and it increases, as the RI and RDI receivers suffer less from the noise due to the large SNR and benefits more from using more samples. When the SNR is large enough, the RI and RDI receivers outperform the RD receiver. Figure 4.19 compares the simulated improved receivers that optimize α first with those that optimize T_N first. One sees that their performance difference is less than 0.5 dB in all the cases considered, as expected.

Table 4.1 shows the optimum values of α and T_N for the simulated receivers in two circumstances (either optimize α first or optimize T_N first) under different SNR scenarios considered in this paper. One can choose the best values of α and T_N for the receiver settings from Table I according to the specific applications. The best values for other conditions may be tabulated in

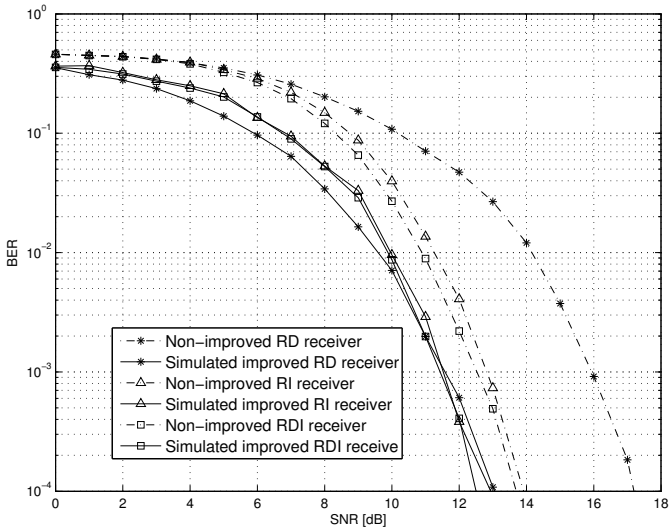

Figure 4.18: The BER versus SNR using neither α_{opt} or $T_{N_{opt},\alpha_{opt}}$ and both α_{opt} and $T_{N_{opt},\alpha_{opt}}$.

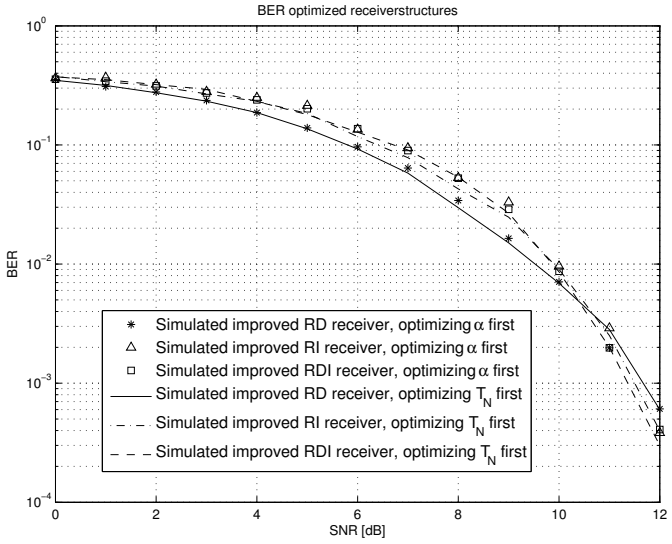

Figure 4.19: Comparison of the simulated improved receivers that optimize α first and the simulated improved receivers that optimize T_N first.

Table 4.1: The Best Values of α and $T_N(ns)$ for the Simulated TR Receivers at different SNRs

SNR (dB)	RD receivers				RI receivers				RDI receivers			
	α_{opt}	$T_{N_{opt},\alpha_{opt}}$	$T_{N_{opt}}$	$\alpha_{opt,T_{N_{opt}}}$	α_{opt}	$T_{N_{opt},\alpha_{opt}}$	$T_{N_{opt}}$	$\alpha_{opt,T_{N_{opt}}}$	α_{opt}	$T_{N_{opt},\alpha_{opt}}$	$T_{N_{opt}}$	$\alpha_{opt,T_{N_{opt}}}$
0	0.39	7.50	8.13	0.46	0.39	13.8	8.13	0.26	0.39	10.6	8.13	0.43
1	0.43	8.13	8.13	0.46	0.46	13.8	7.50	0.20	0.46	13.1	7.50	0.20
2	0.33	8.75	8.13	0.50	0.35	15.0	7.50	0.13	0.35	13.1	8.13	0.20
3	0.43	8.75	8.75	0.46	0.33	18.1	8.75	0.13	0.33	15.6	9.38	0.13
4	0.43	8.75	8.75	0.29	0.35	21.3	9.38	0.13	0.35	15.6	9.38	0.09
5	0.35	9.38	10.6	0.31	0.33	21.3	10.6	0.09	0.33	21.9	11.9	0.09
6	0.35	12.5	10.6	0.26	0.20	21.3	11.9	0.09	0.20	21.3	14.4	0.09
7	0.39	13.8	11.9	0.17	0.20	23.8	13.1	0.09	0.17	23.8	17.5	0.09
8	0.35	14.4	11.9	0.26	0.17	24.4	15.0	0.09	0.17	29.4	18.8	0.09
9	0.33	14.4	13.8	0.26	0.23	28.8	15.0	0.09	0.23	33.8	23.1	0.09
10	0.35	14.4	11.3	0.26	0.17	28.8	16.9	0.09	0.17	32.5	26.9	0.13
11	0.20	15.0	10.0	0.26	0.20	29.4	18.1	0.09	0.20	30.0	36.3	0.17
12	0.23	16.3	15.0	0.26	0.13	28.8	27.5	0.09	0.13	28.1	26.9	0.13

a similar way. These tables can serve as guidelines for receiver design. From these tables, one can estimate the SNR using methods in [85] and then use the estimated SNR to determine the receiver settings.

4.5 Conclusions

The BER performances of generalized UWB TR receivers proposed in the literature have been optimized with respect to the energy allocation factor and the length of the integration interval. For the generalized TB, ML- and GLRT-receivers in [79] and [80], numerical results have shown that the optimization can provide a performance gain of up to 4.6 dB in SNR. The receivers using optimization of the energy allocation factor can achieve better performances by redistributing a fixed amount of energy between the reference and the data symbols only, while the receivers using optimization of both the energy allocation factor and the integration interval length can achieve better performances and simpler structures by using less samples in the correlator. On the other hand, for the RD, RI and RDI receivers in [81], similar optimization results as well as a performance gain of up to 4.2 dB can be achieved. However, in both cases of either only optimizing α or jointly optimizing α and T_N, the SNR must be estimated in order to identify the optimum energy allocation and the optimum length of the integration interval.

This chapter focuses on the optimization with respect to several parameters for the generalized UWB TR receivers. In this case, a number of $\frac{\alpha}{1-\alpha}N_d$ reference symbols and a number of N_d data symbols are transmitted in one observation. Thus, the data rate is $(1-\alpha)\cdot\frac{1}{T_b}(\alpha \in (0,1))$, whereas the data rate for the traditional TR receiver in [53] is $\frac{1}{T_b}$. When the data duration T_b

is fixed, the data rate of the generalized TR receivers is lower that that of the traditional TR receiver. This is due to the penalty of excessive reference symbols in the generalized TB receivers. However, the generalized TR receiver benefits from its better performance and simpler implementation.

Chapter 5

Conclusions and Future Work

5.1 Introduction

This chapter summaries the main findings of the research, presents the conclusions and provides an outline of some ideas for the further work. The research reported in this thesis is mainly based on the optimization for the transmitted-reference (TR) receivers in a ultra-wide bandwidth (UWB) system. By using the approaches proposed in this thesis, all the improved TR receivers can offer future data communications with more flexibility and much improved quality of service (QoS).

This chapter is organized as follows. *Section 5.2* summaries the main findings of the research work, whilst *Section 5.3* presents the main conclusions regarding the optimization. *Section 5.4* discusses the further work and future potential issues of research and development.

5.2 Summary of the main findings

The issue of receiver optimization is investigated in this thesis. Particularly, two types of the TR receivers, traditional autocorrelation TR receivers and generalized TR receivers, are improved in terms of performance. The main findings related to these two types of receivers are presented in *Chapter 3* and *Chapter 4*. These work will be summarized as follows:

- **Optimizations for the traditional TR receiver;**

  In the traditional TR signalling system,a pulse pair is transmitted per frame, where the first pulse corresponds to the reference signal and the T_d-second-delayed pulse corresponds to the data signal. Then, the received data signal is correlated with the received reference signal for data detection. Normally, the time delay T_d between reference and data pulses is larger than the maximum channel delay spread T_{mds} to avoid interference within the pulse pair. However, the value of T_d does not need to be greater than T_{mds} all the time, as this time delay affects the energy allocation as well.

  As discussed in the main content that, if T_d is too large, the interference between two successive pulses per frame can be eliminated but the energy allocated to the data signal will be greatly reduced when the total energy per frame is fixed and hence, the energy of the received data signal gathered at the correlator will not be enough for a reliable decision. This will result in a performance degradation; if T_d is too small, the significantly enhanced inter-pulse interference may degrade the performance as well, although the energy allocated to the data signal increased. Thus, there exists the best tradoff between IPI and energy allocation.

In *Chapter 3*, the traditional TR receiver is optimized with respect to the inter-pulse time delay T_d, which is related to both the IPI term and the energy allocation factor.

- **Optimizations for the generalized TR receivers.**

  The generalized TR receivers were proposed for their improved performances and increased data rates over the traditional TR receiver. In the generalized TR system, each frame contains only one pulse. A number of N_d data symbols is transmitted after a number of N_r reference symbols per block. At the receiver, the template signal used at the correlator is the combination of the N_r previous reference symbols in a block, as in the training-based (TB) TR receiver. For various generalized TR receivers, their templates are slightly different.

  The numbers of N_r and N_d are highly related to the receiver performance. Assuming that the number of data symbols N_d and the total energy per block are fixed, the excellent template signal can be obtained if N_r is too large, while the energy allocated to the data symbols per block is very small such that the received data signal is not reliable for data detection. This will cause a performance degradation. On the other hand, if N_r is too small, the energy distributed to the data symbols is increased but the template gets worse. As a result, the performance will be reduced as well. Thus, the choice of N_r can give the best tradeoff between th numbere of reference symbols and performance.

  Furthermore, the performance can be significantly influenced by the integration interval length at the correlator. This is because: 1). if the integration range is too wide, an excessive noise will be introduced for

correlation and results in a performance reduction, although the most energy of the useful data signal is gathered; 2). if the integration range is too small, much noise can be suppressed but also a great amount of useful signal will be omitted simultaneously. This will cause a performance degradation similarly.

The optimization with respect to the number of reference symbols per block and the integration interval length is presented in *Chapter 4*.

5.3 Conclusions

The objective of the thesis is the optimization of the UWB TR receivers, as described in *Section 5.2*. In a similar way, the major original contributions to knowledge are shown as below:

- **Optimizations for the traditional TR receiver;**

  The time delay T_d within the pulse pair in the traditional TR receiver was optimized in terms of two criteria, as shown in *Chapter 3*. In particular, the optimal T_d was achieved by either maximizing the channel capacity (*Section 3.3*) or minimizing the BER performance (*Section 3.4*) by using three approaches, including the simulation approach, the semi-analytical approach and the analytical approach.

  For the channel capacity criterion, the Gaussian approximation (GA) was in used in order to use the Shannon equation for the capacity calculation. Since the Shannon equation is a monotonous function of the output SINR, this issue of maximizing the capacity is equivalent to that of maximizing the output SINR. First, the simulation method was ap-

plied to find the best value of T_d in *Section 3.3.1*. It showed that there indeed exist an optimum value of $T_{d_{opt}}$ providing the best tradeoff. Also, the channel achievable capacity by using the simulation method was significantly improved over that without the optimization. Second, the semi-analytical method was introduced based on some mathematical calculation and further approximations in *Section 3.3.2*. In this case, the interference-plus-noise term was assumed to be Gaussian. The results from semi-analytical had a very similar profile as those from simulation and a significant capacity improvement could be achieved over the non-improved scheme. Third, the semi-analytical method can be applied to the UWB channel models to conduct the analytical method shown in *Section 3.3.3*. By employing the IEEE 802.15.3a channel models, a theoretical expression of the channel achievable capacity with respect to T_d was derived herein. This pure analytical results were very close to the semi-analytical results. Therefore, all these three optimization approaches could be the guidance for receiver designs.

For the BER criterion, the optimal T_d was achieved by using the 'brute-force' method via simulation. Introducing the GA, the optimal values of T_d minimizing BER from semi-analytical and analytical methods were obtained by using the output SINR values derived from *Section 3.3.2* and *Section 3.3.3*, respectively. Similarly, significant BER performance improvement could be achieved from the three approaches over the non-improved scheme.

- **Optimizations for the generalized TR receivers.**

  Both the number of reference symbols N_r and the integration interval

length T_N were optimized in terms of the BER performance. Instead of employing a joint optimization of both N_r and T_N, two separate optimizations of N_r or T_N were used for time-saving. The optimization of N_r was transformed to be the optimization of the energy allocation factor α.

A group of receivers composed of the TB, ML- and GLRT- receivers was optimized with respect to α at an initial value of $T_d = T_{mds}$ first. The improved receivers provided a lot of performance gains at the optimal α. Then, the optimum values of $T_{N_{opt}}$ for these receivers were obtained at the optimal α got in the first step. A further performance gain could be achieved at the optimal T_N. On the other hand, these receivers were improved by optimizing T_N first at the initial value of $\alpha = \frac{1}{21}$ and then optimizing α at the optimal T_N achieved in the first step. The simulation results illustrated that both optimization schemes can offer significant performance improvement. The difference between the receivers that optimize α first and the receivers that optimize T_N first was very little. Therefore, it was proved that the joint optimization could be replaced by two separate optimizations.

Another group of receivers composed of the RD, RI and RDI receivers was optimized in the same way in *Section 4.4*. In addition, the semi-analytical method was added to compare with the simulation method. In the semi-analytical approach, the GA was used as well for the noise term. However, it was not as accurate as the simulation approach due to the over-estimation of noise.

In conclusion, the contribution of this thesis is in the demonstration that the optimization schemes proposed herein for the UWB TR receivers are novel and can clearly improve the system performance. Specifically, an up to 4.2 dB performance gain can be achieved. This enables the improved receivers can be successfully applied to achieve higher QoS in the next generation communication systems.

5.4 Future Work

The work presented in this thesis can be extended on a range of frontiers. All the optimization approaches discussed herein were based on a single-user communication system and can be applied to a multi-user system where the added multiple-access interference (MAI) needs to be considered. For example, in the traditional TR system with the AcR, the choice of T_d may also impact the receiver performance significantly in the present of MAI. Therefore, the future work can apply the three optimization approaches proposed in *Chapter 3* to a multi-user UWB system. However, it may be very difficult to have a closed-form expression of capacity/BER with respect to T_d due to the MAI term. Similarly, for the generalized TR receivers, all the optimization results in *Chapter 4* could be extended to a multi-user system as well.

In addition, for the RD, RI and RDI generalized TR receivers described in *Section 4.4*, the semi-analytical results of optimization can be further derived by introducing the IEEE 802.15.3a channel models for a specific theoretical result.

Finally, the ideas and schemes presented in this thesis for the receiver optimization could provide other researches with a novel way of thinking in

the domain of receiver designs, not only for UWB communication systems.

References

[1] IEEE standard for information technology–telecommunications and information exchange between systems–local and metropolitan area networks–specific requirements part 11: Wireless lan medium access control (mac) and physical layer (phy) specifications amendment 8: Ieee 802.11 wireless network management. *IEEE Std 802.11v-2011 (Amendment to IEEE Std 802.11-2007 as amended by IEEE Std 802.11k-2008, IEEE Std 802.11r-2008, IEEE Std 802.11y-2008, IEEE Std 802.11w-2009, IEEE Std 802.11n-2009, IEEE Std 802.11p-2010, and IEEE Std 802.11z-2010)*, pages 1–433, Feb. 2011.

[2] F. Subhan, H. Hasbullah, A. Rozyyev, and S.T. Bakhsh. Indoor positioning in bluetooth networks using fingerprinting and lateration approach. In *2011 International Conference on Information Science and Applications (ICISA)*, pages 1–9, April 2011.

[3] Sangjae Lee, Youngae Jeon, Sangsung Choi, Man Soo Han, and Kyoungrok Cho. Gigabit uwb video transmission system for wireless video area network. *IEEE Transactions on Consumer Electronics*, vol. 57, no. 2, pages 395-402, May 2011.

[4] Terence W. Barrett. History of ultra wideband (uwb) radar & communications: Pioneers and innovators. *Progress In Electromagnetics Symposium (PIERS2000)*, pages 285–319, July 2000.

[5] Gerald F. Ross. Transmission and Reception System for Generating and Receiving Base-Band Duration Pulse Signals without Distortion for Short Base-Band Pulse Communication System. *U.S. Patent # 3728632*, 1973.

[6] Gerald F. Ross. Base-band Radiation and Reception System. *U.S. Patent # 3739392*, 1973.

[7] Andreas F. Molish Ian Oppermann Christian Politano Maria G. D. Benedetto, Thomas Kaiser and Domenico Porcino. *UWB Communication Systems: A Comprehensive Overview*. Hindawi Publishing Corporation, 2006.

[8] Federal Communications Commission (FCC). FIRST REPORT AND ORDER In the matter of Revision of Part 15 of the Commission's Rules Regarding Ultra-Wideband Transmission Systems. *FCC 02-48*, page 36, 2002.

[9] Lachlan Michael Mohammad Ghavami and Ryuji Kohno. *Ultra Wideband Signals and Systems in Communication Engineering*. Wiley, July 2004.

[10] C.L. Bennett and G.F. Ross. Time-domain Electromagnetics and its applications. *Proceedings of the IEEE*, vol. 66, no, 3, pages 299-318, March 1978.

[11] H. F. Harmuth. Nonsinusoidal waves for radar and radio communication. *NASA STI/Recon Technical Report A*, vol. 81, pages 494-540, October 1981.

[12] G.R. Aiello and G.D. Rogerson. Ultra-wideband wireless systems. *Microwave Magazine, IEEE*, vol. 4, no. 27, pages 36-47, June 2003.

[13] John G. Proakis. *Digital Communications (4th Edition)*. Mc-Graw-Hill.

[14] R.J. Fontana. Recent system applications of short-pulse ultra-wideband (uwb) technology. *IEEE Transactions on Microwave Theory and Techniques*, vol. 52, no. 9, pages 2087-2104, September 2004.

[15] I.I. Immoreev and P.G.S.D.V. Fedotov. Ultra wideband radar systems: advantages and disadvantages. *2002 IEEE Conference on Ultra Wideband Systems and Technologies, 2002. Digest of Papers*, pages 201–205, 2002.

[16] Yunqiang Yang and A.E. Fathy. See-through-wall imaging using ultra wideband short-pulse radar system. *2005 IEEE Antennas and Propagation Society International Symposium*, vol. 3B, pages 334-337, July 2005.

[17] H.L. Bloecher, J. Dickmann, and M. Andres. Automotive active safety & comfort functions using radar. *IEEE International Conference on Ultra-Wideband, 2009. ICUWB 2009*, pages 490–494, September 2009.

[18] I. Oppermann, L. Stoica, A. Rabbachin, Z. Shelby, and J. Haapola. Uwb wireless sensor networks: Uwen - a practical example. *IEEE Communications Magazine*, vol. 42, no. 12, pages S27-S32, December 2004.

[19] D. Porcino and W. Hirt. Ultra-wideband radio technology: potential and challenges ahead. *IEEE Communications Magazine*, vol. 41, no. 7, pages 66-74, July 2003.

[20] M.Z. Win and R.A. Scholtz. Impulse radio: how it works. *IEEE Communications Letters*, vol. 2, no. 2, pages 36-38, February 1998.

[21] M.Z. Win and R.A. Scholtz. On the robustness of ultra-wide bandwidth signals in dense multipath environments. *IEEE Communications Letters*, vol. 2, no. 2, pages 51-53, February 1998.

[22] A. Saleh and R. Valenzuela. A statistical model for indoor multipath propagation. *IEEE Journal on Selected Areas in Communications*, vol. 5, no. 2, pages 128-137, February 1987.

[23] J.R. Foerster. The effects of multipath interference on the performance of uwb systems in an indoor wireless channel. *IEEE VTS 53rd Vehicular Technology Conference, 2001. VTC 2001 Spring*, vol. 2, pages 1176-1180, 2001.

[24] M.Z. Win, R.A. Scholtz, and M.A. Barnes. Ultra-wide bandwidth signal propagation for indoor wireless communications. *1997 IEEE International Conference on 'Towards the Knowledge Millennium'*, vol. 1, pages 56-60, June 1997.

[25] D. Cassioli, M.Z. Win, and A.F. Molisch. The ultra-wide bandwidth indoor channel: from statistical model to simulations. *IEEE Journal on Selected Areas in Communications*, vol. 20, no. 6, pages 1247-1257, August 2002.

[26] Channel modeling sub-committee report final. *IEEE P802.15 Wireless Personal Area Networks*, page 5, February 2003.

[27] Z. Ahmadian and L. Lampe. Performance analysis of the ieee 802.15.4a uwb system. *IEEE Transactions on Communications*, vol. 57, no. 5, pages 1474-1485, May 2009.

[28] Yunfei Chen and N. Beaulieu. Interference analysis of uwb systems for ieee channel models using first- and second-order moments. *IEEE Transactions on Communications*, vol. 57, no. 3, pages 622-625, March 2009.

[29] R. Scholtz. Multiple access with time-hopping impulse modulation. *IEEE Military Communications Conference, 1993. MILCOM '93. Conference record. 'Communications on the Move'*, vol. 2, pages 447-450, October 1993.

[30] F. Ramirez-Mireles. On the performance of ultra-wide-band signals in gaussian noise and dense multipath. *IEEE Transactions on Vehicular Technology*, vol. 50, no. 1, pages 244-249, January 2001.

[31] C.A. Corral, S. Sibecas, S. Emami, and G. Stratis. Pulse spectrum optimization for ultra-wideband communication. *2002 IEEE Conference on Ultra Wideband Systems and Technologies, 2002. Digest of Papers*, pages 31–35, 2002.

[32] T. Zhang, T.D. Abhayapala, and R.A. Kennedy. Performance of ultra-wideband correlator receiver using gaussian monocycles. *IEEE International Conference on Communications, 2003. ICC '03*, vol. 3, pages 2192-2196, May 2003.

[33] Bo Hu and N.C. Beaulieu. Pulse shapes for ultrawideband communication systems. *IEEE Transactions on Wireless Communications*, vol. 4, no. 4, pages 1789-1797, July 2005.

[34] B. Parr, ByungLok Cho, K. Wallace, and Zhi Ding. A novel ultra-wideband pulse design algorithm. *IEEE Communications Letters*, vol. 7, no. 5, pages 219-221, May 2003.

[35] Xianren Wu, Zhi Tian, T.N. Davidson, and G.B. Giannakis. Optimal waveform design for uwb radios. *IEEE Transactions on Signal Processing*, vol. 54, no. 6, pages 2009-2021, June 2006.

[36] Xiaojing Huang and Yunxin Li. Performances of impulse train modulated ultra-wideband systems. *IEEE International Conference on Communications, 2002. ICC 2002*, vol. 2, pages 758-762, 2002.

[37] Lijia Ge, Guangrong Yue, and S. Affes. On the ber performance of pulse-position-modulation uwb radio in multipath channels. *2002 IEEE Conference on Ultra Wideband Systems and Technologies, 2002. Digest of Papers*, pages 231–234, 2002.

[38] M. Hamalainen, R. Tesi, J. Iinatti, and V. Hovinen. On the performance comparison of different uwb data modulation schemes in awgn channel in the presence of jamming. *IEEE Radio and Wireless Conference, 2002. RAWCON 2002*, pages 83–86, 2002.

[39] I. Guvenc and H. Arslan. On the modulation options for uwb systems. *IEEE Military Communications Conference, 2003. MILCOM 2003*, vol. 2, pages 892-897, October 2003.

[40] Li Zhao and A.M. Haimovich. Multi-user capacity of m-ary ppm ultra-wideband communications. *2002 IEEE Conference on Ultra Wideband Systems and Technologies, 2002. Digest of Papers*, pages 175–179, 2002.

[41] C. Carbonelli and U. Mengali. M-ppm noncoherent receivers for uwb applications. *IEEE Transactions on Wireless Communications*, vol. 5, no. 8, pages 2285-2294, August 2006.

[42] V.S. Somayazulu. Multiple access performance in uwb systems using time hopping vs. direct sequence spreading. *2002 IEEE Wireless Communications and Networking Conference, 2002. WCNC2002*, vol. 2, pages 522-525, March 2002.

[43] Bo Hu and N.C. Beaulieu. Accurate evaluation of multiple-access performance in th-ppm and th-bpsk uwb systems. *IEEE Transactions on Communications*, vol. 52, no. 10, pages 1758-1766, October 2004.

[44] M.Z. Win and R.A. Scholtz. Ultra-wide bandwidth time-hopping spread-spectrum impulse radio for wireless multiple-access communications. *IEEE Transactions on Communications*, vol. 48, no. 4, pages 679-689, April 2000.

[45] Wei-Chung Peng. Book reviews - spread spectrum communications. *IEEE Communications Magazine*, vol. 25, no. 8, pages 60-61, August 1987.

[46] J.R. Foerster. The performance of a direct-sequence spread ultrawideband system in the presence of multipath, narrowband interference, and multiuser interference. *2002 IEEE Conference on Ultra Wideband Systems and Technologies, 2002. Digest of Papers*, pages 87–91, 2002.

[47] J. Nabi and R. Bose. On the performance analysis of multiple access codes for ultra-wideband sensor networks. *ITI 3rd International Conference on Information and Communications Technology, 2005. Enabling Technologies for the New Knowledge Society:*, pages 323–332, December 2005.

[48] M.S. Iacobucci and M.-G. Di Benedetto. Multiple access design for impulse radio communication systems. *IEEE International Conference on Communications, 2002. ICC 2002*, vol. 2, pages 817-820, 2002.

[49] Bo Hu and N.C. Beaulieu. Accurate performance evaluation of time-hopping and direct-sequence uwb systems in multi-user interference. *IEEE Transactions on Communications*, vol. 53, no. 6, pages 1053-1062, June 2005.

[50] B. Mielczarek, M.O. Wessman, and A. Svensson. Performance of coherent uwb rake receivers with channel estimators. *2003 IEEE 58th Vehicular Technology Conference, 2003. VTC 2003-Fall*, vol. 3, pages 1880-1884, October 2003.

[51] J.D. Choi and W.E. Stark. Performance of ultra-wideband communications with suboptimal receivers in multipath channels. *IEEE Journal on Selected Areas in Communications*, vol. 20, no. 9, pages 1754-1766, December 2002.

[52] R. Hoctor and H. Tomlinson. Delay-hopped transmitted-reference rf communications. *2002 IEEE Conference on Ultra Wideband Systems and Technologies, 2002. Digest of Papers*, pages 265–269, 2002.

[53] Yi-Ling Chao and R.A. Scholtz. Optimal and suboptimal receivers for ultra-wideband transmitted reference systems. *IEEE Global Telecommunications Conference, 2003. GLOBECOM '03*, vol. 2, pages 759-763, December 2003.

[54] Yi-Ling Chao and R.A. Scholtz. Ultra-wideband transmitted reference systems. *IEEE Transactions on Vehicular Technology*, vol. 54, no. 5, pages 1556-1569, September 2005.

[55] M. Weisenhorn and W. Hirt. Robust noncoherent receiver exploiting uwb channel properties. *2004 International Workshop on Ultra Wideband Systems, 2004. Joint with Conference on Ultrawideband Systems and Technologies. Joint UWBST IWUWBS*, pages 156–160, May 2004.

[56] Z. Tian and B.M. Sadler. Weighted energy detection of ultra-wideband signals. *2005 IEEE 6th Workshop on Signal Processing Advances in Wireless Communications*, pages 1068–1072, June 2005.

[57] A.A. D'Amico, U. Mengali, and E. Arias-de Reyna. Energy-detection uwb receivers with multiple energy measurements. *IEEE Transactions on Wireless Communications*, vol. 6, no. 7, pages 2652-2659, July 2007.

[58] S. Franz and U. Mitra. On optimal data detection for uwb transmitted reference systems. *IEEE Global Telecommunications Conference, 2003. GLOBECOM '03*, vol. 2, pages 744-748, December 2003.

[59] M.E. Sahin, I. Guvenc, and H. Arslan. Optimization of energy detector receivers for uwb systems. *2005 IEEE 61st Vehicular Technology Conference, 2005. VTC 2005-Spring*, vol. 2, pages 1386-1390, May 2005.

[60] D. Cassioli, M.Z. Win, F. Vatalaro, and A.F. Molisch. Low complexity rake receivers in ultra-wideband channels. *IEEE Transactions on Wireless Communications*, vol. 6, no. 4, pages 1265-1275, April 2007.

[61] Giuseppe Durisi and Sergio Benedetto. Comparison between coherent and noncoherent receivers for uwb communications. *Signal Process. EURASIP J. Appl.*, 2005:359–368, January 2005.

[62] T.Q.S. Quek and M.Z. Win. Analysis of uwb transmitted-reference communication systems in dense multipath channels. *IEEE Journal on Selected Areas in Communications*, vol. 23, no. 9, pages 1863-1874, September 2005.

[63] Yi-Ling Chao and R.A. Scholtz. Multiple access performance of ultra-wideband transmitted reference systems in multipath environments. *2004 IEEE Wireless Communications and Networking Conference, 2004. WCNC*, vol. 3, pages 1788-1793, March 2004.

[64] F. Nekoogar, F. Dowla, and Spiridon A. Integration window position estimation in tr receivers. *Wireless Communications 2005, UCRL-CONF-210686*, pages 126–133, June 2005.

[65] T.Q.S. Quek and M.Z. Win. Ultrawide bandwidth transmitted-reference signaling. *2004 IEEE International Conference on Communications*, vol. 6, pages 3409-3413, June 2004.

[66] Y.-L. Chao. Optimal integration time for uwb transmitted reference correlation receivers. *Conference Record of the Thirty-Eighth Asilomar Conference on Signals, Systems and Computers, 2004*, vol. 1, pages 647-651, November 2004.

[67] Tao Jia and Dong In Kim. Analysis of channel-averaged sinr for indoor uwb rake and transmitted reference systems. *IEEE Transactions on Communications*, vol. 55, no. 10, pages 2022-2032, October 2007.

[68] K. Witrisal and M. Pausini. Statistical analysis of transmitted-reference uwb systems on multipath channels. *The 2006 IEEE 2006 International Conference on Ultra-Wideband*, pages 303–308, September 2006.

[69] K. Witrisal and M. Pausini. Statistical analysis of uwb channel correlation functions. *IEEE Transactions on Vehicular Technology*, vol. 57, no. 3, pages 1359-1373, May 2008.

[70] J. Baringbing and K. Witrisal. Performance evaluation of multiple-access dual-pulse transmitted reference uwb systems. *International Wireless Communications and Mobile Computing Conference, 2008. IWCMC '08*, pages 214–219, August 2008.

[71] S. Franz and U. Mitra. Integration interval optimization and performance analysis for uwb transmitted reference systems. *2004 International Workshop on Ultra Wideband Systems, 2004. Joint with Conference on Ultrawideband Systems and Technologies. Joint UWBST IWUWBS*, pages 26–30, May 2004.

[72] Tao Jia and Dong In Kim. Wlc23-3: Multiuser performance of balanced uwb transmitted-reference system in multipath. *IEEE Global Telecommunications Conference, 2006. GLOBECOM '06*, pages 1–5, December 2006.

[73] Yunfei Chen and N. Beaulieu. Derivations of some equations on interference analysis of ipi, ici, and isi using ieee uwb channel models.

http://www2.warwick.ac.uk/fac/sci/eng/staff/yc/supplementonline.pdf, accessed in May 2009.

[74] I.S. Gradshteyn and I.M. Ryzhik. *Table of Integrals, Series, and Products (Fifth Edition)*. Academic Press, Inc, 1994.

[75] P.P. Mercier, D.C. Daly, M. Bhardwaj, D.D. Wentzloff, F.S. Lee, and A.P. Chandrakasan. Ultra-low-power uwb for sensor network applications. *IEEE International Symposium on Circuits and Systems, 2008. ISCAS 2008*, pages 2562–2565, May 2008.

[76] T. Zasowski, G. Meyer, F. Althaus, and A. Wittneben. Propagation effects in uwb body area networks. *2005 IEEE International Conference on Ultra-Wideband, 2005. ICU 2005*, pages 16–21, September 2005.

[77] Liuqunig Yang and G.B. Giannakis. Optimal pilot waveform assisted modulation for ultra-wideband communications. *Conference Record of the Thirty-Sixth Asilomar Conference on Signals, Systems and Computers, 2002*, vol. 1, pages733-737, November 2002.

[78] Honglei Zhang and D.L. Goeckel. Generalized transmitted-reference uwb systems. *2003 IEEE Conference on Ultra Wideband Systems and Technologies*, pages 147–151, November 2003.

[79] S. Franz and U. Mitra. Generalized uwb transmitted reference systems. *Selected Areas in Communications, IEEE Journal on*, 24(4):780–786, April 2006.

[80] Yunfei Chen and N.C. Beaulieu. New receiver designs for generalized uwb transmitted reference systems. *IEEE International Conference on Communications, 2008. ICC '08*, pages 3923–3927, 2008.

[81] Yunfei Chen and N.C. Beaulieu. Improved receivers for generalized uwb transmitted reference systems. *IEEE Transactions on Wireless Communications*, vol. 7, no. 2, pages 500-504, February 2008.

[82] G. Leus and A.-J. van der Veen. Noise suppression in uwb transmitted reference systems. *2004 IEEE 5th Workshop on Signal Processing Advances in Wireless Communications*, pages 155–159, July 2004.

[83] F. Nekoogar, F. Dowla, and A. Spiridon. Integration window position estimation in tr receivers. *wirelessCom2005, Maui, HI, United States*, pages 66–70, June 2005.

[84] Yunfei Chen, N. Beaulieu, and Shuyi Wang. Novel iterative receivers for tr uwb systems. *IEEE Communications Letters*, vol. 13, no. 4, pages 242-244, April 2009.

[85] Yunfei Chen and N.C. Beaulieu. SNR estimation methods for uwb systems. *IEEE Transactions on Wireless Communications*, vol. 6, no. 10, pages 3836-3845, October 2007.